ALGORITHMS FOR CHANNEL IMPAIRMENT MITIGATION IN BROADBAND WIRELESS COMMUNICATIONS

NGUYEN LE, HUNG

(B.Eng. (Hons.))

A THESIS SUBMITTED FOR THE DEGREE OF

DOCTOR OF PHILOSOPHY

DEPARTMENT OF ELECTRICAL AND COMPUTER ENGINEERING

NATIONAL UNIVERSITY OF SINGAPORE

2007

Acknowledgements

First of all, I would like to express my sincere thank to my academic supervisor, Professor Chi Chung Ko, for the valuable guidance, support and encouragement he has been providing me. Without his research orientation and support, I would not have a chance to pursue my graduate study in the National University of Singapore (NUS). Among a variety of subjects I have learnt in NUS, the most valuable one is “a balance in life” he has conveyed to me. In fact, I lost the balance when I first came to NUS. Gradually, he has been helping my balance get better during the last three years. He is my true mentor.

I am deeply grateful to Professor Tho Le-Ngoc at McGill University for his great guidance on my research work. He has taught me various theoretical backgrounds and practical signal processing techniques in OFDM systems. Also, I have learnt a great deal of his practical experiences and hard work that will be beneficial to my future career. Without his advice, I would be unable to complete the OFDM research work in this thesis.

I would like to thank Mr. Robert Morawski at McGill University for his professional assistance in running numerous computer simulations and developing a hardware implementation of the proposed algorithms for OFDM systems. Without his kind help, I would be unable to obtain such important simulation results for this thesis.

I would like to thank the National University of Singapore for the research scholarship offered to me, by which I could carry out my research work without any financial difficulty.

Finally, I would like to give my deepest gratitude to my parents who have been dedicating their lives to my education. I also wish to thank my wife who always stays by me in any difficult circumstance.

Table of Contents

Summary

Broadband wireless communications has been well recognized as one of the most potential strategies to integrate various high-data-rate and quality communication applications such as high-speed wireless internet, broadcasting and mobile communication services under a common system infrastructure. However, along with these potential benefits, the primary challenges in broadband wireless communications are channel impairments which include interference, multi-path fading propagation and imperfect synchronization. To mitigate such detrimental effects to the receiver performance, this thesis proposes several algorithms for estimating and compensating these channel impairments in early and recent broadband wireless systems.

As one of the early solutions to broadband wireless communications, the frequency hopping spread spectrum (FHSS) technique has been deployed to achieve high robustness against intentional interferences or jammers. However, the anti-jamming feature of the FHSS systems may be significantly neutralized by a follower partial-band jammer. To defeat this effective jammer, this thesis proposes a maximum likelihood (ML)-based joint follower jamming rejection and symbol detection algorithm for slow FH M-ary frequency shift keying (MFSK) systems over quasi-static flat Rayleigh fading channels.

Recently, considered as a very promising candidate for broadband wireless communications, the orthogonal frequency division multiplexing (OFDM) scheme has been extensively employed in various broadband wireless systems to provide high spectral efficiency and robustness against multi-path fading channels. However, the inherent drawback of OFDM-based systems is their susceptibility to synchronization errors such as the carrier and sampling frequency offsets. To estimate the channel impulse response (CIR) and synchronization errors in *uncoded* single-input single-output (SISO)

OFDM-based systems, this thesis proposes a pilot-aided joint channel estimation and synchronization approach with the aid of the standard recursive least squares (RLS) algorithm.

For further improvement in the OFDM receiver performance, the integration of the multiple-input multiple-output (MIMO) architectures and OFDM technique has been widely considered as a potential strategy to enhance data rate, capacity and quality of broadband wireless OFDM systems. However, the primary challenge in MIMO-based systems is the increasing complexity in channel estimation as the number of antennas increases. To perform joint multiantenna channel estimation and synchronization in MIMO scenarios, this thesis develops a vector recursive least squares (RLS)-based scheme for *uncoded* burst-mode MIMO-OFDM systems over multipath Rayleigh fading channels.

Dealing with channel estimation and synchronization in *coded* OFDM transmissions, this thesis introduces a turbo joint channel estimation, synchronization and decoding scheme for convolutionally coded burst-mode MIMO-OFDM systems. To benefit from the spectacular performance of turbo processing, the proposed turbo scheme employs the iterative extrinsic *a posteriori* probability (APP) exchange in the turbo principle to jointly perform channel estimation, synchronization and decoding in an iterative and semi-blind fashion.

List of Tables

List of Figures

Acronyms

AWGN Additive White Gaussian Noise

APP A Posteriori Probability

BER Bit Error Rate

CIR Channel Impulse Response

CFO Carrier Frequency Offset

CP Cyclic Prefix

CRLB Cramer Rao Lower Bound

FHSS Frequency Hopping Spread Spectrum

FH Frequency Hopping

FFT Fast Fourier Transform

FD Frequency Domain

ICI Inter-Carrier Interference

ISI Inter-Symbol Interference

ML Maximum Likelihood

MIMO Multiple-Input Multiple-Output

MFSK M-ary Frequency Shift Keying

OFDM Orthogonal Frequency Division Multiplexing

P/S Parallel-to-Serial converter

ppm part per million

RLS Recursive Least Squares

SFO Sampling Frequency Offset

SER Symbol Error Rate

S/P Serial-to-Parallel converter

SISO Single-Input Single-Output

SIMO Single-Input Multiple-Output

SNR Signal-to-Noise Ratio

SJR Signal-to-Jamming Ratio

TD Time domain

Chapter 1

Introduction

Broadband wireless communications has been well recognized as a potential strategy to integrate various high-data-rate and quality communication applications such as high-speed wireless internet, broadcasting and mobile communications services under a common system infrastructure. However, along with these potential benefits, the primary challenges in broadband wireless communications are the channel impairments which include interference, multi-path fading propagation and imperfect synchronization. Focusing on intentional interference, multipath fading channels, carrier and sampling frequency offsets, this thesis proposes several algorithms for mitigating these channel impairments in FH and OFDM systems. Before introducing the detailed developments of these proposed algorithms from Chapter 2 onwards, Chapter 1 provides a brief history of broadband wireless communications and an overview of these channel impairments. In addition, motivations, scopes and thesis contributions are also presented in this chapter.

1.1 Brief History of Broadband Wireless Communications

In 1897, Guglielmo Marconi developed the world's first wireless transmission to communicate from ship to shore by employing the Morse code [1]. However, due to a limited power of the transmitted signals, Marconi's wireless systems were only able to provide a communication channel with low data rate and over short ranges. Later, in 1906, the invention of the vacuum tube liberated Marconi's first wireless system from their low-data rate and on-and-off keying by amplifying the transmitted analog signals. Then, the use of the amplitude modulation (AM) for high-fidelity analog

transmissions such as voice and music became popular over the world in the 1920s. To alleviate the detrimental effect of noise in AM-based systems, frequency modulation (FM) radio was first developed by Armstrong in 1933. As a natural result of Second World War with electronic supremacy (a war with jamming and anti-jamming strategies) [2], the first patent by G. Guanella on radar was probably considered as the spread spectrum (SS) principle in 1938. Since World War II, numerous intensive researches on the SS principle have been carried out for military and civilian wireless communication applications. Based on a wide variety of practical achievements in the SS technology, a new era of wireless communication applications with high-data-rate transmissions using wide frequency bandwidth, the so-called broadband wireless communications, started around the late 1970s. Specifically, the first proposal for CDMA cellular networks in the USA and Europe (1978-1980) evolved into the GSM and DAMPS standards. Till the mid 1990s, the 2G standard IS-95 became a full spread spectrum/CDMA platform. Today, in the presence of numerous broadband wireless systems sharing a common radio channel, the primary challenges in increasing the data rate, quality and capacity of such systems are channel impairments and limited radio frequencies.

Recently, orthogonal frequency division multiplexing (OFDM) technique, first proposed in 1968 [3], has been extensively employed in various broadband wireless systems to provide high spectral efficiency and robustness against multi-path fading channels. Furthermore, by exploiting significant diversity and capacity gain of the multiple-input multi-output (MIMO) architectures, the integration of MIMO and OFDM techniques [4] has been widely recognized as a very promising strategy to enhance data rate, capacity and quality of the existing broadband wireless systems as well as their next generations.

In this thesis, we focus on the channel impairment mitigation in the early and recent broadband wireless systems such as frequency hopping spread spectrum (FH-SS) and OFDM-based ones, respectively. Specifically, we propose several schemes for channel impairment mitigation in frequency hopping M-ary frequency shift keying (FH-MFSK) and MIMO-OFDM systems. To give an overview of the major channel impairments in such systems, the next section will describe briefly intentional interferences in FH/MFSK systems as well as multi-path fading channels and synchronization errors in OFDM-based systems.

1.2 Channel Impairments

1.2.1 Intentional interferences

In frequency hopping (FH) systems, there are four main types of intentionally interfering (jamming) sources such as barrage noise, single tone, multiple tone and partial-band jammers. Among these types of jammers, the most popular one is the barrage noise jammer which simply transmits a band-limited white Gaussian noise whose power spectrum covers the entire frequency range of a target FH receiver. Consequently, a barrage noise jammer usually induces the same effect as thermal noise, in turn enhancing the noise level at a target FH receiver [5].

Besides barrage noise jamming, the second type of intentional interference is single-tone jamming. A single-tone jammer simply transmits an un-modulated carrier signal at a certain frequency in the currently used FH signal bandwidth. As a result, this type of jamming induces a quite insignificant effect on FH systems since the instantaneous FH frequency bandwidth is small and changes continuously. For FH systems, a more effective tone jamming strategy is the use of multi-tone jamming which transmits various un-modulated carrier signals in the entire FH frequency bandwidth.

To obtain a more efficient jamming strategy in FH systems, partial-band jamming is usually employed. This jamming scheme transmits all its available power to a certain portion of the entire FH signal bandwidth [6]. In fact, such jammers include extremely effective ones which are called follower partial-band jammers [7] (smart or repeater jammers). A follower partial band jammer is able to determine the currently used frequency band of a target FH receiver and injects its interfering signals to that frequency band. To mitigate the detrimental effect of the jamming strategy, this thesis proposes a maximum likelihood (ML)-based algorithm to reject the follower jamming components in FH/MFSK receivers over quasi-static Rayleigh fading channels.

1.2.2 Multi-path fading channels

In wireless propagation channels, the multi-path phenomenon causes a significant degradation in the performance of wireless communication systems with coherent detection. Specifically, under multi-path propagation, the transmitted signal arrives to a receiver via various propagation paths with different delays and attenuations. Consequently, the superposition of many impinging signals from various propagation paths yields a time-variant amplitude response on the received signal, the so-called fading phenomenon. Based on the central-limit theorem, the resulting received signal can be approximated as a complex Gaussian random variable whose envelop has a Rayleigh distribution, and this is thus termed Rayleigh fading [8]. For coherent detection, this channel state information is required for retrieval of the transmitted data.

Besides a time-variant amplitude response on the received signal due to multipath propagation, the time-varying characteristics of each signal path induce frequency spreading, the so-called Doppler spreading [9]. In particular, the Doppler spread B_d is the range of frequencies within which the time-averaged scattering function is non-zero. An essential characteristic of B_d is to indicate the rate of channel variation in

time. Specifically, the larger B_d, the faster channel characteristics change, thus inducing more frequency spreading. Based on the parameter B_d, channels are characterized as fast-fading if the Doppler spread B_d is large compared with the signal bandwidth or as slow-fading if B_d is small compared to the signal bandwidth [9].

In addition, another important parameter of wireless channels is the coherence bandwidth B_c, defined as the reciprocal of the time range over which the frequency-averaged scattering function is non-zero. When the bandwidth of the transmitted signal is larger than the coherence bandwidth, the transmitted signal experiences different attenuations at different frequencies and in turn undergoes frequency-selective fading. Furthermore, the multipath components can be resolved from the received signal, so that the multipath channel can be characterized in a complex linear time-varying system with the channel impulse response (CIR) given by [8]

$$h(t;\tau) = \sum_{l=0}^{L-1} \alpha_l(t)\delta\big(\tau - \tau_l(t)\big), \tag{1.1}$$

where $\alpha_l(t)$ and $\tau_l(t)$ are the time-varying complex attenuation and delay of the *l*-th path, respectively. In burst mode transmissions where channel responses are usually assumed to vary insignificantly over one transmitted data burst, we can assume that the CIR is time-invariant, i.e., the so-called quasi-static fading channels. Unless stated otherwise, the remainder of this thesis assumes the transmitted signals experience quasi-static fading.

1.2.3 Synchronization errors

Unlike single carrier-based systems, multicarrier (MC)-based ones such as MC-CDMA and OFDM systems are particularly vulnerable to synchronization errors due

to the fact that the frequency spacing among subcarriers of MC-based systems is typically very small. In practice, these synchronization errors include the symbol timing offset (STO), carrier frequency offset (CFO) and sampling frequency offset (SFO). Specifically, STO refers to the use of the incorrect position of the FFT window for a set of the received samples in the time domain. Traditionally, timing synchronization is performed by two phases. First, coarse synchronization is established by exploiting the auto-correlation properties of the preamble. Second, fine synchronization is attained by using cross-correlation of the received packet with a known training sequence [10]. After coarse and fine synchronization, residual STO can be absorbed in channel frequency response [11]. Besides the effect of STO, CFO quantifies the mismatch among the carrier frequencies of the RF impinging signals and receiver's local oscillators. In addition, even in the absence of the Doppler effect, the frequency discrepancy between oscillators used in the radio transmitters and receivers is usually unavoidable and therefore the CFO always exits. The presence of CFO destroys the orthogonality among subcarriers. This loss of orthogonality among subcarriers will incur inter-carrier interference (ICI), phase rotation and attenuation in the frequency domain. Likewise, SFO refers to the discrepancy between the sampling frequencies at transmitters and receivers. Similar to the CFO effect, SFO also induces the ICI in the frequency domain, and the phase rotation and attenuation in both time and frequency domains [12].

1.3 Motivations and Scopes

As one of the early solutions to broadband wireless communications, frequency hopping spread spectrum (FHSS) technique has been deployed to achieve high robustness against intentional interferences or jammers. However, the anti-jamming feat-

ure of FHSS systems may be significantly neutralized by a follower partial-band jammer [7]. Hence, follower jamming mitigation is required to maintain a reliable communication channel in such severely jamming scenarios. Addressing the issue, this thesis investigates the follower partial band jamming mitigation for slow FH M-ary frequency shift keying (MFSK) systems over quasi-static Rayleigh fading channels.

Recently, considered as a very strong candidate for broadband wireless communications, orthogonal frequency division multiplexing (OFDM) scheme has been extensively employed in various broadband wireless systems to provide high spectral efficiency and robustness against multi-path fading. However, the inherent drawback of OFDM-based systems is their susceptibility to synchronization errors such as carrier and sampling frequency offsets. Therefore, compensation of these frequency offsets is of crucial importance in implementing such systems. In addition, so far, most studies on OFDM systems have considered channel estimation and synchronization separately [29]-[31]. Channel estimation is performed by assuming that perfect synchronization has been established [32]-[33], although channel estimation could be degraded by imperfect synchronization and vice versa. Since synchronization and channel estimation are mutually related, joint channel estimation and synchronization could provide better accuracy at the cost of higher complexity. Focusing on joint channel estimation and synchronization issues, this thesis considers the joint CIR, CFO and SFO estimation problem in uncoded single-input single-output (SISO) OFDM systems over quasi-static Rayleigh multi-path fading channels.

Known as a revolutionary concept for wireless transmissions, multiple-input multiple-output (MIMO) architectures [9] are able to offer a spectacular increase in the spectral efficiency of wireless communication channels by increasing the number

of transmit and receive antennas. As a result, the integration of the multiple-input multiple-output (MIMO) architectures and OFDM technique has been widely considered as a potential strategy to enhance data rate, capacity and quality of broadband wireless OFDM systems. However, MIMO-based transmissions lend themselves to a highly computational complexity in channel estimation. For joint multiantenna channel estimation and synchronization in MIMO-OFDM systems, some algorithms [45]-[46] have been proposed recently but the detrimental SFO effect has been omitted in these studies. Taking into account the SFO effect, this thesis investigates the joint CIR, CFO and SFO estimation with the aid of the vector recursive least squares (RLS) algorithm [49] for *uncoded* burst-mode MIMO-OFDM systems over quasi-static multipath Rayleigh fading channels.

For further improvement in the performance of coded MIMO-OFDM systems, turbo processing has been well recognized as a very strong solution to perform channel estimation and decoding in an iterative fashion [62]. In fact, the principle behind the astonishing performance of turbo processing is the iterative exchange of extrinsic *a posteriori* probabilities (APPs) among the constituent functional blocks in MIMO-OFDM receivers. Based on the iterative APP exchange, the thesis considers the joint channel estimation, synchronization and decoding problem with the aid of the vector RLS algorithm in convolutionally coded MIMO-OFDM systems over quasi-static multipath Rayleigh fading channels.

1.4 Thesis Contributions

This thesis proposes several algorithms for mitigating major channel impairments such as jamming, multipath fading propagation and imperfect synchronization in early and recent broadband wireless communication systems. Specifically, a ML-based joi-

nt follower jamming rejection and symbol detection scheme is developed for FH-MFSK systems. For channel estimation and synchronization in *uncoded* OFDM transmissions, this thesis develops pilot-aided schemes for SISO and MIMO configurations. Finally, in *coded* wireless OFDM transmissions, a turbo joint channel estimation, synchronization and decoding approach is developed for convolutionally coded MIMO-OFDM systems. The above proposed schemes are summarized as follows.

As one of the most detrimental channel impairments in FHSS systems (early broadband wireless systems), follower partial-band jamming is able to significantly degrade the FH receiver performance. By exploiting the unknown spatial correlation of the jamming components between receiving antenna elements, a closed-form expression for the ML estimates of the jamming components is derived, leading to joint interference rejection and symbol detection being carried out in a unified ML framework with a low computational complexity. Analysis and simulation results show that the proposed ML-based joint follower jamming rejection and symbol detection scheme is able to remove jamming and outperforms the conventional and sample matrix inversion (SMI)-based beamformers in the presence of a follower partial-band jammer.

For channel estimation and synchronization in recent broadband wireless communication systems, this thesis proposes pilot-aided schemes for the joint CIR, CFO and SFO estimation in burst-mode *uncoded* OFDM systems with SISO and MIMO configurations. In addition, we also present a simple ICI reduction technique in the time domain and a ML coarse estimation of CFO and SFO to further enhance the performance of these proposed schemes. Numerous analysis and simulation results show that the proposed schemes provide a near-optimum receiver performance in quasi-static Rayleigh multi-path fading channels over large ranges of CFO and SFO values.

For channel estimation and synchronization in *coded* transmissions, a turbo joint channel estimation, synchronization and decoding scheme is developed for convolutionally coded MIMO-OFDM systems over quasi-static Rayleigh multi-path fading channels. By exploiting the iterative extrinsic *a posteriori* probability (APP) exchange in the turbo principle, joint channel estimation and synchronization is performed in a doubly iterative and semi-blind fashion with the aid of the vector RLS algorithm. The spectacular benefits of iteratively exchanging the extrinsic soft information in the turbo receiver enable joint estimation of CIR, CFO and SFO and provide low mean-squared-error (MSE) estimates and a near-ideal receiver performance.

1.5 Thesis Organization

The thesis consists of six chapters. This chapter introduced an overview of broadband wireless communications and its major channel impairments. The motivations, scope and thesis contributions were also presented in this chapter. Chapter 2 will provide the literature of existing algorithms for anti-jamming in FH/MFSK systems and the proposed ML-based jamming rejection and symbol detection for such systems. The detailed development of the pilot-aided joint channel estimation and synchronization approach for *uncoded* SISO-OFDM systems will be presented in Chapter 3. Chapter 4 will introduce the vector RLS-based joint CIR, CFO and SFO estimation scheme in *uncoded* MIMO-OFDM systems. For channel impairment mitigation in *coded* OFDM transmissions, a turbo joint channel estimation, synchronization and decoding scheme will be developed in Chapter 5. Finally, Chapter 6 will summarize the research work in this thesis and provide some suggestions for future work.

Chapter 2

Jamming Mitigation in Frequency Hopping Systems

As one of the early solutions for broadband wireless communications, frequency hopping spread spectrum (FHSS) technique has been deployed to achieve high robustness against intentional interferences or jammers. However, the anti-jamming feature of FHSS systems may be significantly neutralized by partial-band jamming. Focusing on anti-jamming issues, this chapter presents the literature of existing algorithms for partial-band jamming mitigation in FH systems. In addition, a signal model of received FH signals is formulated in the presence of a follower partial-band jammer. Based on the signal model, a ML-based joint jamming rejection and symbol detection scheme is derived. Finally, analysis and simulation results are presented to validate the anti-jamming performance of the proposed scheme.

2.1 Introduction

The use of frequency-hopping spread-spectrum (FHSS) techniques for highly secure data transmission has been employed intensively in civilian and military wireless communications. However, in a severely jammed propagation channel, the received jamming signal, whose power is comparable with or much greater than the signal power, will very likely induce an unacceptable degradation to the FH detection performance [8]. In such circumstances, the use of an anti-jamming approach is crucial to alleviate these detrimental effects so as to maintain a reliable communication channel in the presence of intentional interferers. Specifically, the

performance of FHSS systems can be severely degraded in the presence of an intermittent jammer, such as a pulsed noise or a partial band jammer [8], that is present for only a fraction of the time. The detrimental effect caused by intermittent jamming may be compensated by appropriate channel coding. Unfortunately, even with channel coding, the performance of FHSS systems may still be significantly degraded in the presence of a follower partial-band jammer that has the capability to determine the frequency slot of the spread-spectrum bandwidth currently being used during some initial observation interval, and then injects the jamming signal in that frequency slot [7]. Fast hopping may be used to protect against such interference by prohibiting a follower jammer from having sufficient time to determine the desired signal's frequency slot and transmit an interfering signal. However, there is a penalty incurred in subdividing a signal into several FH elements. This is due to the fact that the energy from these separate elements has to be combined noncoherently. In addition, in FH systems, the transmitters and receivers contain clocks that must be synchronized. That is, the transmitters and receivers must hop at the same rate at the same time. The faster the hopping rate, the higher the jam-ming resistance, and the more accurate the clocks must be. This means that a highly accurate clock is required to allow a very fast hop rate for the purpose of defeating a follower jammer. It has been shown in [13] that under certain environments, the required accuracies can be achieved only with atomic clocks. As a result, some systems may still have limitations that do not allow for fast hopping [14].

Investigations on FHSS systems in the presence of partial-band jamming have been carried out in [6], [15]-[20] while studies on follower jamming mitigation have been well documented in [14], [21]-[22], [71]. Specifically, in [14], a countermeasure to a follower partial-band Gaussian noise jammer was proposed for FHSS communicatio-

ns. The proposed scheme makes use of randomized decisions by the transmitter and the receiver to lure the jammer so that system performance can be improved. Of course, this implies that both the transmitter and receiver have to require a higher level of synchronization. In [21], the spatial dimension provided by an antenna array was exploited to achieve a better rejection of the follower jammer based on the classical sample matrix inversion (SMI) algorithm. However, this algorithm requires identical antenna gains for all receive antenna elements at the direction of arrival (DOA) of the jammer and does not work properly over flat fading channels. Similarly, while a variety of broadband source tracking algorithms [23]-[25] are available, they may not function properly under a flat fading scenario.

In this chapter, we formulate a signal model that takes into consideration the effect of a follower jammer explicitly, and then propose a maximum likelihood (ML)-based joint interference cancellation and symbol detection scheme for slow FH/MFSK systems over quasi-static flat fading channels. The scheme is based on a two-element array where, at each element, N samples are extracted from the received signals within each transmitted symbol interval. By exploiting the unknown spatial correlation of the jamming components between the two antenna elements, a closed-form expression for the ML estimates of the jamming components is derived, leading to interference rejection and symbol detection being carried out in a unified ML framework.

Note that in present broadband wireless communication systems such as GSM and Bluetooth based systems as well as other potential future ones using FH techniques, there is always the threat of Denial-of-Service (DoS) attack by intentional interferers [26]-[27]. Specifically, the former is very vulnerable to jamming attack [26]. Under severely jamming scenarios where the jamming power is much greater than the signal power and the channel suffers from quasi-static flat fading, the proposed ML-based

interference rejection structure and algorithm would provide a basis for the formulation of an appropriate solution to maintain a reliable communication channel.

The rest of this chapter is organized as follows. Section 2.2 describes the system model. The derivation of the proposed interference rejection scheme is presented in Section 2.3. The performance of the proposed scheme is analyzed in section 2.4, where an approximate expression for SER is derived. Simulation results and relevant discussions are given in Section 2.5. Finally, Section 2.6 summarizes this chapter.

2.2 System Model

Consider a MFSK modulated slow FH system. To suppress the detrimental effects of a follower partial band jammer, we explore the use of a simple two-element receiving array, where the received signal from each element is down converted and sampled at N times the symbol rate. The samples collected from the two antenna elements over one symbol duration will be used to estimate the desired information symbol by using a ML-based detection scheme, which will be described in more details in Section 2.3.

Without loss of generality, consider the detection of the symbol in a hop over the interval $0 < t < T_s$, where T_s is the symbol duration. The complex envelop of the transmitted signal can be expressed by

$$s(t) = e^{j2\pi(f_i + d_0 f_d)t}, \tag{2.1}$$

where f_i is the hopping frequency, $d_0 \in [0, 1, \ldots, M-1]$ represents the information symbol, and f_d stands for the frequency spacing between two adjacent MFSK tones. Note that, unlike conventional MFSK systems, the proposed scheme does not require the MFSK tones to be orthogonal.

As described in [5], a follower jammer first measures the hopping frequency and the spectrum of the desired hop and then injects the available transmitting power discrim-

inately to the currently used frequency slot. Without perfect knowledge of the desired signal but knowing the hopping frequency of the desired signal, such a jammer will most likely transmit a signal that is different, perhaps noise like, from the desired signal and that will cover the entire band of the latter. The complex envelop of a follower partial-band jamming signal can thus be represented as

$$J(t) = n_J(t)e^{j2\pi(f_i + B_J/2)t}, \tag{2.2}$$

where $n_J(t)$ is a baseband equivalent band-limited signal with bandwidth B_J and can be modeled as a zero mean band-limited Gaussian random process. The exponential term in (2.2) indicates that this baseband signal is up converted to cover the bandwidth occupied by all M data tones in the frequency slot currently occupied by the desired signal in all the hops.

Assuming that the desired signal and the follower jamming signal experience a quasi-static flat Rayleigh fading channel, the received signal at the *p*-th antenna element will be given by

$$r_p(t) = \alpha_p s(t) + \beta_p J(t) + w_p(t), p = 1,2, \tag{2.3}$$

where $w_p(t)$ is the complex white Gaussian receiver noise, and the complex coefficients α_p and β_p account for the overall effects of phase shifts, fading and antenna response for the desired signal and the jamming signal at the *p*th antenna element, respectively. Under a quasi-static flat fading channel, these fading coefficients can be assumed to be constant over one hop duration, equivalently a coherent interval.

Note that unlike the signal models in [6], [17], [21] which are derived for multiple partial-band and follower jamming signals coming from different directions, the signal model used in this chapter is more applicable for a single follower partial-band jammer with known timing in a slow flat fading scenario.

At the *p*th antenna element, the received signal is sampled at *N* times the symbol

rate. Using Equations (2.1), (2.2) and (2.3), the *n*-th sample is

$$r_{p,n} = \alpha_p \exp\left(j\omega_n(d_0)\right) + \beta_p J_n + w_{p,n}, \tag{2.4}$$

where

$$\begin{aligned} r_{p,n} &= r_p\left(\left(\tfrac{1}{2N} + \tfrac{n}{N}\right)T_s\right) \\ \omega_n(d_0) &= 2\pi\left(f_i + d_0 f_d\right)\left(\tfrac{1}{2N} + \tfrac{n}{N}\right)T_s, \\ J_n &= J\left(\left(\tfrac{1}{2N} + \tfrac{n}{N}\right)T_s\right), \end{aligned} \tag{2.5}$$

and $w_{p,n} = w_p\left(\left(\tfrac{1}{2N} + \tfrac{n}{N}\right)T_s\right)$, for n = 0, 1, …, N-1. It is noted that N must be greater than one. In addition, the sampling rate could be much greater than tone spacing. This depends on the number of collected samples per MFSK symbol duration for processing.

Based on (2.4), the signal-to-jamming power ratio (SJR) and signal-to-noise power ratio (SNR) are $\text{SJR} = P_S / P_J$ and $\text{SNR} = P_S / P_N$, respectively, with $P_S = E\left(\left|\alpha_p \exp\left[j\omega_n(d_0)\right]\right|^2\right) = E\left(\left|\alpha_p\right|^2\right)$, $P_J = E\left(\left|\beta_p\right|^2\right)E\left(\left|J_n\right|^2\right)$ and $P_N = E\left(\left|w_{p,n}\right|^2\right)$.

For convenience, Equation (2.4) can be written in vector form for the N samples from the two antenna elements as follows:

$$\mathbf{r}_1 = \alpha_1 \mathbf{s}(d_0) + \mathbf{v} + \mathbf{w}_1, \tag{2.6}$$

and

$$\mathbf{r}_2 = \alpha_2 \mathbf{s}(d_0) + \zeta\mathbf{v} + \mathbf{w}_2, \tag{2.7}$$

where

$$\begin{aligned} \mathbf{r}_p &= \left[r_{p,0}, r_{p,1}, ..., r_{p,N-1}\right]^T, \; p = 1, 2, \\ \mathbf{s}(d_0) &= \left[\exp\left(j\omega_0(d_0)\right), \exp\left(j\omega_1(d_0)\right), ..., \exp\left(j\omega_{N-1}(d_0)\right)\right]^T, \\ \mathbf{v} &= \beta_1\left[J_0, J_1, ..., J_{N-1}\right]^T, \end{aligned} \tag{2.8}$$

$$\xi = \beta_2 / \beta_1 ,$$

and $$\mathbf{w}_p = \left[w_{p,0}, w_{p,1}, ..., w_{p,N-1} \right]^T , p = 1, 2.$$

As the hopping frequency and spectrum of the desired signal need to be found, a follower jammer will not transmit any jamming signal during the initial measurement phase, and will be activated only after some delay following the beginning of each frequency hop [7], [21]. As a result, it would be reasonable to assume that the desired signal's channel gains, α_p (p = 1, 2), have been estimated and known to the receiver prior to the onset of the follower jamming signal. This is because the ML-based channel estimation, described in Appendix A, can be easily performed blindly within a very short interval at the beginning of a hop. In the presence of the desired signal's channel knowledge, the main problem in jamming rejection and symbol detection is thus to estimate the data symbol d_0 from received signal vectors $\mathbf{r}_p$ (p = 1, 2) in the presence of unknown jamming components ξ and $\mathbf{v}$ as well as independent receiver noise $\mathbf{w}_p$ (p = 1, 2).

As described in Appendix B, using the available channel estimates of the desired signal $\hat{\alpha}_p, p = 1,2$, a simple beamforming structure with weighting vector $\mathbf{g} = \left[\hat{\alpha}_2 \quad -\hat{\alpha}_1 \right]^T$ can be employed to place a null toward the desired signal. Deploying the technique in [21], the onset of the jamming signal can be detected by determining the time when a significant increase in the output signal power has occurred. Based on the detected jammed or unjammed status of the system, an appropriate algorithm can be employed for subsequent jamming rejection and symbol detection. In particular, the unjammed symbols are detected by using the conventional ML technique, while the jammed symbols can be detected by the proposed approach which will be described in details in Section 2.3.

2.3 ML-Based Joint Jamming Rejection and Symbol Detection

In this section, a ML-based joint interference rejection and detection scheme is formulated to effectively suppress the received jamming components. Noting that the jamming components from the two antenna elements are spatially correlated through some unknown coefficients ξ, the vector of jamming components **v** and ξ will be treated as deterministic quantities to be estimated by the ML technique. This approach is different from the conventional one, where the jamming components are simply regarded as receiver noise.

Since MFSK modulation is employed, the desired symbol d_0 is given by only one of the alphabet {0, 1, … , M–1}. A joint ML estimation of d_0, ξ and **v** can thus be expressed as

$$\hat{\xi}, \hat{\mathbf{v}}, \hat{d}_0 = \arg \min_{\xi, \mathbf{v}, d} \left\{ \left\| \mathbf{r}_1 - \alpha_1 \mathbf{s}(d) - \mathbf{v} \right\|^2 + \left\| \mathbf{r}_2 - \alpha_2 \mathbf{s}(d) - \xi \mathbf{v} \right\|^2 \right\}, \tag{2.9}$$

where $d \in \{0,1,...,M-1\}$ is the candidate symbol to be searched in the ML cost function.

For convenience, let us define

$$\mathbf{z}_p(d) = \mathbf{r}_p - \alpha_p \mathbf{s}(d), \text{ for } p = 1, 2, \tag{2.10}$$

so that the cost function in (2.9) becomes

$$\Gamma(d) = \left\| \mathbf{z}_1(d) - \mathbf{v} \right\|^2 + \left\| \mathbf{z}_2(d) - \xi \mathbf{v} \right\|^2 . \tag{2.11}$$

Differentiating the cost function $\mathbf{\Gamma}(d)$ with respect to **v** and ξ, respectively, and setting the results to zero, we obtain

$$\mathbf{v} = \frac{\mathbf{z}_1(d) + \xi^* \mathbf{z}_2(d)}{1 + |\xi|^2}, \tag{2.12}$$

and

$$\xi = \frac{\mathbf{v}^H \mathbf{z}_2(d)}{\|\mathbf{v}\|^2}. \tag{2.13}$$

Substituting (2.12) into (2.11) yields

$$\Gamma(d) = \frac{\|\mathbf{z}_2(d) - \xi \mathbf{z}_1(d)\|^2}{1 + |\xi|^2}, \tag{2.14}$$

and by substituting (2.12) into (2.13), we get

$$a(d)\xi^2 + b(d)\xi - a^*(d) = 0, \tag{2.15}$$

where

$$a(d) = \mathbf{z}_2^H(d)\mathbf{z}_1(d), \tag{2.16}$$

and

$$b(d) = \|\mathbf{z}_1(d)\|^2 - \|\mathbf{z}_2(d)\|^2. \tag{2.17}$$

As a result, the closed-form expressions for the ML estimates of ξ which are the solutions to (2.15) can be determined by

$$\xi_1(d) = \frac{-b(d) - \sqrt{b^2(d) + 4|a(d)|^2}}{2a(d)}, \tag{2.18}$$

and

$$\xi_2(d) = \frac{-b(d) + \sqrt{b^2(d) + 4|a(d)|^2}}{2a(d)}. \tag{2.19}$$

In accordance with (2.9), (2.14), (2.18) and (2.19), an ML estimate of the transmitted symbol d_0 is therefore

$$\hat{d}_0 = \arg\min_d \{\Gamma_1(d), \Gamma_2(d); d = 0,1..., M-1\}, \tag{2.20}$$

where

$$\Gamma_i(d) = \frac{\|\mathbf{z}_2(d) - \xi_i(d)\mathbf{z}_1(d)\|^2}{1 + |\xi_i(d)|^2}, \text{ for } i = 1, 2. \tag{2.21}$$

Equations (2.18) and (2.19) indicate that there are two possible estimates of ξ for a fixed value of *d*. Consequently, in accordance with (2.20), it seems that we have to calculate the two cost functions $\Gamma_1(d)$ and $\Gamma_2(d)$ corresponding to a fixed *d* for the purpose of estimating the desired symbol. Fortunately, as shown in Appendix C, $\Gamma_2(d)$ is always smaller than $\Gamma_1(d)$ for a fixed value of *d*. Therefore, it is sufficient to just compute the cost function $\Gamma_2(d)$ corresponding to $\xi_2(d)$ in (2.19). As a result, the decision rule of (2.20) can be simplified to be given by

$$\hat{d}_0 = \arg\min_d \{\Gamma_2(d); d = 0,1...,M-1\}. \tag{2.22}$$

The detailed procedure for implementing the proposed ML-based interference rejection and detection algorithm can be summarized as follows:

1. initialize the candidate symbol $d = 0$;
2. calculate both $\mathbf{z}_1(d)$ and $\mathbf{z}_2(d)$ based on (2.5), (2.8), (2.10) as well as knowledge of α_1 and α_2 (by using blind ML estimation in Appendix A);
3. compute both $a(d)$ and $b(d)$ using (2.16) and (2.17);
4. calculate $\xi_2(d)$ using (2.19);
5. compute $\Gamma_2(d)$ based on (2.21);
6. if $d = M-1$, go to Step 7; otherwise $d = d+1$ and return to Step 2;
7. obtain the ML estimate of the transmitted symbol $\hat{d}_0$ based on (2.22).

The computational burden of the proposed algorithm is mainly due to Steps 2, 3 and 5, since only these three steps involve vector operations. The numbers of real addition and real multiplication used in these steps are shown in Table 2.1. It is easy to see that the computational complexity of the proposed algorithm is O(*NM*) in terms of the number of real additions and multiplications needed.

Note that the proposed algorithm and structure is based on the use of two receive

antennas to remove unknown but spatially correlated jamming. With a single antenna, it will not be possible to remove the jamming, which is in the same frequency band as the signal. The use of more than two antennas will lead to better performance if there is only a single jammer. However, the cost may be significantly larger in terms of the space needed and the additional receiving electronics, especially in a mobile application where space and power supply is restricted.

Table 2.1: Computational complexity of the proposed algorithm.

Step	Number of real addition	Number of real multiplication
2	$8NM$	$8NM$
3	$8NM$ -$3M$	$8NM$
5	$6NM$+M	$6NM$+$3M$

2.4 Performance analysis

In the section, an approximate expression for the symbol error rate (SER) of the proposed ML-based joint jamming rejection and symbol detection scheme is derived. For the sake of simplicity, we consider only BFSK signaling over a jamming dominant channel, noting that the case for M-ary signaling can be similarly analyzed.

Taking the two possible BFSK symbols to be equiprobable, using the decision rule of (2.22), and assuming, without loss of generality, that the transmitted symbol value is $d_0 = 0$, the SER can be easily shown to be

$$P_e = \Pr\{f(0) > f(1)\}, \tag{2.23}$$

where the two conditional cost functions $f(0)$ and $f(1)$ are given by

$$f(m) = \Gamma_2(d = m)\big|_{d_0 = 0}, m = 0,1. \tag{2.24}$$

Similarly, the resulting input signal vectors now become

$$\mathbf{r}_1 = \alpha_1 \mathbf{s}(0) + \mathbf{v} + \mathbf{w}_1 , \tag{2.25}$$

and

$$\mathbf{r}_2 = \alpha_2 \mathbf{s}(0) + \xi \mathbf{v} + \mathbf{w}_2 . \tag{2.26}$$

Using (2.10), (2.21), (2.24), (2.25) and (2.26), the conditional cost function $f(0)$ can be determined by

$$f(0) = \frac{\left\| \xi \mathbf{v} + \mathbf{w}_2 - \xi_2^+(0)(\mathbf{v} + \mathbf{w}_1) \right\|^2}{1 + \left| \xi_2^+(0) \right|^2} , \tag{2.27}$$

where

$$\xi_2^+(0) \equiv \xi_2(d = 0)\big|_{d_0 = 0}$$

$$= \frac{\left\| \xi \mathbf{v} + \mathbf{w}_2 \right\|^2 - \left\| \mathbf{v} + \mathbf{w}_1 \right\|^2 + \sqrt{\left(\left\| \mathbf{v} + \mathbf{w}_1 \right\|^2 - \left\| \xi \mathbf{v} + \mathbf{w}_2 \right\|^2 \right)^2 + 4 \left| \left[\xi \mathbf{v} + \mathbf{w}_2 \right]^H \left[\mathbf{v} + \mathbf{w}_1 \right] \right|^2}}{2 \left[\xi \mathbf{v} + \mathbf{w}_2 \right]^H \left[\mathbf{v} + \mathbf{w}_1 \right]} . \tag{2.28}$$

After some manipulation and simplification, we have

$$f(0) = \frac{\left\| \xi \mathbf{v} + \mathbf{w}_2 \right\|^2 + \left\| \mathbf{v} + \mathbf{w}_1 \right\|^2 - \chi_0}{2} , \tag{2.29}$$

where $\chi_0 = \sqrt{\left(\left\| \xi \mathbf{v} + \mathbf{w}_2 \right\|^2 - \left\| \mathbf{v} + \mathbf{w}_1 \right\|^2 \right)^2 + 4 \left| \left[\xi \mathbf{v} + \mathbf{w}_2 \right]^H \left[\mathbf{v} + \mathbf{w}_1 \right] \right|^2}$.

Under a severely jammed channel, where the power of the jamming signal is much greater than that of receiver noise $\mathbf{w}_p$ (p = 1, 2), the high order terms with respect to receiver noise $\mathbf{w}_p$ (p = 1, 2) can be omitted in a power series expansion of χ_0. As a result, χ_0 can be approximated by using just the zeroth and first order terms with respect to $\mathbf{w}_1$ and $\mathbf{w}_2$. The conditional cost function $f(0)$ can therefore be approximated by

$$f(0) \approx \frac{\|\xi\mathbf{v}+\mathbf{w}_2\|^2 + \|\mathbf{v}+\mathbf{w}_1\|^2 - \overbrace{\|\mathbf{v}\|^2\left(1+|\xi|^2\right)}^{\text{zeroth order term}} - \overbrace{2\,\mathrm{Re}\left\{\mathbf{w}_2^H\mathbf{v}\xi\right\} - 2\,\mathrm{Re}\left\{\mathbf{w}_1^H\mathbf{v}\right\}}^{\text{first order term}}}{2}. \quad (2.30)$$

Similarly, substituting (2.10), (2.21), (2.25) and (2.26) into (2.24) yields the conditional cost function $f(1)$ as

$$f(1) = \frac{\|\mathbf{s}_2+\xi\mathbf{v}+\mathbf{w}_2\|^2 + \|\mathbf{s}_1+\mathbf{v}+\mathbf{w}_1\|^2 - \chi_1}{2}, \quad (2.31)$$

where $\chi_1 = \sqrt{\left(\|\mathbf{s}_2+\xi\mathbf{v}+\mathbf{w}_2\|^2 - \|\mathbf{s}_1+\mathbf{v}+\mathbf{w}_1\|^2\right)^2 + 4\left|[\mathbf{s}_2+\xi\mathbf{v}+\mathbf{w}_2]^H[\mathbf{s}_1+\mathbf{v}+\mathbf{w}_1]\right|^2}$

and $\mathbf{s}_p = \alpha_p[\mathbf{s}(0)-\mathbf{s}(1)]$ with p =1, 2.

Using a power series expansion of χ_1 and carrying out the same analysis as for χ_0, it can be shown that $f(1)$ can be approximated by

$$f(1) \approx \frac{\|\mathbf{s}_1+\mathbf{v}+\mathbf{w}_1\|^2 + \|\mathbf{s}_2+\xi\mathbf{v}+\mathbf{w}_2\|^2 - \overbrace{\sqrt{q_0}}^{\text{zeroth order term}} - \overbrace{\mathrm{Re}\left\{\mathbf{w}_1^H\frac{\mathbf{q}_1}{2\sqrt{q_0}}\right\} - \mathrm{Re}\left\{\mathbf{w}_2^H\frac{\mathbf{q}_2}{2\sqrt{q_0}}\right\}}^{\text{first order term}}}{2}, \quad (2.32)$$

where $q_0 = \left(\|\mathbf{s}_2+\xi\mathbf{v}\|^2 - \|\mathbf{s}_1+\mathbf{v}\|^2\right)^2 + 4\left|[\mathbf{s}_2+\xi\mathbf{v}]^H[\mathbf{s}_1+\mathbf{v}]\right|^2$,

$\mathbf{q}_1 = 4(\mathbf{s}_1+\mathbf{v})\left(\|\mathbf{s}_1+\mathbf{v}\|^2 - \|\mathbf{s}_2+\xi\mathbf{v}\|^2\right) + 8(\mathbf{s}_2+\xi\mathbf{v})[\mathbf{s}_2+\xi\mathbf{v}]^H[\mathbf{s}_1+\mathbf{v}]$,

and $\mathbf{q}_2 = 4(\mathbf{s}_2+\xi\mathbf{v})\left(\|\mathbf{s}_2+\xi\mathbf{v}\|^2 - \|\mathbf{s}_1+\mathbf{v}\|^2\right) + 8(\mathbf{s}_1+\mathbf{v})[\mathbf{s}_1+\mathbf{v}]^H[\mathbf{s}_2+\xi\mathbf{v}]$.

By substituting (2.30) and (2.32) into (2.23), the SER is thus determined approximately by

$$P_e \approx \Pr\{\Delta > 0\}, \quad (2.33)$$

where

$$\Delta = -\|\mathbf{s}_2+\mathbf{v}\xi\|^2 - \|\mathbf{s}_1+\mathbf{v}\|^2 + \sqrt{q_0} + \mathrm{Re}\left\{\mathbf{w}_2^H\left(\frac{\mathbf{q}_2}{2\sqrt{q_0}} - 2\mathbf{v}\xi - 2\mathbf{s}_2\right)\right\} + \mathrm{Re}\left\{\mathbf{w}_1^H\left(\frac{\mathbf{q}_1}{2\sqrt{q_0}} - 2\mathbf{v} - 2\mathbf{s}_1\right)\right\}.$$

Note that the quantity Δ includes the linear combination of the real and imaginary parts of the independent Gaussian receiver noise samples $w_{p,n}$. As a result, Δ is also Gaussian distributed and its mean μ_Δ and variance σ_Δ^2 can therefore be computed by

$$\mu_\Delta = -\left\|\mathbf{s}_2 + \mathbf{v}\xi\right\|^2 - \left\|\mathbf{s}_1 + \mathbf{v}\right\|^2 + \sqrt{q_0}\,, \tag{2.34}$$

and

$$\sigma_\Delta^2 = \sigma^2\left(\left\|\frac{\mathbf{q}_2}{2\sqrt{q_0}} - 2\mathbf{v}\xi - 2\mathbf{s}_2\right\|^2 + \left\|\frac{\mathbf{q}_1}{2\sqrt{q_0}} - 2\mathbf{v} - 2\mathbf{s}_1\right\|^2\right), \tag{2.35}$$

where σ^2 is the variance of the real and imaginary parts of the zero-mean white Gaussian receiver noise samples $w_{p,n}$.

In accordance with (2.33), (2.34) and (2.35), the SER can be computed approximately by

$$P_e \approx Q\left(-\frac{\mu_\Delta}{\sqrt{\sigma_\Delta^2}}\right), \tag{2.36}$$

where $Q(x) = \frac{1}{\sqrt{2\pi}}\int_x^{+\infty} \exp\left(-\frac{t^2}{2}\right)dt$. It is noted that (2.36) is a conditional error probability, given channel gains of jamming and desired signals.

2.5 Simulation Results and Discussions

Numerical simulations have been conducted to validate the performance of the proposed interference suppression scheme for a slow FH system. In this system, each hop has 4 MFSK symbols, the symbol rate is 200000 symbols per second, and the hop rate is 50000 hops per second. The frequency spacing is 100 kHz. The ratio of the unjammed interval to the hop duration, R_U, is given by 0.025 for all except the last result (Figure 2.5). Channel gains of jamming and desired signals are complex

Gaussian random variables with variance values of 1. The jammer's bandwidth is equal to the bandwidth occupied by the all M data tones in each hop.

Figure 2.1 shows the SER of the proposed scheme versus the signal-to-noise ratio (SNR) when the signal-to-jamming ratio (SJR) is -25dB and -40dB. BFSK modulation is used and the number of samples per symbol is $N = 4$. For comparison, the results of using the conventional beamformer [28] and the SMI-based beamformer are also plotted. As can be seen, the performance of the proposed scheme differs only slightly for the various SJRs used, which is highly desirable in military communications. Also, unlike the conventional beamformer, no error floor exists for the proposed scheme. This is because the latter regards the jamming components as deterministic quantities to be estimated while the conventional beamformer simply treats the jamming components as receiver noise. Furthermore, the proposed scheme is able to offer a better performance than the other methods since it is a ML-based approach.

However, in the unlikely event that $\alpha_p = \beta_p$, as when both signal and jammer are from the same direction or there is no distinction between the signal and the jammer in terms of channel gains, all the algorithms will fail. In fact, since there is no distinction between the signal and the jammer in terms of transmission characteristics and the jamming signal is unknown, it will not be possible for any statistical signal processing algorithm to reject the jamming signal. Similarly, when two jammers are present and both are unknown, it will not be possible for the proposed scheme, the SMI method and other similar techniques to work properly. This is because the array is a two-element one and the presence of two jammers will give rise to an under-determined system where the number of unknown parameters is more than number of the degrees of freedom that the system has.

Figure 2.2 illustrates the performance of the proposed detection scheme under vari-

ous modulation levels. The SJR is -10 dB and the number of samples per symbol is $N = 4$. As observed, the performance of the proposed scheme degrades as the modulation level increases.

Figure 2.3 investigates the performance of the proposed scheme as the number of samples per symbol is changed. BFSK modulation is used and SJR is -10 dB. It can be seen that the proposed scheme has a better performance as the number of samples per symbol is increased. The average conditional error probabilities of the proposed scheme are also plotted in Figure 2.3. The validity of the performance analysis for the proposed scheme is also demonstrated in Figure 2.3 from noting that the SER values from simulation are remarkably close to the corresponding analytical curve.

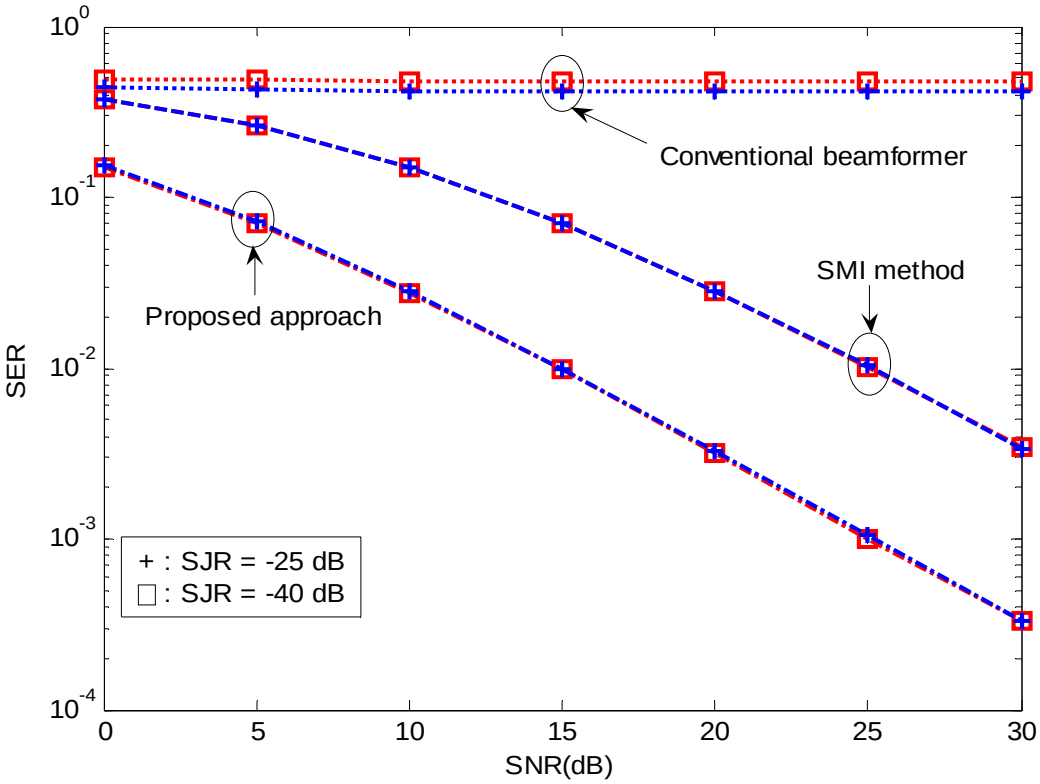

Figure 2.1: Performance of the proposed approach under various SJRs with BFSK modulation and $N = 4$.

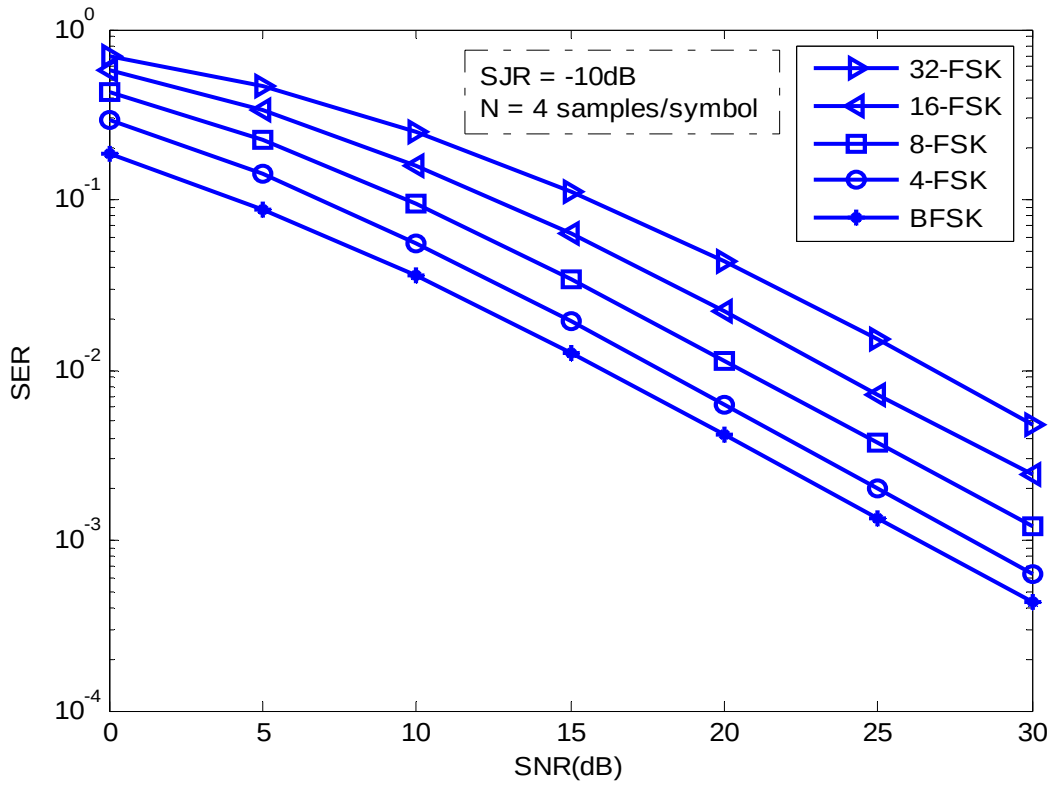

Figure 2.2: Performance of the proposed scheme under various modulation levels and N=4 samples/symbol.

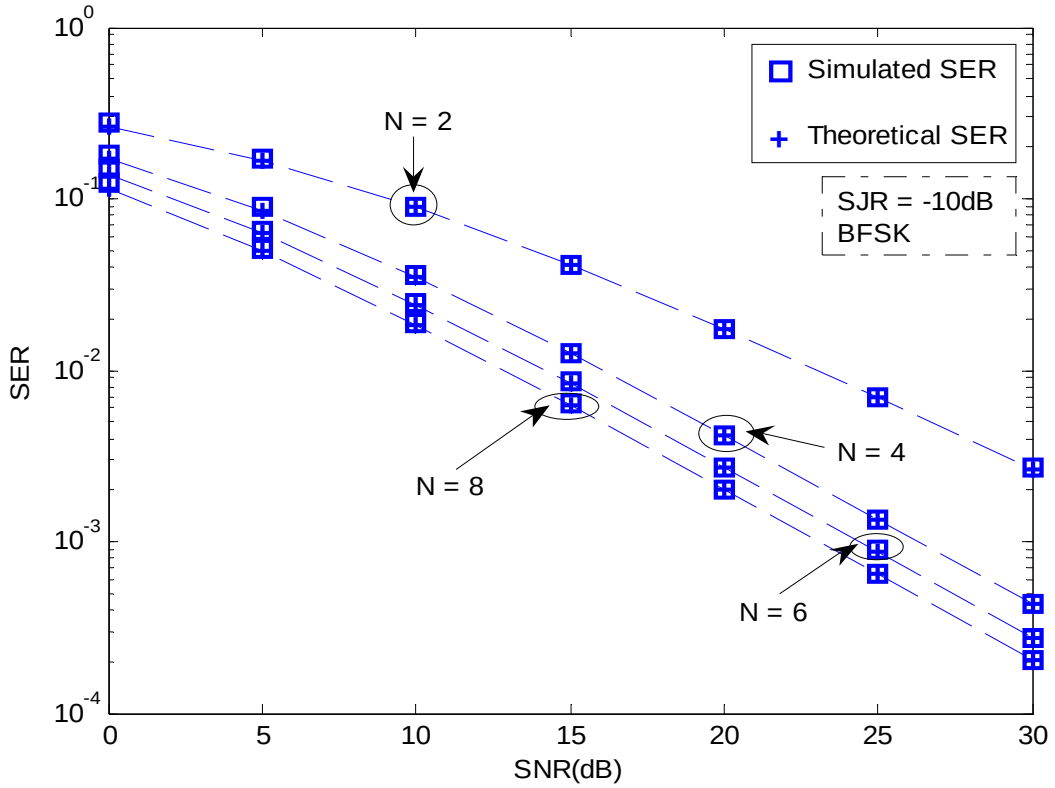

Figure 2.3: Performance of the proposed scheme under various numbers of samples per symbol and the tightness of the theoretical and simulated SER values for BFSK signaling.

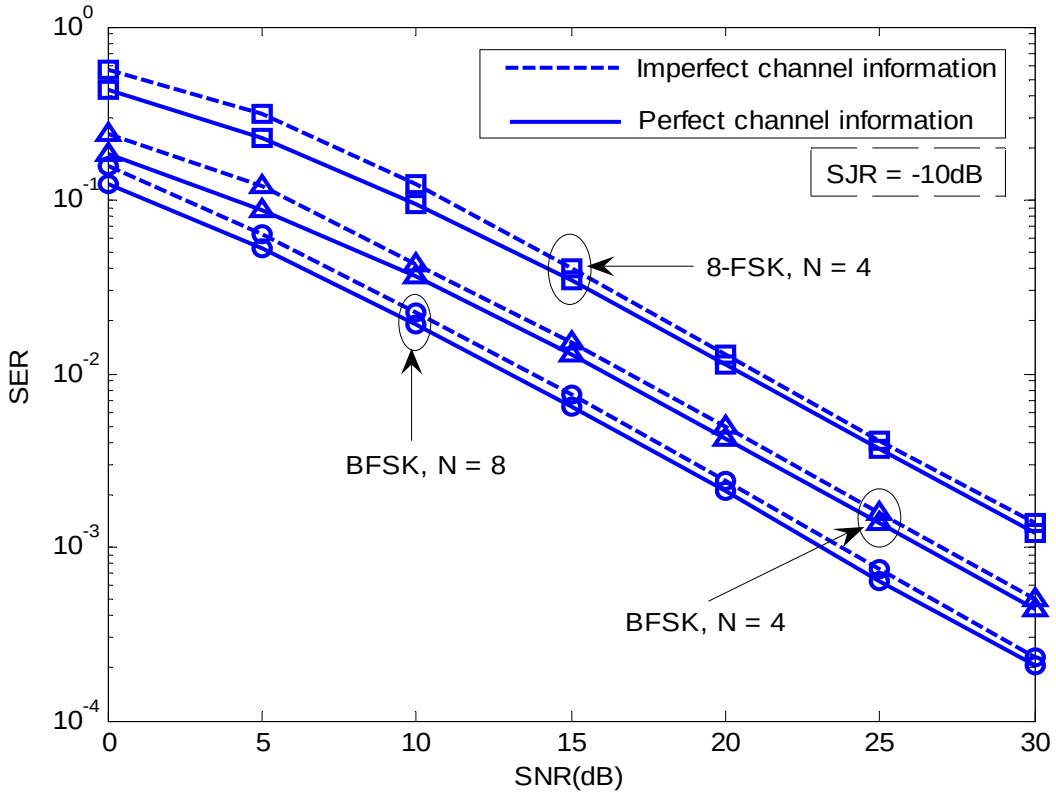

Figure 2.4: Performance of the proposed scheme when the desired signal's channel gains are blindly estimated by using the ML technique in Appendix A within the unjammed interval of a hop.

The results from Figures 2.1, 2.2 and 2.3 have been obtained by assuming perfect channel estimation. To investigate the effect of imperfect channel estimation, Figure 2.4 shows the performance of the proposed scheme with imperfect knowledge of the desired signal's channel gains, blindly estimated by using the ML technique (as described in Appendix A) within the unjammed interval of a hop. Obviously, at SJR=-10dB and using just 4 received samples in a very short unjammed interval of a hop to estimate the channel gains, the resulting SER performance in the case of imperfect channel estimation is very close to that in the case of perfect channel estimation.

Figure 2.5 investigates the timing of the jamming signal on the system performance. The values of R_U used for the three sets of results are 0.025, 0.25 and 0.5, and the results are obtained as follows. The dotted curves are obtained from using 10 samples of the received signals at the beginning of each hop in the ML approach (as described

in Appendix A) to estimate the desired signal's channel response. Then, a simple beamforming structure is employed to place a null toward the desired signal (as described in Appendix B). Using the technique in [21], the onset of jamming can then be detected by determining the time when a significant increase in the signal power at the beamformer's output has occurred.

Based on the detected jammed or unjammed status of the system, detection of the jammed symbols are carried out by the proposed approach, while that for the unjammed symbols are performed by using the conventional ML technique. The curves in Figure 2.5 denote the overall SER results, including the SER performance in both the jammed and unjammed portions of each hop.

As described, the dotted curves in Figure 2.5 are obtained with imperfect channel estimates. On the other hand, the solid curves are based on using the exact channel response of the desired signal. The minor performance degradation between the two

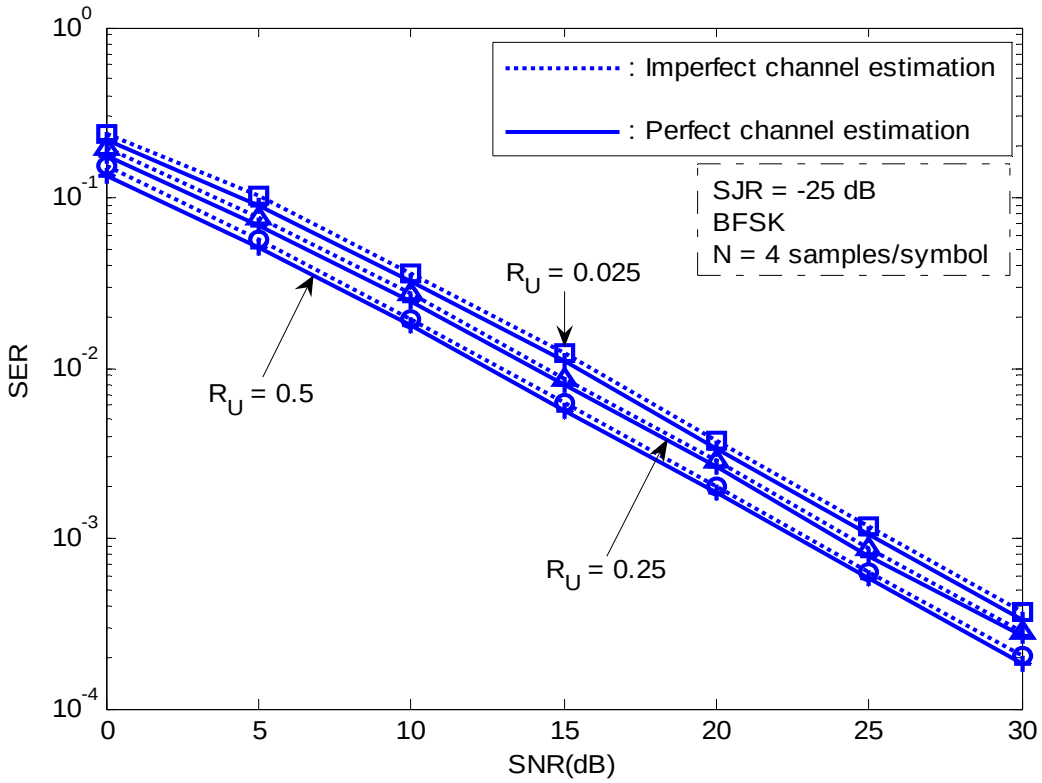

Figure 2.5: Performance of the proposed scheme with various unjammed intervals in a hop.

sets of curves again indicates that the new algorithm does not require very accurate channel information.

The effect of the timing of jamming signal can be studied in more detail by comparing the three sets of results in Figure 2.5, each for a different value of R_U. Note that the lower the value of R_U, the more jammed the hop will be. As can be seen, while an increase in the jamming duration will worsen the SER performance, the use of the new algorithm has the effect that such deterioration becomes rather insignificant.

Finally, Figure 2.6 examines the issue of jamming timing estimation. Specifically, the result is obtained from using the blind ML channel estimation algorithm given in Appendix A to estimate the channel gains of the desired signal, followed by implementing the beamformer in Appendix B to reject the desired signal based on these estimated gains, and then using the algorithm in [21] to detect the onset of jamming.

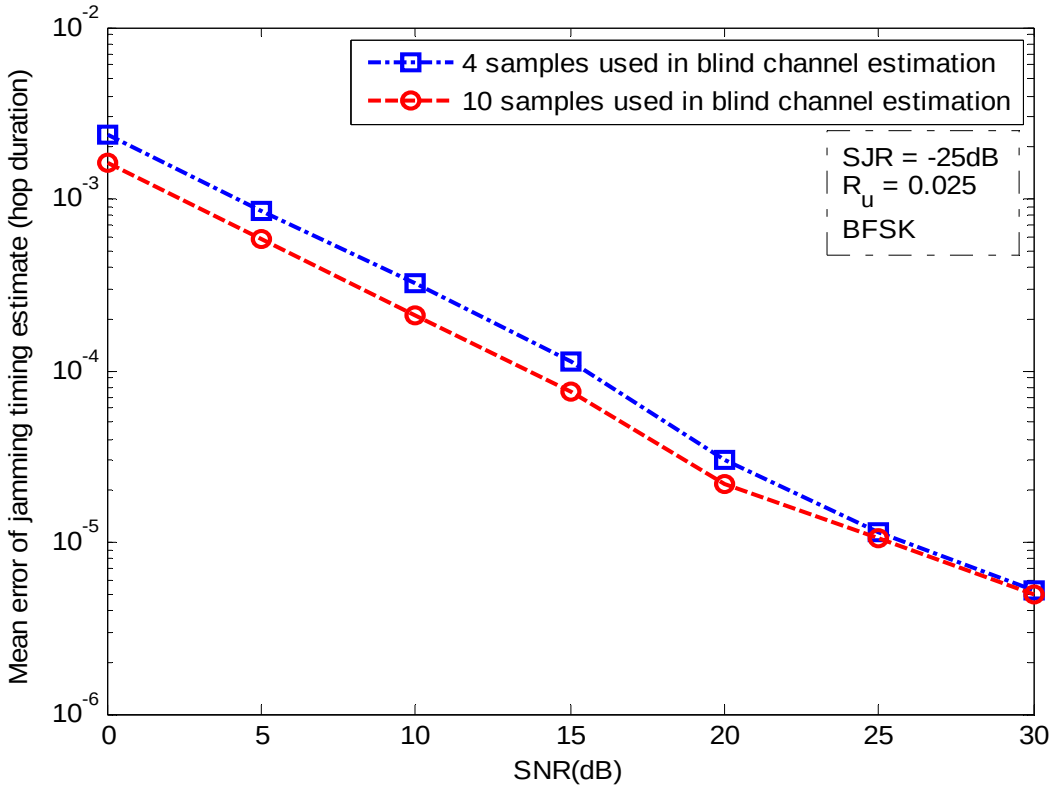

Figure 2.6: Estimation of jamming timing.

The two curves in the figure show how the mean jamming timing estimate error, normalized with respect to the hop duration, changes as a function of SNR when 4 and 10 samples are used in the blind ML channel estimation procedure. As can be seen, using 10 received samples will give a more accurate timing estimation. However, this difference is rather insignificant, especially when the SNR is large. The reason is that we can obtain highly accurate timing estimation with a small number of used samples under high SNR regimes. Also, even with a small number of samples, accurate timing estimate can be quite readily performed under low SNR regimes.

It should also be noted that other mitigation techniques, such as channel coding and interleaving, could also be used for the anti-jamming purpose. In fact, channel coding and interleaving are effective to intermittent jamming, such as a pulsed noise or a partial band jammer. However, even with channel coding and interleaving, the performance of FHSS systems will still deteriorate significantly in the presence of a follower jammer which is on most of the time. On the other hand, the proposed algorithm is able to suppress such a jammer. On the issue of complexity, the proposed algorithm operates only at the receiver and, as discussed in Section 2.3, the implementation complexity is low. Comparatively, channel coding and interleaving techniques need to be used at both the transmitter and receiver, while interleaving will increase delay. Nevertheless, to further enhance performance, an appropriate channel coding and interleaving scheme may be used on top of the proposed algorithm.

2.6 Chapter Summary

In this chapter, a novel maximum likelihood (ML)-based joint interference cancellation and symbol detection scheme was proposed for slow FH/MFSK systems in the presence of a follower partial-band jammer over quasi-static flat Rayleigh fading

channels. Based on unknown spatial correlation of jamming components from two antenna elements, a ML cost function was formulated to jointly perform symbol detection and interference rejection in an integrated ML operation. Based on a derived closed-form expression for the ML estimates of received jamming components, the proposed scheme possesses a low computational complexity. It is robust against imperfect channel estimates, and has a much better SER performance than the conventional beamformer and the SMI method in the presence of a follower partial-band jammer.

Chapter 3

Channel Estimation and Synchronization for SISO-OFDM Systems

Dealing with multipath fading and imperfect synchronization issues in recent broadband wireless communication systems, Chapter 3 focuses on the joint estimation and tracking of channel impulse response, carrier and sampling frequency offsets in *uncoded* SISO-OFDM systems. In particular, this chapter first provides the literature of existing approaches for channel estimation and synchronization in uncoded SISO-OFDM systems. Then, a standard RLS-based joint estimation of CIR, CFO and SFO scheme is proposed for burst mode SISO-OFDM systems over quasi-static multipath fading channels. To further widen the allowable ranges of CFO and SFO values, a ML coarse CFO and SFO estimation is introduced to provide properly initial guesses of CFO and SFO for the iterative joint CIR, CFO and SFO estimation. Finally, simulation results are presented to show a near-optimum BER performance of the proposed scheme.

3.1 Introduction

Orthogonal frequency division multiplexing (OFDM) technique has been employed intensively in various broadband communications systems to exploit its robustness and high spectral efficiency in frequency-selective fading channels. However, along with these potential benefits of multicarrier-based transmissions, the inherent drawback is their vulnerability to synchronization errors such as CFO and SFO. So far, most studies on OFDM systems have considered channel estimation and synchronization

separately [29]-[31]. Channel estimation is performed by assuming that perfect synchronization has been established [32]-[33], although channel estimation could be degraded by imperfect synchronization and vice versa. Since synchronization and channel estimation are mutually related, joint channel estimation and synchronization could provide better accuracy at the cost of higher complexity. A few joint channel estimation and synchronization techniques have been recently proposed in [34]-[37]. However, the SFO is assumed to be zero in [34]-[35], while the CFO is excluded in [36]. In [37], both CFO and SFO are considered in a joint synchronization and channel estimation scheme performed in the time domain (TD) to reduce the number of channel coefficients to be estimated. The TD joint estimation of channel distortion, CFO and SFO parameters requires the TD version of the recovered signals for adaptive computation, and hence, needs an IFFT block, which is equivalent to an OFDM modulator [37]. To reduce complexity, it is desired to avoid this IFFT by performing the joint estimation of CFO, SFO and channel response in the frequency domain (FD). In addition, the TD joint estimation approach [37] may result in significant instability in terms of considerable ripple/fluctuation in the mean squared error (MSE) of CFO and SFO estimates due to the possibility of error propagation under decision-directed operation mode [37]. To avoid such instability in CFO and SFO estimation, a pilot-aided estimation approach using FD observations would be an appropriate candidate. However, CFO and SFO introduce rotations in the time domain, which in turn yield large inter-carrier interference (ICI) in the frequency domain, and hence greatly degrade the FD estimation performance. Therefore, ICI reduction is required before performing a pilot-aided estimation of CIR, CFO and SFO with FD observations.

In this chapter, we propose a pilot-aided joint channel estimation and synchroniza-

tion scheme that eliminates the need for an IFFT block [37] without sacrificing performance and convergence speed. To achieve fast convergence and high performance, we develop a cost function of the SFO, CFO and CIR coefficients based on the received signal samples and pilot tones in the frequency domain. An accompanying recursive least square (RLS) estimation and tracking algorithm is then formulated. Since the number of CIR coefficients that need to be estimated is smaller than when the channel transfer function is used, the algorithm has low complexity. Through formulating and analyzing the ICI introduced by rotation due to CFO and SFO, a TD CFO and SFO compensation scheme is introduced to eliminate the ICI in FD. In addition, a simple maximum-likelihood (ML) scheme based on the preamble is developed for coarse estimation of initial CFO and SFO values to be used in the suppression of dominant ICI effects and in fine RLS estimation and tracking.

The rest of the chapter is organized as follows. Section 3.2 describes the system model and analyzes the effects of CFO, SFO and channel distortion. Based on these results, an ICI reduction technique is introduced in Section 3.3 along with an analysis of the residual ICI to illustrate the feasibility of joint channel estimation and synchronization in the frequency domain. Section 3.4 presents the derivations and development of the RLS-based joint channel estimation and synchronization algorithm. Section 3.5 derives the ML scheme based on the preamble for the coarse estimation of the initial CFO and SFO. Simulation results for various conditions and schemes in both AWGN and Rayleigh multipath fading channels along with Cramer-Rao lower bounds (CRLB) are presented and discussed in Section 3.6. Finally, Section 3.7 summarizes this chapter.

3.2 System Model

Figure 3.1 shows a simplified block diagram of an OFDM transmitter using M-ary modulation (e.g., M-QAM). The serial-to-parallel converter (S/P) groups the input bit stream into a sequence of *Q*-bit tuples, $\{\mathbf{d}_{m,k}\}$, where $\mathbf{d}_{m,k} = [d_{m,k,q}, q = 0,1,...,Q-1]$ and $Q = \log_2 M$ bits, and maps each *Q*-bit tuple, $\mathbf{d}_{m,k}$, to a complex-valued symbol, $X_m(k) \in \mathbf{A}$ where **A** is the M-ary modulation signaling set, and *m*, *k* denote the OFDM symbol and subcarrier indices, respectively. Each OFDM symbol consists of $K<N$ information bearing sub-carriers, where *N* is FFT size. After cyclic prefix (CP) insertion and D/A converter, the transmitted baseband signal can be represented as

$$s(t) = \frac{1}{N} \sum_{m=-\infty}^{+\infty} \sum_{k=-K/2}^{K/2-1} X_m(k) e^{j\frac{2\pi k}{NT}(t-T_g-mT_s)} U(t-mT_s) \qquad (3.1)$$

where *T* is the sampling period at the output of IFFT, N_g denotes the number of CP samples, $T_s = (N+N_g)T$ and $T_g = N_g T$ are the OFDM symbol length after CP insertion and CP length, respectively. $u(t)$ is the unit step function, and $U(t) = u(t) - u(t-T_s)$.

In burst-mode transmissions, the OFDM signal is assumed to be transmitted over a time-invariant multi-path fading channel within one burst duration. Specifically, the quasi-static channel response can be represented by

$$h(\tau) = \sum_{l=0}^{L-1} \tilde{h}_l \delta(\tau - \tau_l), \qquad (3.2)$$

where $\tilde{h}_l$ are the complex path gains and *L* is the total number of resolvable (effecti-ve) paths.

Frequency differences between oscillators used in the radio transmitter and receivers, and channel-induced Doppler shifts cause a *net* carrier frequency offset

(CFO) of Δf in the received signal where f is the operating radio carrier frequency. In the presence of the net CFO Δf, the received signal can be determined by

$$r(t) = e^{j2\pi\Delta ft}\sum_{l=0}^{L-1}\tilde{h}_l s(t-\tau_l) + w(t). \tag{3.3}$$

At the receiver, the received signal is sampled at rate 1/*T'*. Since *T'*≠*T*, the received samples are also affected by SFO. After sampling the received signal $r(t)$ at time instant $t_n = nT'$ (due to SFO) and CP removal, the *n*-th received sample of the *m*-th OFDM symbol in the time-domain is determined by

$$r_{m,n} = \frac{e^{j\frac{2\pi}{N}(N_m+n)\varepsilon_\eta}}{N}\sum_{k=-K/2}^{K/2-1} X_m(k)H(k)e^{j\frac{2\pi k}{N}n(1+\eta)}e^{j\frac{2\pi k}{N}\eta N_m} + w_{m,n}, \tag{3.4}$$

where $n = 0,1,...,N-1$ and $N_m = N_g + m(N+N_g)$. The complex-valued Gaussian noise sample, $w_{m,n}$, has zero mean and variance of σ^2. $H(k) = \sum_{l=0}^{L-1} h_l e^{-j\frac{2\pi k}{N}l}$ is the channel response at the *k*-th sub-carrier and $\mathbf{h} = [h_0 \;\; h_1 \;\cdots\; h_{L-1}]^T$ is the corresponding effective channel impulse response (CIR) that incorporates path-delay induced phase rotation at receiver side. To completely remove the inter-symbol interference (ISI), the CP must be longer than the channel spread, *L*. The SFO and CFO terms are represented in terms of the transmit sampling period *T* as $\eta = \Delta T/T$, $\Delta T = T' - T$ and $\varepsilon = \Delta fNT = (\Delta f / f)(NTf)$, respectively, and $\varepsilon_\eta = (1+\eta)\varepsilon$. In practice, both relative frequency differences, $\Delta T/T$, and $\Delta f/f$, are within the allowable tolerance, which is typically 10ppm (10E-6) or less. However, since the radio carrier frequency, *f*, is normally much higher than the sampling freque-ncy 1/*T*, the factor *NTf* can make the CFO term ε large while the SFO term satisfies η <<1.

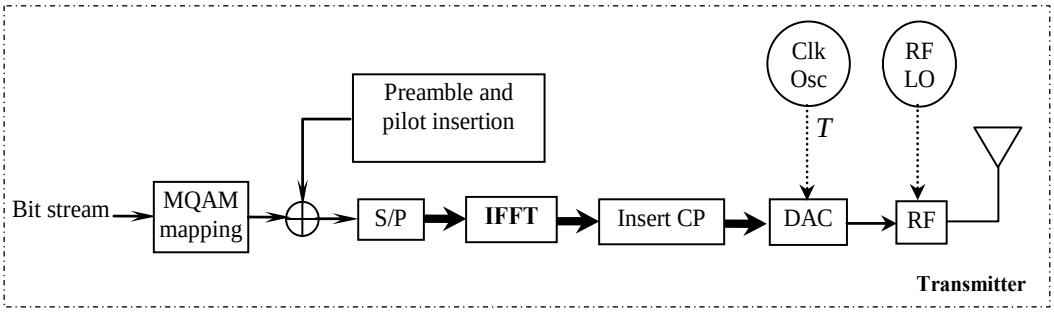

Figure 3.1: Burst-mode OFDM transmitter.

Based on (3.4), the signal to noise ratio (SNR) in the time domain is

$$SNR = \frac{P_S}{P_N}, \tag{3.5}$$

where $P_S = \frac{1}{N^2} E\left\{ \left| \sum_{k=-K/2}^{K/2-1} X_m(k) H(k) e^{j\frac{2\pi k}{N} n(1+\eta)} e^{j\frac{2\pi k}{N} \eta N_m} \right|^2 \right\}$ and $P_N = \sigma^2$.

Assumed that the coefficients of CIR, $\{h_0, h_1, ...h_{L-1}\}$, are independent zero-mean complex random variables, after some manipulations, the SNR can be obtained as

$$SNR = KE\left\{ \left| X_m(k) \right|^2 \right\} E\left\{ \sum_{l=0}^{L-1} \left| h_l \right|^2 \right\} \Big/ N^2 \sigma^2 . \tag{3.6}$$

Unlike traditional FD channel estimation, the CIR $\{h_0, h_1, ...h_{L-1}\}$ in the proposed esti-mation approach is obtained based on the observation of the received sub-carriers in the frequency domain. After FFT, the received FD sample is $Y_m(k) = \sum_{n=0}^{N-1} r_{m,n} e^{-j\frac{2\pi}{N} nk}$. From (3.4), we can derive

$$Y_m(k) = \sum_{i=-K/2}^{K/2-1} X_m(i) H(i) e^{j\frac{2\pi}{N} N_m \varepsilon_i} \rho_{i,k} + W_m(k), \tag{3.7}$$

where $\rho_{i,k} = \frac{1}{N} \sum_{n=0}^{N-1} e^{j\frac{2\pi}{N} n(\varepsilon_i + i - k)} \approx \text{sinc}(\varepsilon_i + i - k) e^{j\pi(\varepsilon_i + i - k)}$ stands for the ICI

coefficient, $\varepsilon_i = i\eta + \varepsilon_\eta$, $\mathrm{sinc}(x) = \frac{\sin(\pi x)}{(\pi x)}$, and $W_m(k) = \sum_{n=0}^{N-1} w(n+N_m) e^{-j\frac{2\pi}{N}nk}$. It is noted that the frequency-domain expression of the received samples in [12, Eq. 37] is an approximation of (3.7). In the first summation in (3.7), the term *i=k* corresponds to the sub-carrier of interest, while the other terms with *i≠k* represent ICI. As can be observed from the above expression for $\rho_{i,k}$, the term, $\varepsilon_i = i\eta + \varepsilon_\eta$, needs to be removed in order to suppress ICI. Obviously, in an *ideal* case with *zero* SFO and CFO, ε_i=0, $\rho_{i,k} = 1$ for $i=k$ and $\rho_{i,k} = 0$ (ICI does not exist) for $i \neq k$. Therefore, $Y_m(k) = X_m(k)H(k) + W_m(k)$ and we have perfect orthogonality among sub-carriers preserved at the receiver. Thus, to mitigate ICI, the effect of CFO and SFO on FD sub-carriers needs to be compensated.

3.3 ICI Reduction by TD CFO-SFO Compensation

As shown in (3.4) and (3.7), the SFO and CFO introduce rotation in the time domain and both attenuation and ICI in the frequency domain. Attenuation can be compensated in a symbol-by-symbol manner. However, removing ICI requires knowledge of all the detected symbols in the frequency domain. Hence, ideally, it is better to remove the rotation in the time domain to prevent ICI in the frequency domain. Based on the derivations to obtain (3.7), it is noted that only the common factor $e^{j\frac{2\pi\varepsilon_\eta n}{N}}$ and individual coefficients $e^{j\frac{2\pi kn\eta}{N}}$ embedded in the summation at (3.4) result in the ICI in (3.7). The common factor can be removed from the received time-domain sample. However, the correction of the individual coefficients requires knowledge of the detected symbols in the frequency domain, and this is not available. Fortunately, the

common factor has a major influence in $\rho_{i,k}$ due to the large CFO term, ε, while the effect of the individual coefficient is minor in $\rho_{i,k}$ since the SFO term satisfies η<<1 in practice. As a result, to suppress the common factor, the received time-domain sample in (3.4) can be multiplied by $e^{-j\frac{2\pi\varepsilon_\eta^c n}{N}}$ prior to FFT as shown in Figure 3.2, where

$$r_{m,n}^c = r_{m,n} e^{-j\frac{2\pi}{N} n\varepsilon_\eta^c}, \tag{3.8}$$

$\varepsilon_\eta^c = (1+\eta^c)\varepsilon^c$, and ε^c and η^c are the estimated CFO and SFO[1], respectively.

After FFT, the resulting FD sub-carrier is

$$Y_m^c(k) = \sum_{n=0}^{N-1} r_{m,n}^c e^{-j\frac{2\pi}{N} nk}. \tag{3.9}$$

After some manipulation, this can be shown to be

$$Y_m^c(k) = \sum_{i=-K/2}^{K/2-1} X_m(i)H(i)e^{j\frac{2\pi}{N} N_m\varepsilon_i} \rho_{i,k}^c + W_m^c(k), \tag{3.10}$$

where $W_m^c(k) = \sum_{n=0}^{N-1} w_m(n+N_m) e^{-j\frac{2\pi}{N} n(1+\eta^c)\varepsilon^c} e^{-j\frac{2\pi}{N} nk}$ and

$\rho_{i,k}^c = \frac{1}{N}\sum_{n=0}^{N-1} e^{j\frac{2\pi}{N} n[i\eta+(1+\eta)\varepsilon-(1+\eta^c)\varepsilon^c+i-k]}$.

Hence, after the TD CFO-SFO compensation, the resulting ICI coefficient becomes

$$\rho_{i,k}^c = \frac{1}{N}\sum_{n=0}^{N-1} e^{j\frac{2\pi}{N} n[i\eta+\varepsilon_\eta-\varepsilon_\eta^c+i-k]}. \tag{3.11}$$

[1] Estimation of CFO and SFO will be discussed in Section 3.4.

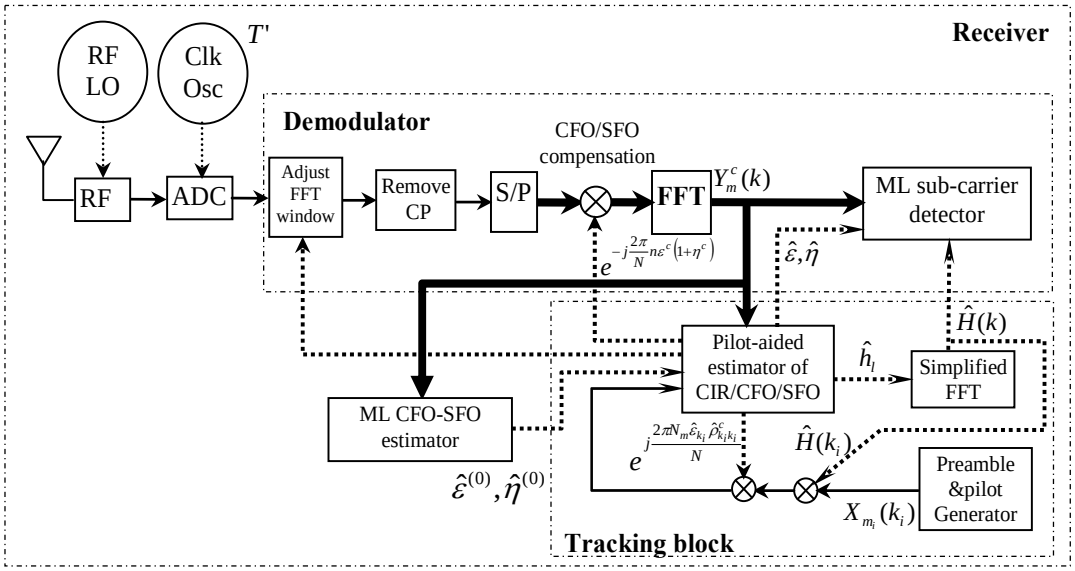

Figure 3.2: Burst-mode OFDM Receiver using joint CIR/CFO/SFO estimation and tracking.

As shown in (3.11), there exists residual ICI due to the term, $i\eta$, even with the use of the TD CFO-SFO compensation with perfect estimates of CFO and SFO ($\varepsilon^c = \varepsilon$ and $\eta^c = \eta$). Fortunately, for practical SFO values, the residual ICI is negligible since $i\eta$ is quite insignificant in contributing to the ICI coefficient, $\rho_{i,k}$, after the TD CFO-SFO compensation.

The residual ICI can be quantified by the ICI-to-signal ratio (ISR) defined as

$$ISR = \frac{P_{ICI}}{P_s}, \tag{3.12}$$

where $P_{ICI} = E\left(\left|\sum_{\substack{i=-K/2 \\ i\neq k}}^{K/2-1} X_m(i)H(i)e^{j\frac{2\pi N_m\varepsilon_i}{N}}\rho^c_{i,k}\right|^2\right)$ and $P_s = E\left(\left|X_m(k)\right|^2\left|H(k)\right|^2\left|\rho^c_{k,k}\right|^2\right)$

After some manipulation, we arrive at

$$ISR = \left(\sum_{k=-K/2}^{K/2-1}\sum_{\substack{i=-K/2 \\ i\neq k}}^{K/2-1}\left|\rho^c_{i,k}\right|^2\right) \Bigg/ \sum_{k=-K/2}^{K/2-1}\left|\rho^c_{k,k}\right|^2 . \tag{3.13}$$

Figure 3.3 shows the "ISR versus SFO (η) and CFO (ε)" plots based on (3.13) for the two cases with and without TD CFO-SFO compensation. *Without* TD CFO-SFO compensation, the solid-line plots in Figure 3.3 indicate that the contributions of SFO and CFO to residual ICI can be approximately represented by $\log(\text{ISR}) \approx a\log(c\eta+\varepsilon)+b$ where a = 2, b = 0.7, and c = 10. In other words, both η and ε contribute to the ICI and η has a dominant effect as compared to ε by about c times. However, as mentioned earlier, $\eta = \Delta T/T$ and $\varepsilon = (\Delta f / f)(NTf)$. Hence, in practice, even if the frequency differences, $\Delta T/T$, and $\Delta f/f$, can be kept within the same allowable tolerance of typically 10ppm (10E-6) or less, the factor NTf is usually larger than 10 and the CFO term, ε, can introduce unacceptably large ICI. *With* the TD CFO-SFO compensation,

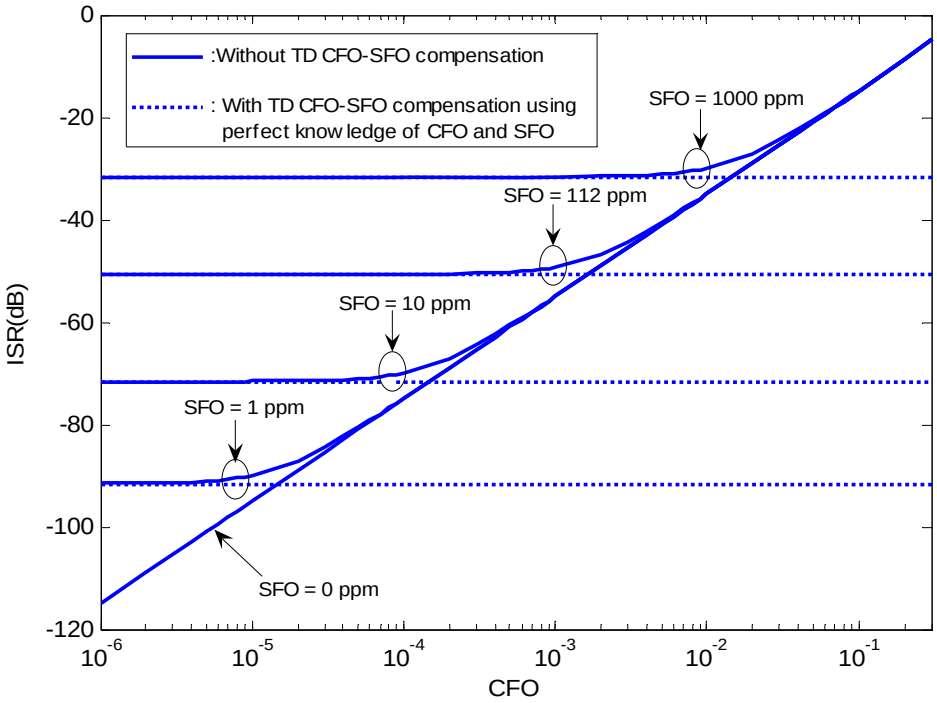

Figure 3.3: ISR versus CFO and SFO.

the dotted-line plots in Figure 3.3 show that the effect of CFO is totally eliminated when $\varepsilon^c = \varepsilon$ and $\eta^c = \eta$, and the contribution of SFO to residual ICI due to the irreducible term, $i\eta$, in $\rho_{i,k}$ of (3.11) can be approximately represented by

log(ISR)≈$a$log($c\eta$)+b. Furthermore, from Figure 3.3, for a typical SFO ($\eta = \Delta T/T$) in the range of 1-10ppm, the residual ICI is negligible with *ISR*<-70dB. The ICI will also affect the receiver performance, especially when its power becomes comparable to that of AWGN. It is obvious that CFO and SFO need to be estimated not only for compensating the CFO-SFO induced attenuation in FD but also for mitigating ICI.

3.4 Joint CIR, CFO and SFO Estimation

Based on the observation of the received sub-carriers in FD (after FFT), the proposed pilot-aided algorithm attempts to estimate CIR, CFO and SFO. To exploit the use of the standard RLS approach [8], we define the LS cost function corresponding to the use of *i* pilot tones over OFDM symbols (each OFDM symbol has 4 pilot tones) in a burst as follows,

$$C\left(\hat{\mathbf{h}}^{(i)}, \hat{\varepsilon}^{(i)}, \hat{\eta}^{(i)}\right) = \sum_{p=1}^{i} \lambda^{i-p} \left| e_{i,p} \right|^2 , \tag{3.14}$$

where λ is called the forgetting factor of the RLS algorithm,

$$\hat{\mathbf{h}}^{(i)} = \left[\hat{h}_0^{(i)}, \hat{h}_1^{(i)}, ... \hat{h}_{L-1}^{(i)}\right]^T , \hat{H}^{(i)}(k_p) = \sum_{l=0}^{L-1} \hat{h}_l^{(i)} e^{-j\frac{2\pi k_p l}{N}} ,$$

$$e_{i,p} = Y_{m_p}^c\left(k_p\right) - X_{m_p}(k_p)\hat{H}^{(i)}(k_p) e^{j\frac{2\pi}{N} N_m \hat{\varepsilon}_{k_p}^{(i)}} \hat{\rho}_{i,k_p,k_p}^c , p = 1,...,i ,$$

$$\hat{\varepsilon}_{k_p}^{(i)} = k_p \hat{\eta}^{(i)} + (1+\hat{\eta}^{(i)})\hat{\varepsilon}^{(i)}, \qquad \hat{\rho}_{i,k_p,k_p}^c = \frac{1}{N}\sum_{n=0}^{N-1} e^{j\frac{2\pi}{N} n\left[k_p \hat{\eta}^{(i)} + (1+\hat{\eta}^{(i)})\hat{\varepsilon}^{(i)} - (1+\eta^c)\varepsilon^c\right]}, \quad \text{the}$$

index *i* denotes the number of pilot tones used for the RLS estimation from the first iteration to the *i*-th iteration (the *current* iteration). In fact, each pilot tone corresponds to one iteration of the RLS estimation. $X_{m_p}\left(k_p\right)$ is the value of the *p*-th pilot tone (at sub-carrier k_p of the m_p^{th} OFDM symbol) used at the *p*-th iteration (a *past* iteration)

in the RLS-based estimation. It is noted that all tones are employed as pilot ones in the preamble of a burst.

To make use of the standard RLS approach [8] for estimating the unknown CIR, CFO, SFO, the non-linear estimation error, $e_{i,p}$, needs to be linearized about the existing estimates by using the following first-order Taylor's series approximation:

$$e_{i,p} \approx Y_{m_p}^c(k_p) - \left\{ f\left(X_{m_p}(k_p), \hat{\boldsymbol{\omega}}_{i-1}\right) + \nabla f^T\left(X_{m_p}(k_p), \hat{\boldsymbol{\omega}}_{i-1}\right)\left(\hat{\boldsymbol{\omega}}_i - \hat{\boldsymbol{\omega}}_{i-1}\right)\right\}, \quad (3.15)$$

where

$f\left(X_{m_p}(k_p), \hat{\boldsymbol{\omega}}_{i-1}\right) = X_{m_p}(k_p)\hat{H}^{(i-1)}(k_p)e^{j\frac{2\pi}{N}N_m\hat{\varepsilon}_{k_p}^{(i-1)}}\hat{\rho}_{i-1,k_p,k_p}^c$ and

$\hat{\boldsymbol{\omega}}_i = \left[\hat{\omega}_{i,0}, \hat{\omega}_{i,1}, ..., \hat{\omega}_{i,2L+1}\right]^T$ is the $(2L+2)\times 1$ weight vector that contains the CIR, CFO and SFO estimates at the i-th iteration of the RLS approach, i.e., $\hat{\omega}_{i,l} = \mathrm{Re}\left\{\hat{h}_l^{(i)}\right\}$,

$\hat{\omega}_{i,l+L} = \mathrm{Im}\left\{\hat{h}_l^{(i)}\right\}$, $l = 0,1,...,(L-1)$, $\hat{\omega}_{i,2L} = \hat{\varepsilon}^{(i)}$ and $\hat{\omega}_{i,2L+1} = \hat{\eta}^{(i)}$.

The gradient vector can be determined by

$$\nabla f\left(X_{m_p}(k_p), \hat{\boldsymbol{\omega}}_i\right) = \left[\frac{\partial f\left(X_{m_p}(k_p), \hat{\boldsymbol{\omega}}_i\right)}{\partial \hat{\omega}_{i,0}}, ..., \frac{\partial f\left(X_{m_p}(k_p), \hat{\boldsymbol{\omega}}_i\right)}{\partial \hat{\omega}_{i,2L+1}}\right]^T, \quad (3.16)$$

where $\dfrac{\partial f\left(X_{m_p}(k_p), \hat{\boldsymbol{\omega}}_i\right)}{\partial \hat{\omega}_{i,l}} = X_{m_p}(k_p)e^{-j\frac{2\pi l k_p}{N}}e^{j\frac{2\pi}{N}N_m\hat{\varepsilon}_{k_p}^{(i)}}\hat{\rho}_{i,k_p,k_p}^c$,

$$\frac{\partial f\left(X_{m_p}(k_p), \hat{\boldsymbol{\omega}}_i\right)}{\partial \hat{\omega}_{i,l+L}} = j\frac{\partial f\left(X_{m_p}(k_p), \hat{\boldsymbol{\omega}}_i\right)}{\partial \hat{\omega}_{i,l}}, \text{with } l = 0,...,L-1,$$

$$\frac{\partial f\left(X_{m_p}(k_p), \hat{\boldsymbol{\omega}}_i\right)}{\partial \hat{\omega}_{i,2L}} = \left(1+\hat{\eta}^{(i)}\right)\Omega_{i,p}, \quad \frac{\partial f\left(X_{m_p}(k_p), \hat{\boldsymbol{\omega}}_i\right)}{\partial \hat{\omega}_{i,2L+1}} = \left(k_p + \hat{\varepsilon}^{(i)}\right)\Omega_{i,p}$$

$$\Omega_{i,p} = X_{m_p}(k_p)\hat{H}^{(i)}(k_p)e^{j\frac{2\pi}{N}N_m\hat{\varepsilon}_{k_p}^{(i)}}\left[j\frac{2\pi}{N}N_m\hat{\rho}_{i,k_p,k_p}^c + \frac{1}{N}\sum_{n=0}^{N-1}j\frac{2\pi}{N}ne^{j\frac{2\pi}{N}n\left[\hat{\varepsilon}_{k_p}^{(i)}-\varepsilon_\eta^c\right]}\right].$$

Subsequently, we can formulate the standard RLS-based joint CIR, CFO, SFO estimation algorithm as follows.

Initialization: Select $\hat{\boldsymbol{\omega}}_1$ using the ML CFO-SFO estimation (to be described in Section 3.5) and $\mathbf{P}_1 = \gamma^{-1}\mathbf{I}_{2L+2}$, where γ is the regularization parameter, $\mathbf{I}_{2L+2}$ is the (2*L*+2)×(2*L*+2) identity matrix.

Iterative Procedure:

1) Update the parameters at the *i*-th iteration

$$\mathbf{K}_i = \frac{\mathbf{P}_{i-1}\nabla f^*\left(X_{m_i}(k_i), \hat{\boldsymbol{\omega}}_{i-1}\right)}{\lambda + \nabla f^T\left(X_{m_i}(k_i), \hat{\boldsymbol{\omega}}_{i-1}\right)\mathbf{P}_{i-1}\nabla f^*\left(X_{m_i}(k_i), \hat{\boldsymbol{\omega}}_{i-1}\right)}, \tag{3.17}$$

with λ denoting the forgetting factor.

$$\mathbf{P}_i = \lambda^{-1}\left(\mathbf{P}_{i-1} - \mathbf{K}_i\nabla f^T\left(X_{m_i}(k_i), \hat{\boldsymbol{\omega}}_{i-1}\right)\mathbf{P}_{i-1}\right), \tag{3.18}$$

$$e_i = Y_{m_i}^c(k_i) - f\left(X_{m_i}(k_i), \hat{\boldsymbol{\omega}}_{i-1}\right). \tag{3.19}$$

2) Update estimates at the *i*-th iteration

$$\hat{\boldsymbol{\omega}}_i = \hat{\boldsymbol{\omega}}_{i-1} + e_i\mathbf{K}_i\,. \tag{3.20}$$

It is noted that the use of the RLS-based algorithm gives the joint estimation technique rapid acquisition and low steady-state error. In burst-mode OFDM transmissions, rapid acquisition will enable the estimation technique to function properly with reduced or short preamble length while maintaining a certain minimum error in the estimation.

In the OFDM receiver (Figure 3.2), the CIR, CFO, SFO estimates are updated on a symbol-by-symbol basis for the ML sub-carrier detector, while the tracking block updates the CIR, CFO and SFO estimates in an iteration-by-iteration manner. Moreover, since the number of CIR coefficients is much smaller than the FFT size, a simplified FFT with reduced complexity can be employed to generate channel transfer

function for both the ML sub-carrier detector in the demodulator and reconstruction of the transmitted signal in the tracking block.

Like other iterative estimation techniques, the RLS-based estimation approach also requires appropriate initial guesses of estimated parameters to achieve its proper convergence. For this reason, a simple ML estimator is proposed to obtain coarse estimates of CFO and SFO to be used as initial guesses for estimated parameters in the RLS-based iterative estimation.

3.5 ML CFO and SFO Estimator

Due to the possibility of multiple local minima caused by the non-linearity of the cost function, the initial guesses of estimated parameters for adaptive estimation must fall in a specific vicinity of their actual values. Consequently, large initial errors between the initial guesses and true values would cause the instability of the RLS-based iterative computation. To alleviate such deterioration, we propose a simple ML estimator to obtain coarse estimates of the initial CFO and SFO values after acquisition phase by using the two long training symbols in the preamble.

To obtain a simple ML coarse estimation of CFO and SFO values, it is desirable to decompose the received signal components into two parts. In particular, the first part should only depend on CFO and SFO while the second part, comprising the remaining unknown components (such as CIR, AWGN and ICI), is approximately uncorrelated and Gaussian-distributed. Based on the FD observations corresponding to two long identical training symbols in the preamble, a simple ML coarse CFO and SFO estimation can be obtained by introducing the following term

$$Y(k) \equiv \frac{X_{m_1}(k) Y_{m_1+1}(k)}{X_{m_1+1}(k) Y_{m_1}(k)} = e^{j\frac{2\pi N_S}{N}[k\eta + \varepsilon(1+\eta)]} + E(k), \qquad (3.21)$$

where $N_s = N + N_g$, m_1 and (m_1+1) denote the time indices of the first and second long training symbols in the preamble, respectively. The FD error sample, $E(k)$, can be expressed by

$$E(k) = \frac{X_{m_1}(k)W_{m_1+1}(k) - X_{m_1+1}(k)W_{m_1}(k)e^{j\frac{2\pi N_s}{N}\varepsilon_k}}{X_{m_1+1}(k)X_{m_1}(k)H(k)e^{j\frac{2\pi(N_g+m_1N_s)}{N}\varepsilon_k}\delta_{kk} + X_{m_1+1}(k)W_{m_1}(k)}.$$

The ICI parts are herein absorbed in $W_m(k)$ with $m = m_1$, and (m_1+1), and assumed to be Gaussian distributed [31]. For the sake of simplicity, the FD error sample, $E(k)$, can be approximated to be Gaussian-distributed and uncorrelated with the first part in the righ-hand side of (3.21). This assumption is supported by the measured Gaussian-shape histograms of the real and imaginary parts of $E(k)$ and its measured auto-correlation that is approximately a delta function as shown in Figure 3.4.

As a result, based on the use of the FD received sub-carriers corresponding to two long training symbols, we define the following ML cost function,

$$f(\varepsilon,\eta) = \sum_{k\in I_p}\left|Y(k) - e^{j\frac{2\pi N_s}{N}[k\eta+\varepsilon(1+\eta)]}\right|^2, \qquad (3.22)$$

where I_p is the set of sub-carrier indices of pilot tones in the preamble.

Hence, without using CIR knowledge, the coarse estimates of CFO and SFO can be simply obtained by

$$\hat{\varepsilon},\hat{\eta} = \arg\min_{\varepsilon,\eta}\sum_{k\in I_p}\left|Y(k) - e^{j\frac{2\pi N_s}{N}[k\eta+\varepsilon(1+\eta)]}\right|^2. \qquad (3.23)$$

Based on (3.23), the coarse estimates of CFO and SFO can be obtained by using a two-dimensional search over their practical ranges with given step sizes. The above coarse CFO and SFO estimates are then used as initial guesses of CFO and SFO for

the RLS-based joint CIR, CFO and SFO estimation & tracking (in Section 3.4) while the initial guesses of CIR are obtained by using the RLS scheme and the preamble.

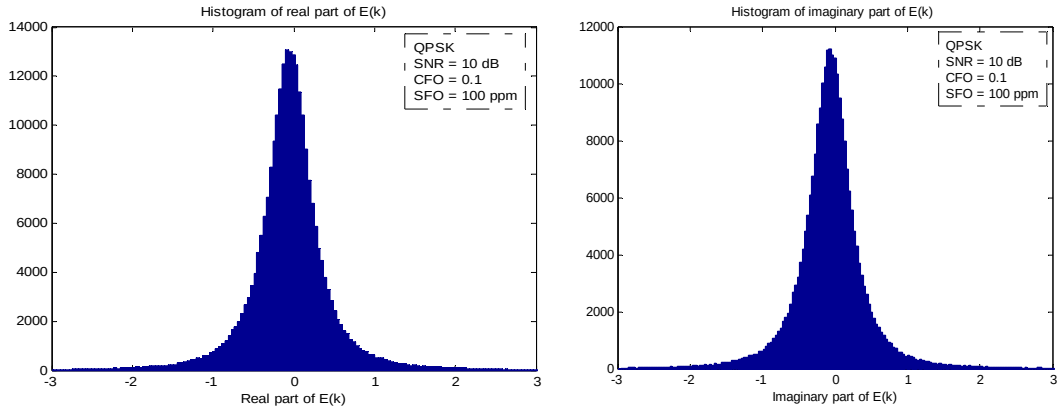

(a) Histograms (probability density functions) of the real and imaginary parts.

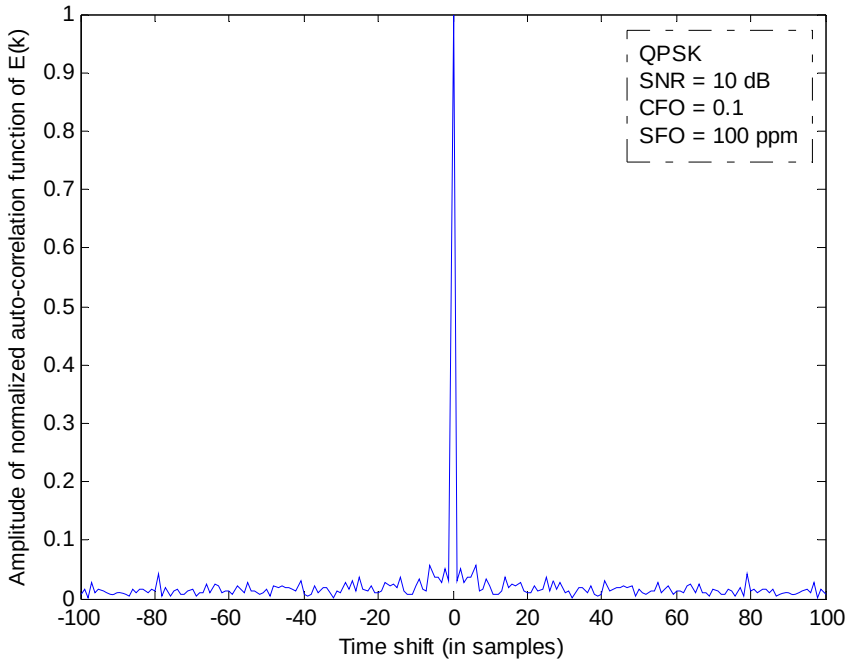

(b) auto-correlation function

Figure 3.4: Probability density and auto-correlation functions of the FD error sample, *E(k)*.

3.6 Simulation Results and Discussions

Computer simulation has been conducted to evaluate the performance of the proposed joint channel estimation and synchronization scheme. We set the OFDM system parameters based on the IEEE 802.11a uncoded systems [38]. Signal constellations of

QPSK, 16-QAM and 64-QAM are employed for OFDM symbols of 48 data sub-carriers and 4 equally spaced pilot tones of the same power. A burst format of two long identical training symbols and 225 data OFDM symbols is used in the simulation. In the joint estimation implementation, to ensure the convergence of acquisition phase for iterative computation of a coarse CIR estimate, the elements of gradient vector corresponding to CFO and SFO parameters are set to zeros in the first long training symbol, and residual CFO values are obtained by correlation-based acquisition phase during the short training symbols in preamble. As an example, we consider an exponentially decaying Rayleigh fading channel with L=5 and a RMS delay spread of 25ns. In the TD CFO-SFO compensator, the terms ε^c and η^c are updated on a symbol-by-symbol basis by using the existing CFO and SFO estimates, respectively. For the coarse CFO and SFO estimation, the step size for searching ML CFO estimate is 0.0001. Due to the actual value of SFO very close to zero, the coarse SFO estimate can be set to zero.

Figure 3.5 shows the simulated mean squared errors[2] (MSE) of the CIR, CFO and SFO estimates and their corresponding CRLB's[3]. It is observed that a forgetting factor smaller than 0.99 results in instability. In addition, the numerical results demonstrate that the proposed estimation algorithm achieves the best performance in term of MSE values with forgetting factor λ=1 and regularization parameter γ = 10. The CRLBs are derived based on an assumption that all 52 data tones (of each OFDM symbol) are used for pilot-aided estimation. For the joint CIR, CFO and SFO estimation in Section 3.6, we only employ 4 pilot tones out of 52 data tones in each OFDM symbol for estimation. As a result, MSE performance gap is large as shown in Figure 3.5.

[2] normalized to the signal power.
[3] See Appendix D for derivations of the CRLB's

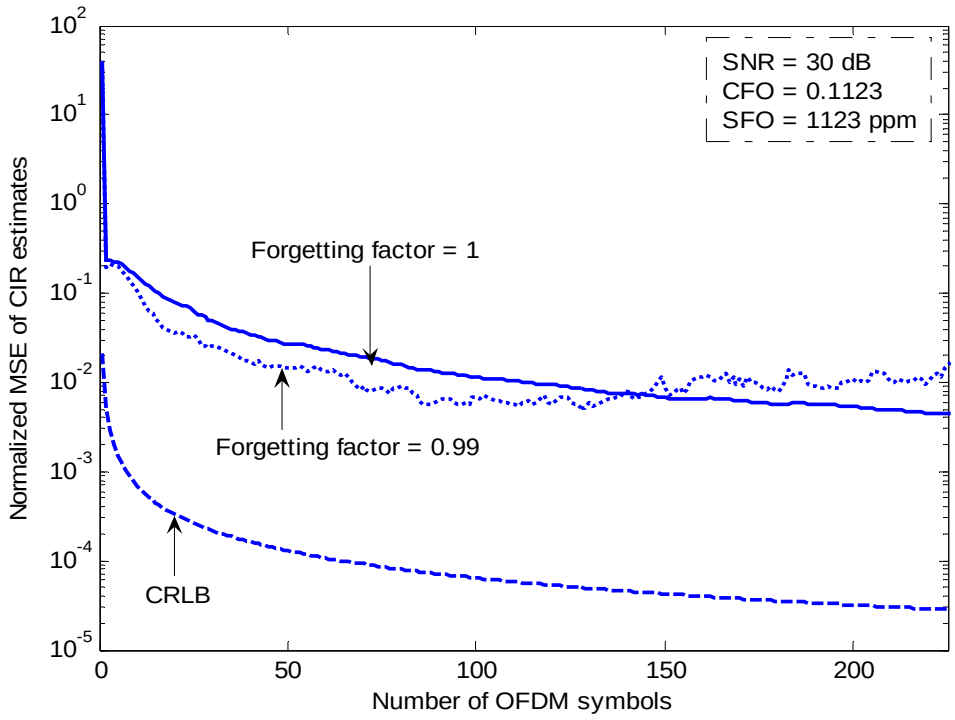

(a) CIR

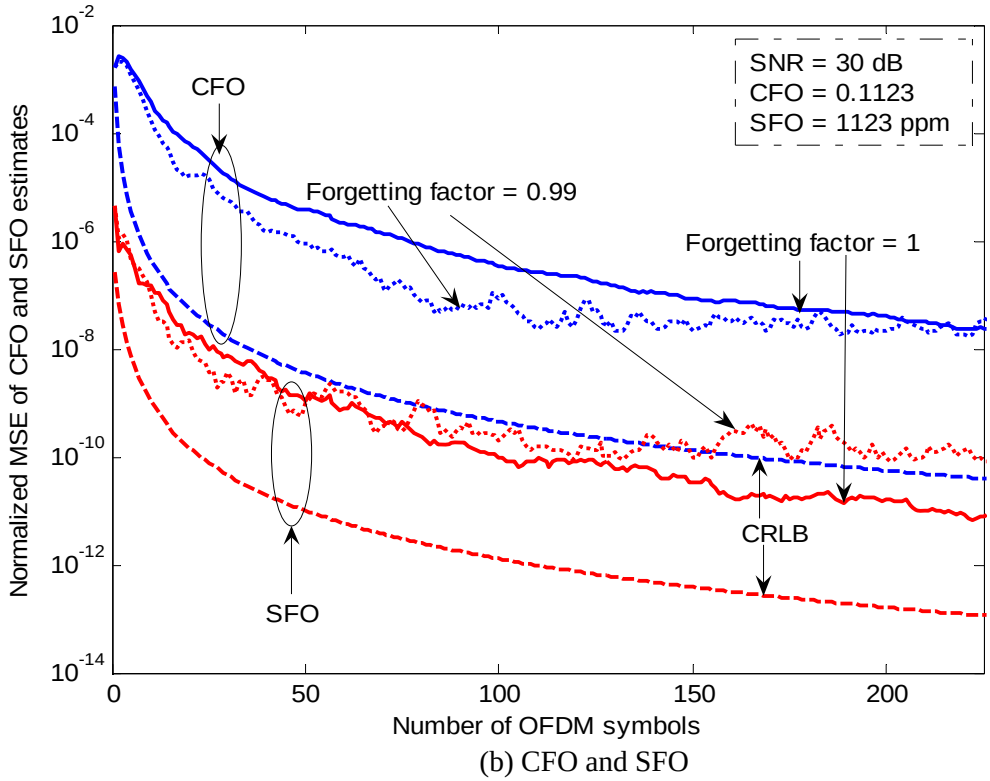

(b) CFO and SFO

Figure 3.5: Normalized MSEs and CRLBs of CIR, CFO and SFO estimates.

As an ultimate performance metric, we investigate the bit error rate (BER) of the OFDM system using ML detection and the proposed estimation algorithm in various

scenarios. In the OFDM receiver, after FFT, the ML criterion is used to detect the transmitted FD data symbol $X_m(k)$ as follows:

$$\hat{X}_m(k) = \arg\min_{X_m(k)} \left\{ \left| Y_m^c(k) - X_m(k)\hat{H}(k)e^{j\frac{2\pi}{N}N_m\hat{\varepsilon}_k}\hat{\rho}_{kk}^c \right|^2 \right\}. \qquad (3.24)$$

Figure 3.6 shows the BER-versus-SNR performance curves in both AWGN (for QPSK) and Rayleigh fading (for QPSK, 16-QAM and 64-QAM) channels. As reference, the *ideal* cases with perfect synchronization (SFO=CFO=0) and channel estimation are included. The *analytical* and *simulation* results for the *ideal* cases are in excellent agreement for both AWGN (Curves H and G in Figure 3.6 (a)) and Rayleigh multipath fading (Curves E and D in Figure 3.6 as well as Curves H and G in Figure 3.6 (b)) channels. To obtain an insight of the contribution of various components of the proposed algorithm, we next consider the case with CFO (ε= 0.212) and SFO (η= 112E-6) in a Rayleigh multipath fading channel.

Without ML CFO-SFO estimator, the performance (A in Figure 3.6(a)) is very bad with unacceptably high BER (about 0.5). This clearly indicates that bad guesses for initial values of SFO and CFO lead to wrong estimates, which in turn yield unacceptable detection error rate. Curve A in Figure 3.6(b) and Curves B in Figure 3.6 show that, *without* ICI reduction, the original ICI is high and becomes a dominant disturbance at high SNR. Hence, at high SNR, even with the use of the ML CFO-SFO estimator in the absence of ICI reduction, the large original ICI is the performance-limiting factor that keeps the BER under QPSK, 16-QAM and 64-QAM constellations at around 1E-2, 1E-1 and 2E-1, respectively.

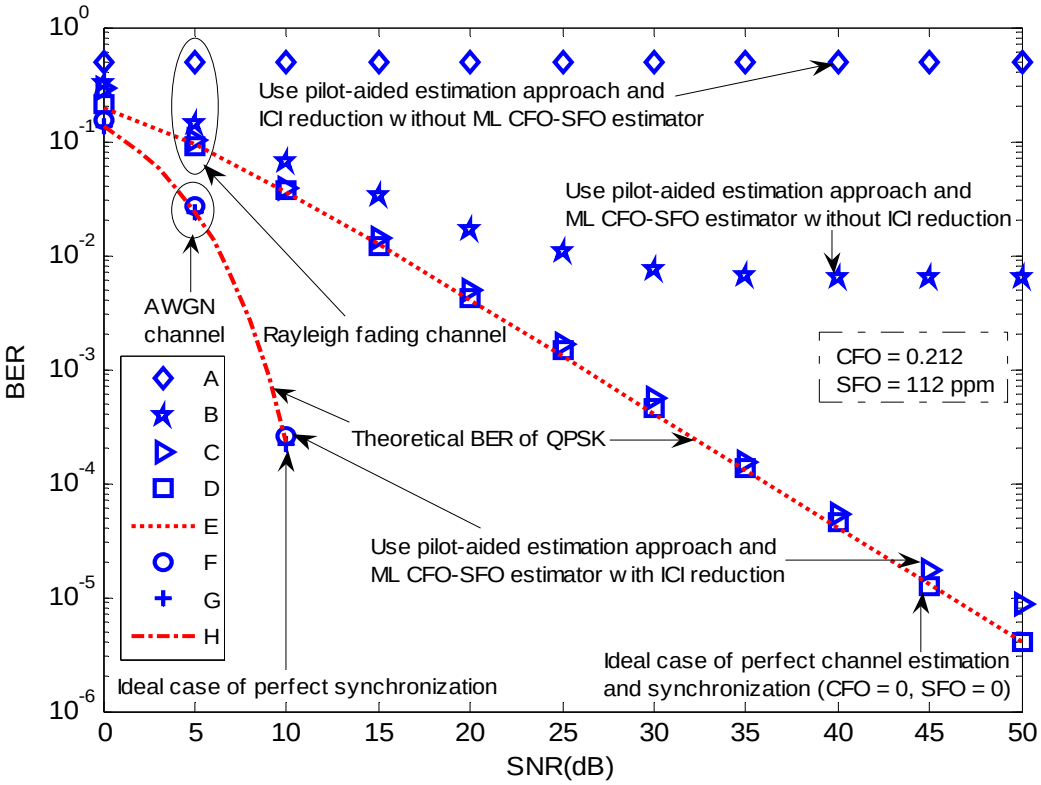

(a) QPSK constellation

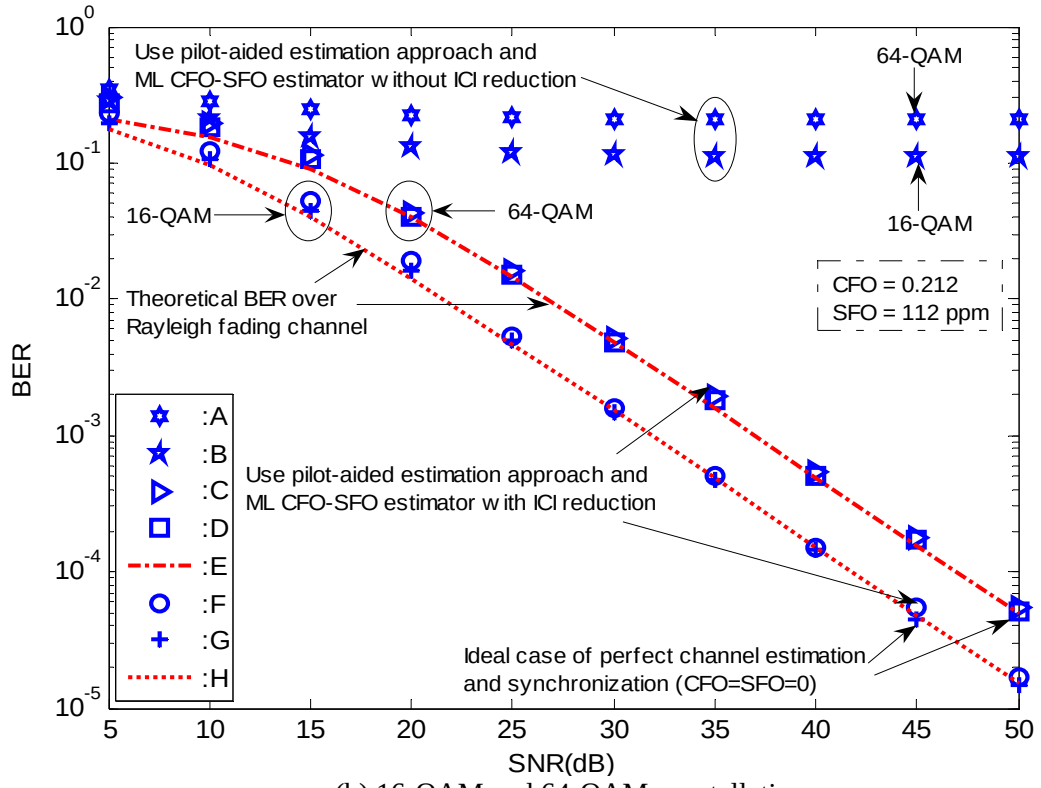

(b) 16-QAM and 64-QAM constellations

Figure 3.6: BER of the ML sub-carrier detector versus SNR with M-QAM constellations over a Rayleigh channel. (CFO=0.212 and SFO=112ppm)

With ML CFO-SFO estimation and ICI reduction, the proposed algorithm provides an excellent performance that approaches the performance in the *ideal* cases (with perfect channel estimation and synchronization) for both AWGN (Curve F in Figure 3.6(a)) and Rayleigh multi-path fading (Curves C in Figure 3.6 and Curve F in Figure 3.6(b)) channels. It indicates the needs for ICI reduction with accurate ML CFO-SFO estimation. The small residual ICI only gives rise to small performance degradation under QPSK constellation at very high SNR around 50dB. For this, we perform further investigations of SFO and CFO values at high SNR of 30dB and 50dB in the Rayleigh multi-path fading channel.

Figure 3.7 shows the BER-versus-CFO (ε) curves. Of course, for the *ideal* case (with perfect channel estimation and synchronization), the reference BER, shown by Curves F (*analytical* results) and E (*simulation* results), is the same over the entire range of CFO values. Curve A confirms that, even with perfect estimates of CIR and SFO, the BER performance is dramatically degraded if CFO effect is neglected at the receiver. Curves B and C show separate contributions of the ICI reduction and ML-CFO-SFO estimation, respectively. They provide a similar performance improvement for small CFO values. As CFO value increases, the ML-CFO-SFO estimation is more effective than the ICI reduction. With both features included, the proposed algorithm offers a performance (Curve D in Figure 3.7(a)) that is extremely close to that for the *ideal* case (with perfect channel estimation and synchronization), even in the presence of large CFO (ε=0.21) and SFO (η=1123ppm). The effects of residual ICI is indicated by a small increase in performance difference between Curves D an F at high SNR=50dB in Figure 3.7(b).

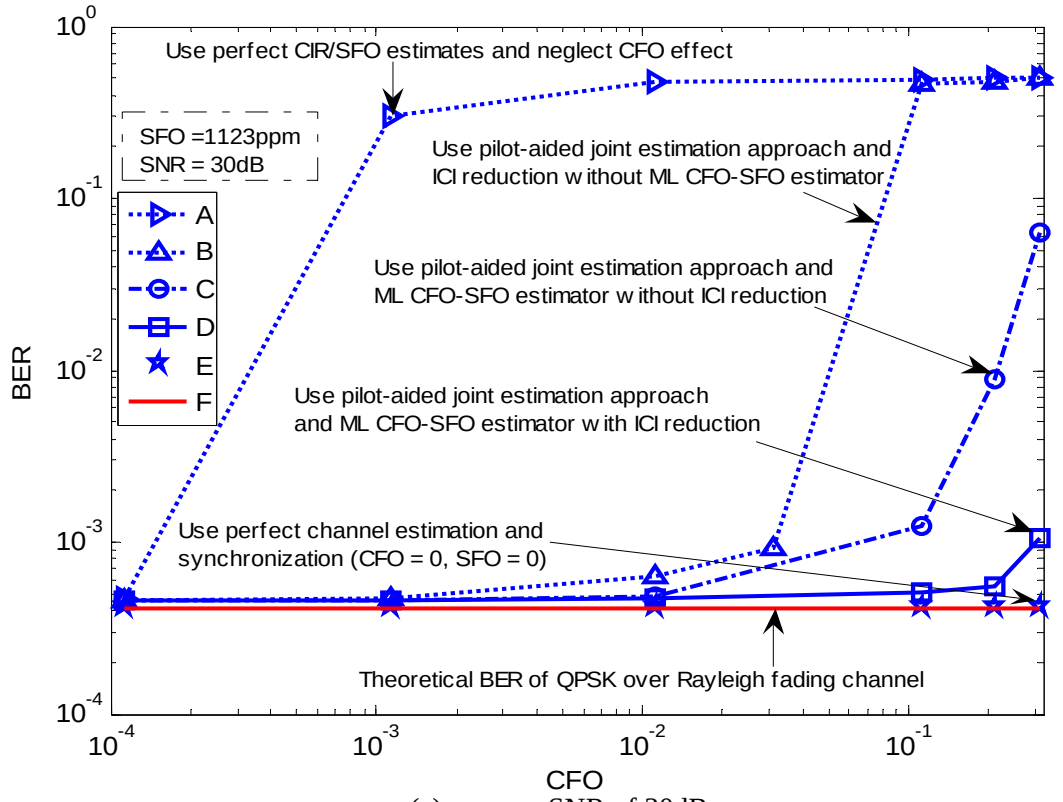

(a) average SNR of 30dB

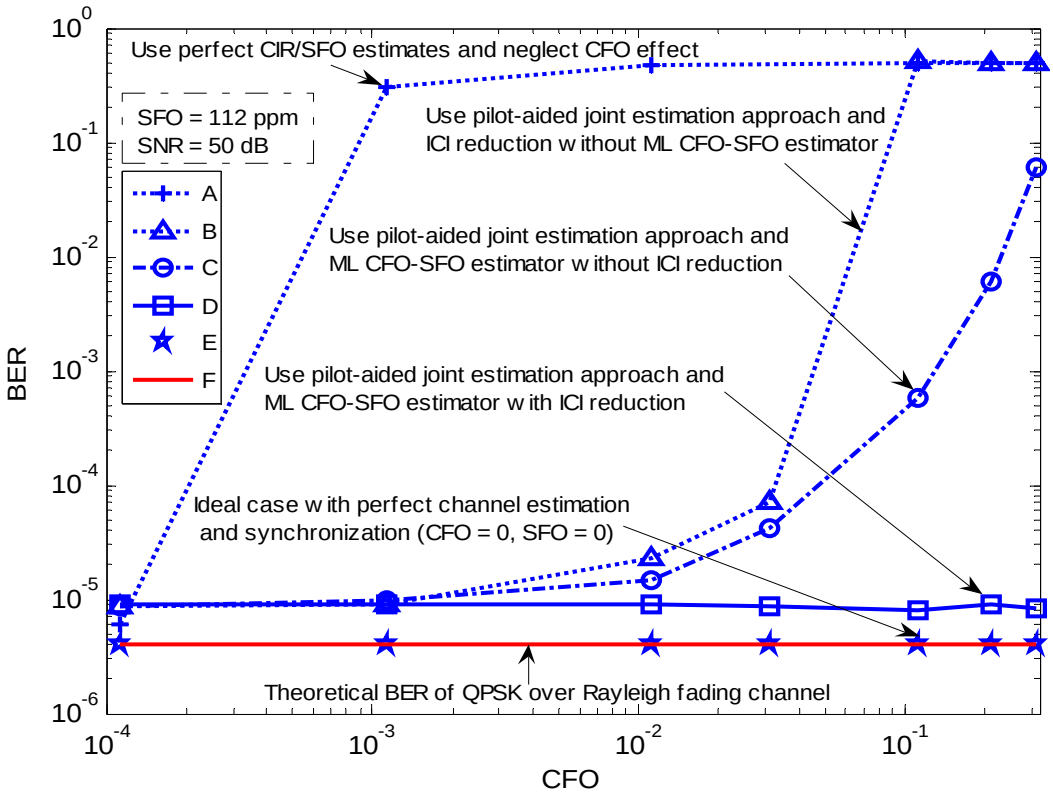

(b) average SNR of 50 dB

Figure 3.7: BER of the ML sub-carrier detector versus CFO with 4QAM in a Rayleigh channel.

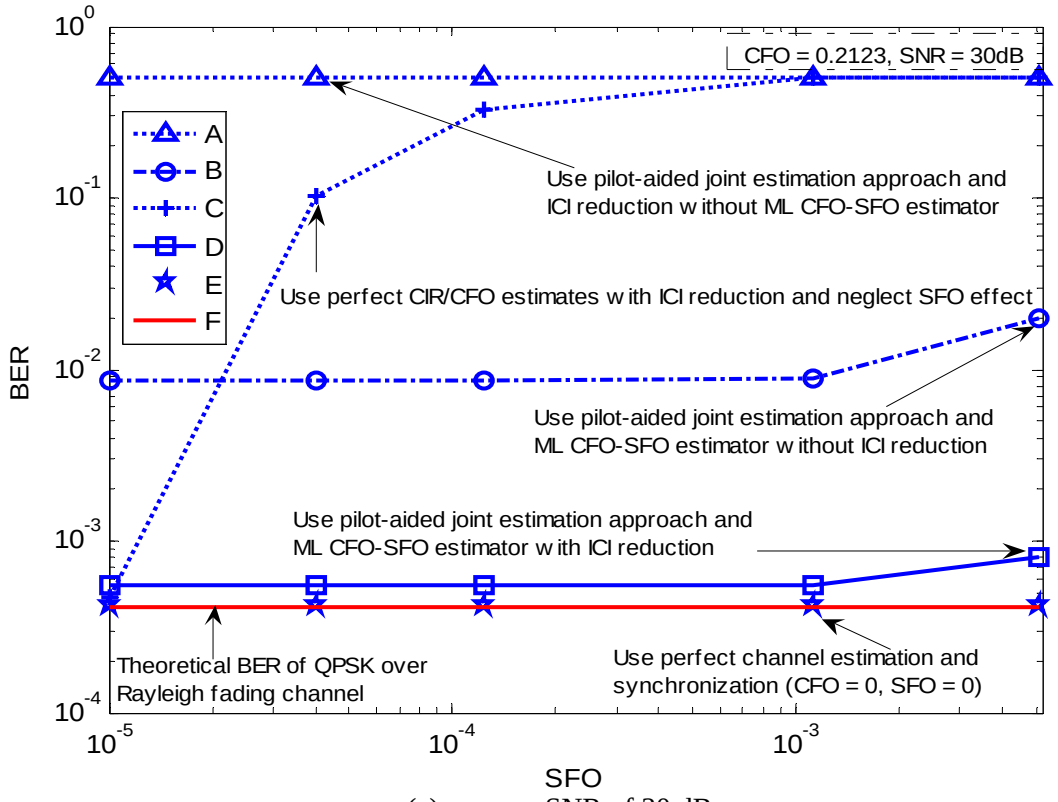

(a) average SNR of 30 dB

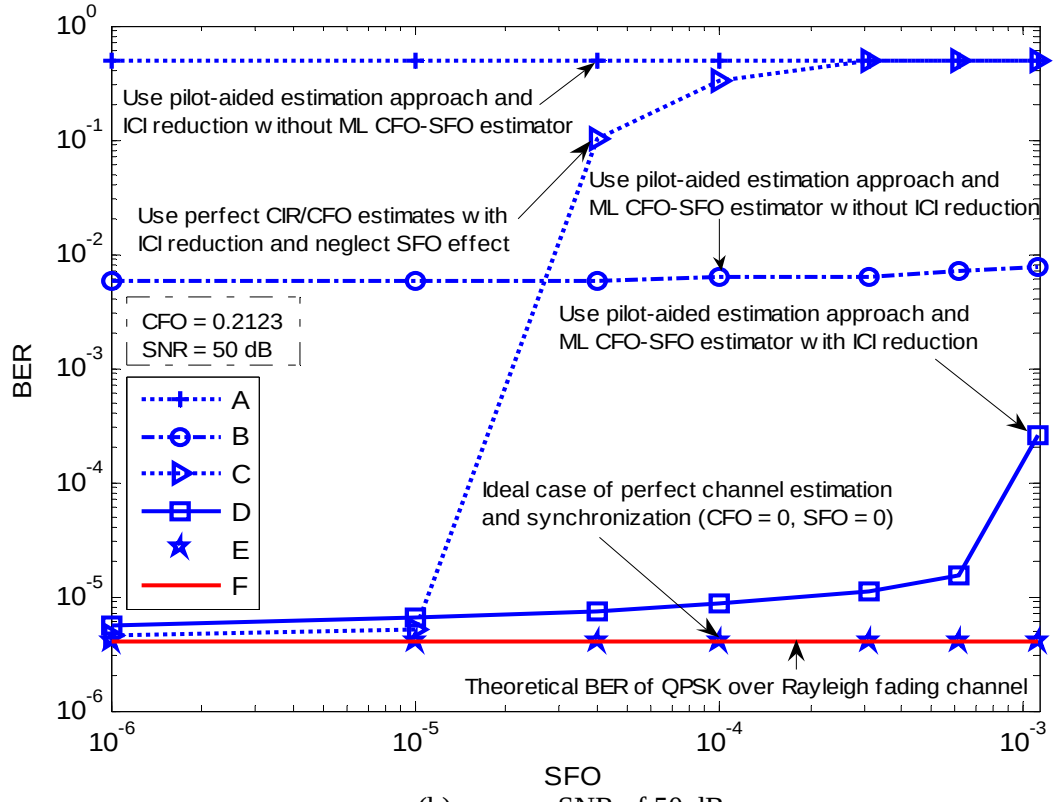

(b) average SNR of 50 dB

Figure 3.8: BER of the ML sub-carrier detector versus SFO with 4QAM over a Rayleigh channel.

Figure 3.8 shows the BER-versus-SFO (η) curves for ε = 0.2123. Curves F (*analytical* results) and E (*simulation* results) for the *ideal* case (with perfect channel estimation and synchronization) are included as reference BER, which is unchanged over the entire range of SFO values. Curves A and B also confirm that the ML CFO and SFO estimation is more effective than the ICI reduction. Furthermore, they show the dominant effects of ε = 0.2123 as they remain unchanged for a wide range of SFO values extending up to 1,000ppm (1E-3). The proposed algorithm using both ML CFO-SFO estimation and ICI reduction provides a performance (Curve D) remarkably close to *ideal* one for high CFO, ε = 0.2123, and over a wide SFO range up to 1,000ppm at SNR of 30dB and 300ppm at SNR of 50dB as shown in Figure 3.8 (a) and (b), respectively[4]. The performance degradation at high SNR that is mainly due to the residual ICI as discussed in the previous section is confirmed by the increase in the BER difference between Curves D and F in Figure 3.8 (b) for η>100ppm. As mentioned, synchronization and channel estimation are mutually related, joint channel estimation and synchronization could provide better accuracy at the cost of higher complexity.

3.7 Chapter Summary

In this chapter, a low-complexity, high-performance pilot-aided joint synchronization and channel estimation scheme suitable for burst-mode OFDM systems was proposed. The proposed estimation and tracking algorithm exploits both frequency domain (FD) and time domain (TD) to achieve low complexity by operating with small number of parameters and avoiding the use of IFFT in [37]. A linear model of the estimation error is formulated to develop a RLS-based algorithm. Furthermore, a simple ML

[4] It is noted the practical SFO values in IEEE 802.11a are only up to 40 ppm

SFO and CFO estimator was devised to provide initial guesses in the proposed RLS-based algorithm, to enhance the detection performance, and to eliminate the dominant ICI induced by SFO and CFO. Accurate initial guesses in turn reduce the convergence time, and enhance the stability of the proposed RLS-based algorithm. Analytical and simulation results for various cases in both AWGN and Rayleigh multi-path fading channels confirm the effectiveness of the various features and quantify their contributions in the system performance. The proposed pilot-aided joint channel estimation and synchronization scheme provides a near-optimum receiver performance that is remarkably close to the ideal case of perfect channel estimation and synchronization in both AWGN and Rayleigh multipath fading channels for large ranges of CFO and SFO values.

Chapter 4

Joint Estimation of Multi-antenna Channel Response and Frequency Offsets for MIMO-OFDM Systems

Known as a revolutionary concept for wireless transmissions, multiple-input multiple-output (MIMO) architectures [9] are able to offer a spectacular increase in the spectral efficiency of wireless communication channels by increasing the number of transmit and receive antennas. However, MIMO-based transmissions lead to a highly computational complexity in channel estimation. Dealing with this issue, this chapter focuses on the joint multiantenna channel estimation and synchronization in *uncoded* MIMO-OFDM systems.

4.1 Introduction

In broadband wireless communications, it is common to deploy multiple-input multiple-output (MIMO) configurations to achieve significant diversity and capacity gains [40]. At the same time, orthogonal frequency division multiplexing (OFDM) techniques are extensively employed to attain high spectral efficiency and robustness against multi-path fading channels [4]. Hence, the integration of MIMO and OFDM techniques has been widely recognized as a very promising strategy to enhance data rate, capacity and quality for broadband wireless systems. However, along with these potential merits, the primary challenge in MIMO-based systems is an increase in the complexity in channel estimation as the number of antennas increases [41]. Furthermore, the inherent drawback of OFDM-based systems is their susceptibility to synchro-

nization errors such as carrier frequency offset (CFO) and sampling frequency offset (SFO) [29], [31], [36] and [41]. Thus, the estimation of the multiantenna channel responses and frequency offsets is of crucial importance in physical layer implementations in MIMO-OFDM systems. So far, most studies on the issue are focused on the multiantenna channel estimation and synchronization (CFO and SFO estimation) separately [29], [31], [42]-[44]. More specifically, the multiantenna channel estimation is performed by assuming that perfect synchronization (i.e., perfect compensation of CFO and SFO) has been established [42]-[44], even though channel estimation would be degraded by imperfect synchronization and vice versa. Since synchronization and channel estimation are mutually related, the *joint* multiantenna channel estimation and synchronization could provide better performance at the cost of higher complexity. For the estimation of CIR and CFO in MIMO-OFDM systems, a few techniques have been recently proposed [41], [45]-[46]. In [41], a pilot-aided approach is proposed for *sequential* estimation of carrier frequency offset and multiantenna channel response by inserting hopping pilots in each OFDM symbol. These hopping pilots enable estimation of CFO and CIR to be performed separately in a sequential fashion. However, the bit error rate (BER) performance of the sequential estimation approach [41] is significantly worse than the ideal one of the case of perfect synchronization and channel estimation. This considerable BER degradation would be due to the *mutual* effect between channel estimation and synchronization that are performed in a sequential fashion. To avoid this mutual effect, studies on the *joint* estimation of the frequency offset and channel response in MIMO-OFDM systems have been addressed in [45]-[46]. However, only CFO is considered as a synchronization error parameter to be estimated in these approaches.

To the best of our knowledge, all existing algorithms for either joint or sequential

estimation of multiantenna channel responses and frequency offset in uncoded MIMO-OFDM systems have neglected the SFO effect in their studies. However, as demonstrated in [47], the detrimental effect of the SFO (even for a very small SFO) will likely lead to a significant degradation of the OFDM receiver performance even with the use of perfect CIR and CFO knowledge. Specifically, the SFO induces a sampling delay that drifts linearly in time over the OFDM symbol. Without any SFO compensation, this delay hampers OFDM receivers as soon as the product of the relative SFO and the number of sub-carriers becomes comparable to one [36]. Consequently, OFDM receivers become more vulnerable to the SFO effect as the used FFT size increases.

Taking into account the SFO effect, this chapter presents a proposed pilot-aided scheme for the joint estimation of CIR, CFO and SFO in MIMO-OFDM systems with the aid of the vector RLS algorithm [49]. Specifically, unlike the standard RLS approach [8] that is applicable to an adaptive filter with a single output, the vector RLS algorithm [49] is employed to function as an adaptive filter with multiple outputs for the joint CIR, CFO and SFO estimation in multiantenna OFDM receivers. The analytical and simulation results show that the proposed pilot-aided estimation and tracking approach is able to offer fast convergence, high stability and a near-optimum BER performance.

The rest of the chapter is organized as follows. Section 4.2 describes the MIMO-OFDM system model. Section 4.3 presents the proposed pilot-aided joint CIR, CFO and SFO estimation scheme. Analytical and simulated results with relevant discussions for various scenarios are presented in Section 4.4. Finally, Section 4.5 summarizes the chapter.

4.2 System Model

Figure 4.1 shows a simplified block diagram of an MIMO-OFDM transmitter using N_t transmit antennas and M-ary modulation (e.g., M-QAM). The input bit stream is first multiplexed in space and time before being grouped by the serial-to-parallel converter (S/P) to yield N_t sequences of Q-bit tuples, $\{\mathbf{d}_{m,k}^u\}$, where $\mathbf{d}_{m,k}^u = [d_{m,k,q}^u, q = 0,1,...,Q-1]$ with $u = 1,...,N_t$ and $Q = \log_2 M$ bits. Then, each Q-bit tuple, $\mathbf{d}_{m,k}^u$, is mapped to a complex-valued symbol, $X_{u,m}(k) \in \mathbf{A}$, where $\mathbf{A}$ is the M-ary modulation signaling set, and u, m and k denote the indices of the transmit anten-nas, OFDM symbols and sub-carriers, respectively. Each OFDM symbol consists of $K<N$ information bearing sub-carriers, where N is FFT size. After cyclic prefix (CP) insertion and digital-to-analogous converter (DAC), the transmitted baseband signal at the u-th transmit antenna can be represented as

$$s_u(t) = \frac{1}{N} \sum_{m=-\infty}^{+\infty} \sum_{k=-K/2}^{K/2-1} X_{u,m}(k) e^{j\frac{2\pi k}{NT}(t-T_g-mT_s)} U(t-mT_s) \tag{4.1}$$

where T is the sampling period at the output of IFFT, N_g denotes the number of CP samples, $T_g = N_g T$, $T_s = (N+N_g)T$ is the OFDM symbol length after CP insertion, $u(t)$ is the unit step function, and $U(t) = u(t) - u(t-T_s)$.

In burst-mode transmissions, the OFDM signal is assumed to be transmitted over a time-invariant multi-path fading channel within one burst duration. Specifically, the quasi-static channel response between the u-th transmit antenna and the v-th receive antenna can be represented by

$$h_{u,v}(\tau) = \sum_{l=0}^{L-1} \tilde{h}_{u,v,l} \delta(\tau - \tau_l), \tag{4.2}$$

where $\tilde{h}_{u,v,l}$ is the path gains and L is the total number of resolvable (effective) paths.

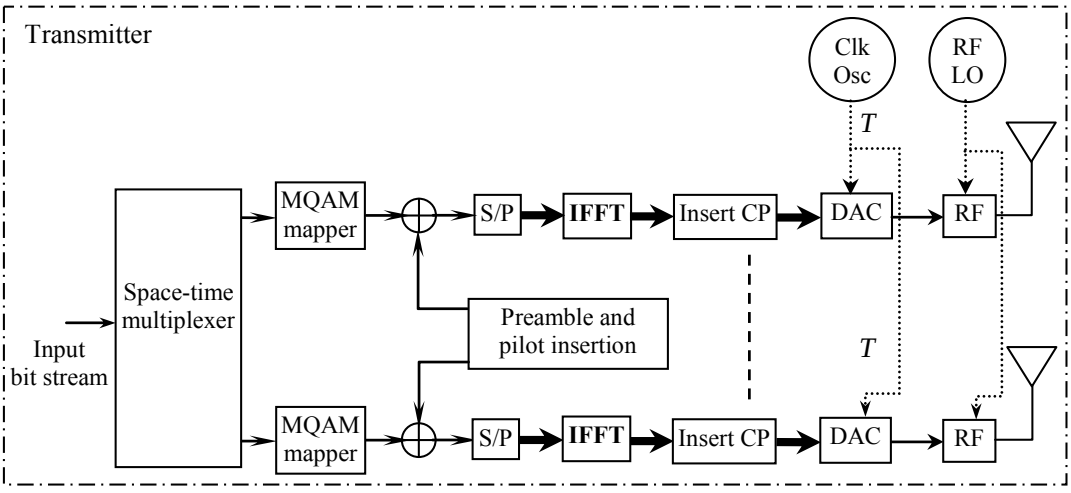

Figure 4.1: Burst-mode OFDM transmitter.

Frequency discrepancies between oscillators used in the radio transmitters and receivers, and channel-induced Doppler shifts cause a *net* carrier frequency offset (CFO) of Δf in the received signal where f is the operating radio carrier frequency. In practice, it would be reasonable to assume that all pairs of transmit-receive antennas experience a common CFO [29], [41]. Furthermore, the impinging signals at all receive antennas are sampled at rate $1/T'$. Since $T' \neq T$, the time alignment of received samples are also affected by sampling frequency offset (SFO), which is also common for all transmit-receive antenna pairs under the realistic assumption that collocated antennas' DACs are driven by a common clock oscillator. In the presence of the net CFO Δf, the received signal at the v-th receive antenna element can be determined by

$$r_v(t) = e^{j2\pi\Delta f t} \sum_{u=1}^{N_t} \sum_{l=0}^{L-1} \tilde{h}_{u,v,l}\, s_u(t-\tau_l) + w_v(t). \tag{4.3}$$

After sampling the received signal $r_v(t)$ at time instant $t_n = nT'$ (due to the presence of SFO) and CP removal, the n-th received sample of the m-th OFDM symbol in the time-domain at the v-th receive antenna element is determined by

$$r_{v,m,n} = \frac{e^{j\frac{2\pi}{N}(N_m+n)\varepsilon_\eta}}{N} \sum_{k=-K/2}^{K/2-1} e^{j\frac{2\pi k}{N}n(1+\eta)} e^{j\frac{2\pi k}{N}\eta N_m} \sum_{u=1}^{N_t} X_{u,m}(k)H_{u,v}(k) + w_{v,m,n}, \quad (4.4)$$

where $n = 0,1,...,N-1$ and $N_m = N_g + m(N+N_g)$. $w_{v,m,n}$ is the complex-valued Gau-ssian noise sample with a zero mean and a variance of σ^2. $H_{u,v}(k) = \sum_{l=0}^{L-1} h_{u,v,l} e^{-j\frac{2\pi k}{N}l}$ is the channel frequency response (CFR) at the *k*-th subcarrier for the pair of the *u*-th transmit antenna and the *v*-th receive antenna, and $\mathbf{h}_{u,v} = [h_{u,v,0} \;\; h_{u,v,1} \;\cdots\; h_{u,v,L-1}]^T$ is the corresponding *effective* channel impulse response (CIR) that incorporates path-delay induced phase rotation at receiver side. To completely remove the inter-symbol interference (ISI), the CP length must be longer than the channel spread, *L*. The SFO and CFO terms are represented in terms of the transmit sampling period *T* as $\eta = \Delta T/T$, $\Delta T = T' - T$ and $\varepsilon = \Delta fNT = (\Delta f / f)(NTf)$, respectively, and $\varepsilon_\eta = (1+\eta)\varepsilon$. In practice, both relative frequency differences, $\Delta T/T$, and $\Delta f/f$, are within the allowable tolerance, which is typically 10ppm (10E-6) or less. However, since the radio carrier frequency, *f*, is normally much higher than the sampling freque-ncy $1/T$, the factor *NTf* can make the CFO term ε large while the SFO term satisfies $\eta << 1$ [47].

Based on (4.4), the signal-to-noise ratio (SNR) at the *v*-th receive antenna in the time domain is

$$SNR_v = \frac{P_{S,v}}{P_N}, \quad (4.5)$$

where $P_{S,v} = \frac{1}{N^2} E\left\{ \left| \sum_{k=-K/2}^{K/2-1} e^{j\frac{2\pi k}{N}n(1+\eta)} e^{j\frac{2\pi k}{N}\eta N_m} \sum_{u=1}^{N_t} X_{u,m}(k)H_{u,v}(k) \right|^2 \right\}$ and $P_N = \sigma^2$.

Assume that the coefficients of CIR, $\{h_{u,v,0}, h_{u,v,1}, ..., h_{u,v,L-1}\}$, are independent zero-mean complex random variables with common variances $\{\sigma_0^2, \sigma_1^2, ..., \sigma_{L-1}^2\}$ for all pairs of transmit-receive antennas, and all receive antennas experience the same AWGN power. After some manipulation, it can be shown that the SNR values at all receive antennas are equal and given by

$$SNR = \frac{KN_t E_s \sum_{l=0}^{L-1} \sigma_l^2}{N^2 \sigma^2}. \quad (4.6)$$

where $E_s = E\left\{\left|X_{u,m}(k)\right|^2\right\}$ is the average energy of M-QAM symbols.

To reduce the computational complexity in the multiantenna channel estimation, the proposed estimation approach attempts to estimate the CIR $\{h_{u,v,0}, h_{u,v,1}, ..., h_{u,v,L-1}\}$ instead of CFR $H_{u,v}(k)$ by using the observations of the received sub-carriers in the frequency domain (FD). After FFT, the received FD sample at the *v*-th receive anten-na is $Y_{v,m}(k) = \sum_{n=0}^{N-1} r_{v,m,n} e^{-j\frac{2\pi}{N}nk}$. Based on (4.4), we obtain the following

$$Y_{v,m}(k) = \sum_{i=-K/2}^{K/2-1} e^{j\frac{2\pi}{N}N_m\varepsilon_i} \rho_{i,k} \sum_{u=1}^{N_t} X_{u,m}(i) H_{u,v}(i) + W_{v,m}(k), \quad (4.7)$$

where $\rho_{i,k} = \frac{1}{N}\sum_{n=0}^{N-1} e^{j\frac{2\pi}{N}n(\varepsilon_i+i-k)} \approx \mathrm{sinc}(\varepsilon_i + i - k) e^{j\pi(\varepsilon_i+i-k)}$ stands for the ICI coefficient, $\varepsilon_i = i\eta + \varepsilon_\eta$, $\mathrm{sinc}(x) = \frac{\sin(\pi x)}{(\pi x)}$, and $W_{v,m}(k) = \sum_{n=0}^{N-1} w_{v,m}(n + N_m) e^{-j\frac{2\pi}{N}nk}$.

It is noted that the frequency-domain expression of the received samples in [12, Eq. 37] is an approximation of (4.7) in the case of SISO-OFDM. In the first summation in

(4.7), the term $i=k$ corresponds to the sub-carrier of interest, while the other terms with $i \neq k$ represent ICI. As can be observed from the above expression for $\rho_{i,k}$, the term, $\varepsilon_i = i\eta + \varepsilon_\eta$, needs to be removed in order to suppress ICI. Obviously, in an *ideal* case with *zero* SFO and CFO, $\varepsilon_i=0$, $\rho_{i,k}=1$ for $i=k$ and $\rho_{i,k}=0$ (ICI does not exist) for $i \neq k$. Therefore, $Y_{v,m}(k) = \sum_{u=1}^{N_t} X_{u,m}(k) H_{u,v}(k) + W_{v,m}(k)$ and perfect orthogonality among sub-carriers is preserved at the receiver. Thus, to mitigate ICI, the contribution of CFO and SFO to received sub-carriers needs to be compensated. As a result, the estimates of CFO and SFO are required to compensate the detrimental effects of synchronization errors while the multiantenna channel estimates are required for the subsequent MIMO symbol detection.

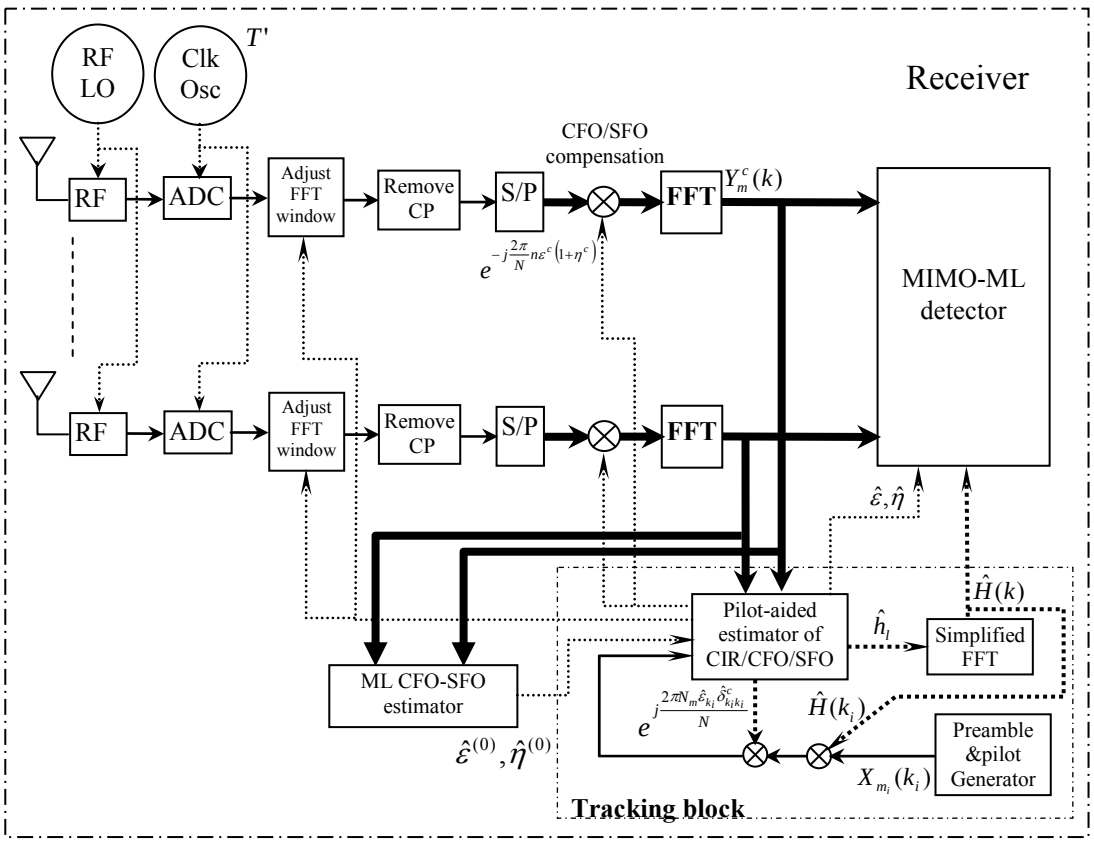

Figure 4.2: Burst-mode OFDM receiver with joint CIR/CFO/SFO estimation and tracking.

4.3 Joint Estimation of CIR, CFO and SFO

4.3.1 ICI Reduction at Multiple Receive Antennas

Similar to the ICI reduction method for SISO-OFDM in [47], ICI reduction in MIMO-OFDM can be analyzed as follows. As can be observed in (4.4) and (4.7), SFO and CFO introduce phase rotation in the time domain and in turn both attenuation and ICI in the frequency domain. CFO-SFO-induced attenuation can be compensated in a symbol-by-symbol manner. However, cancellation of ICI requires knowledge of all the detected symbols in the frequency domain. Hence, ideally, it is better to compensate the phase rotation in the time domain to avoid ICI in the frequency domain. Based on the derivations to obtain (4.7), it is noted that only the common factor $e^{j\frac{2\pi\varepsilon_\eta n}{N}}$ and individual coefficients $e^{j\frac{2\pi kn\eta}{N}}$ embedded in the summation at (4.4) result in the ICI in (4.7). The common factor can be removed from the received time-domain sample. However, the correction of the individual coefficients requires knowledge of the detected symbols in the frequency domain, and this is not available. Fortunately, the common factor has a major influence in $\rho_{i,k}$ due to the large CFO term, ε, while the effect of the individual coefficient is minor in $\rho_{i,k}$ since the SFO term satisfies η<<1 in practice. As a result, to suppress the common factor, the received time-domain sample in (4.4) can be multiplied by $e^{-j\frac{2\pi\varepsilon_\eta^c n}{N}}$ prior to FFT as shown in Figure 4.2, where

$$r_{v,m,n}^c = r_{v,m,n} e^{-j\frac{2\pi}{N}n\varepsilon_\eta^c}, \tag{4.8}$$

$\varepsilon_\eta^c = (1+\eta^c)\varepsilon^c$, and ε^c and η^c are the estimates of CFO and SFO[1], respectively.

[1] Estimation of CFO and SFO will be described in subsection 4.3.3.

After FFT, the resulting FD sub-carriers at the *v*-th receive antenna is

$$Y_{v,m}^{c}(k) = \sum_{n=0}^{N-1} r_{v,m,n}^{c} e^{-j\frac{2\pi}{N}nk} . \tag{4.9}$$

After some manipulation, (4.9) can be shown to be

$$Y_{v,m}^{c}(k) = \sum_{i=-K/2}^{K/2-1} e^{j\frac{2\pi}{N}N_m\varepsilon_i} \rho_{i,k}^{c} \sum_{u=1}^{N_t} X_{u,m}(i)H_{u,v}(i) + W_{v,m}^{c}(k), \tag{4.10}$$

where $W_{v,m}^{c}(k) = \sum_{n=0}^{N-1} w_{v,m}(n+N_m) e^{-j\frac{2\pi}{N}n(1+\eta^c)\varepsilon^c} e^{-j\frac{2\pi}{N}nk}$ and

$$\rho_{i,k}^{c} = \frac{1}{N}\sum_{n=0}^{N-1} e^{j\frac{2\pi}{N}n\left[i\eta+(1+\eta)\varepsilon-(1+\eta^c)\varepsilon^c+i-k\right]} .$$

After the TD CFO-SFO compensation, the resulting ICI coefficient becomes

$$\rho_{i,k}^{c} = \frac{1}{N}\sum_{n=0}^{N-1} e^{j\frac{2\pi}{N}n\left[i\eta+\varepsilon_\eta-\varepsilon_\eta^c+i-k\right]} . \tag{4.11}$$

As shown in (4.11), there exists residual ICI due to the term, $i\eta$, even with the use of the TD CFO-SFO compensation with perfect estimates of CFO and SFO ($\varepsilon^c = \varepsilon$ and $\eta^c = \eta$). Fortunately, for practical SFO values, the residual ICI is negligible since $i\eta$ is quite insignificant in contributing to the ICI coefficient, $\rho_{i,k}$, after the TD CFO-SFO compensation.

4.3.2 Brief Description of the Vector RLS Approach in [49]

Unlike the standard RLS algorithm [8] for minimizing a summation of squared values of the error samples from a single output of an adaptive filter, the vector RLS approach [49] is employed to function as an adaptive filter with multiple outputs. Specifically, the vector RLS approach can be implemented as follows.

Input parameters: The existing estimate of tap-weight vector $\hat{\boldsymbol{\omega}}_{i-1}$, the input signal matrix $\mathbf{X}_{i,N_r} = \left[\mathbf{x}_i^{(1)} \ \cdots \ \mathbf{x}_i^{(N_r)}\right]$, the reference output vector $\mathbf{d}_{i,N_r} = \left[d_i^{(1)} \ \ldots \ d_i^{(N_r)}\right]^T$ and the existing matrix $\mathbf{P}_{i-1}^{-1}$.

Output parameters: The filter output $\mathbf{y}_{i,N_r} = \mathbf{X}_{i,N_r}^T \hat{\omega}_{i\text{-}1}$, the updated estimate of tap-weight vector $\hat{\boldsymbol{\omega}}_i$ and the updated matrix $\mathbf{P}_i^{-1}$.

Iterative Procedure:

1) Compute the gain matrix $\mathbf{K}_i$ at the *i*-th iteration:

$$\mathbf{K}_i = \mathbf{P}_{i-1}^{-1}\mathbf{X}_{i,N_r}^* \left[\mathbf{X}_{i,N_r}^T \mathbf{P}_{i-1}^{-1}\mathbf{X}_{i,N_r}^* + \lambda \mathbf{I}_{N_r}\right]^{-1}. \tag{4.12}$$

2) Filter at the *i*-th iteration:

$$\mathbf{y}_{i,N_r} = \mathbf{X}_{i,N_r}^T \hat{\omega}_{i\text{-}1}. \tag{4.13}$$

3) Compute error estimation at the *i*-th iteration

$$\mathbf{e}_{i,N_r} = \mathbf{d}_{i,N_r} - \mathbf{y}_{i,N_r}. \tag{4.14}$$

4) Update tap-weight vector at the *i*-th iteration

$$\hat{\boldsymbol{\omega}}_i = \hat{\boldsymbol{\omega}}_{i-1} + \mathbf{K}_i \mathbf{e}_{i,N_r}. \tag{4.15}$$

5) Update matrix $\mathbf{P}_i^{-1}$ at the *i*-th iteration

$$\mathbf{P}_i^{-1} = \lambda^{-1}\left(\mathbf{P}_{i-1}^{-1} - \mathbf{K}_i \mathbf{X}_{i,N_r}^T \mathbf{P}_{i-1}^{-1}\right). \tag{4.16}$$

4.3.3 Vector RLS-Based Joint Estimation of CIR, CFO and SFO

Based on the use of the received samples and pilot tones in FD, a pilot-aided algorithm is devised to estimate and track the CIR, CFO and SFO in MIMO-OFDM systems. To exploit the vector RLS algorithm for this estimation and tracking task, we

introduce a LS cost function corresponding to the use of *i* pilot tones over OFDM symbols in a burst as follows:

$$C\left(\hat{\mathbf{h}}_{u,v}^{(i)}, \hat{\varepsilon}^{(i)}, \hat{\eta}^{(i)}\right) = \sum_{p=1}^{i} \lambda^{i-p} \sum_{v=1}^{N_r} \left| e_{i,p,v} \right|^2 , \tag{4.17}$$

where λ is referred to the forgetting factor of the RLS algorithm, $\hat{\mathbf{h}}_{u,v}^{(i)} = \left[\hat{h}_{u,v,0}^{(i)}, \hat{h}_{u,v,1}^{(i)}, ... \hat{h}_{u,v,L-1}^{(i)}\right]^T, u = 1,..., N_t, v = 1,..., N_r,$

$e_{i,p,v} = Y_{v,m_p}^{c}\left(k_p\right) - f_v\left(X_{u,m_p}\left(k_p\right), \hat{\boldsymbol{\omega}}_i\right),$

$f_v\left(X_{u,m_p}\left(k_p\right), \hat{\boldsymbol{\omega}}_i\right) = e^{j\frac{2\pi}{N} N_{m_p} \hat{\varepsilon}_{k_p}^{(i)}} \hat{\rho}_{k_p}^{c} \sum_{u=1}^{N_t} X_{u,m_p}(k_p) \hat{H}_{u,v}^{(i)}(k_p),$

$\hat{H}_{u,v}^{(i)}(k_p) = \sum_{l=0}^{L-1} \hat{h}_{u,v,l}^{(i)} e^{-j\frac{2\pi k_p l}{N}}$, $\hat{\varepsilon}_{k_p}^{(i)} = k_p \hat{\eta}^{(i)} + (1 + \hat{\eta}^{(i)}) \hat{\varepsilon}^{(i)},$

$\hat{\rho}_{k_p}^{c} = \frac{1}{N} \sum_{n=0}^{N-1} e^{j\frac{2\pi}{N} n\left[k_p \hat{\eta}^{(i)} + (1+\hat{\eta}^{(i)})\hat{\varepsilon}^{(i)} - (1+\eta^c)\varepsilon^c\right]}$ and

$p = 1,..., i$ denotes the index of the *p*-th pilot tone in the set of *i* pilot tones used for the vector RLS-based estimation from the first iteration to the *i*-th iteration. $X_{u,m_p}\left(k_p\right)$ is the value of the *p*-th pilot tone at sub-carrier k_p of the m_p-th OFDM symbol from the *u*-th transmit antenna in the vector RLS-based estimation. It is noted that all tones are employed as pilots in the preamble of a burst.

To exploit the vector RLS approach for estimating the unknown CIR, CFO and SFO, the non-linear estimation error $e_{i,p,v}$ needs to be linearized about the existing estimates of CIR, CFO and SFO by using the following first-order Taylor's series approximation:

$$e_{i,p,v} \approx Y_{v,m_p}^{c}(k_p) - \left\{ f_v\left(X_{u,m_p}\left(k_p\right), \hat{\boldsymbol{\omega}}_{i-1}\right) + \nabla f_v^T\left(X_{u,m_p}\left(k_p\right), \hat{\boldsymbol{\omega}}_{i-1}\right)\left(\hat{\boldsymbol{\omega}}_i - \hat{\boldsymbol{\omega}}_{i-1}\right) \right\}, \tag{4.18}$$

where $\hat{\boldsymbol{\omega}}_i = \left[\hat{\omega}_{i,0}, \hat{\omega}_{i,1}, ..., \hat{\omega}_{i,2LN_tN_r+1}\right]^T$ is the $(2LN_tN_r+2)\times 1$ weight vector that contains the CIR, CFO and SFO estimates at the i-th iteration of the vector RLS approach. More specifically, elements of $\hat{\boldsymbol{\omega}}_i$ are assigned as follows:

$$\hat{\omega}_{i,l+2L(u-1)+2LN_t(v-1)} = \mathrm{Re}\left\{\hat{h}^{(i)}_{u,v,l}\right\},$$

$$\hat{\omega}_{i,l+L+2L(u-1)+2LN_t(v-1)} = \mathrm{Im}\left\{\hat{h}^{(i)}_{u,v,l}\right\},$$

$$\hat{\omega}_{i,2LN_tN_r} = \hat{\varepsilon}^{(i)},$$

and $\hat{\omega}_{i,2LN_tN_r+1} = \hat{\eta}^{(i)}$ with $u = 1,...,N_t$, $v = 1,...,N_r$ and $l = 0,...,L-1$.

The gradient vector of $f_v\left(X_{u,m_p}(k_p), \hat{\boldsymbol{\omega}}_{i-1}\right)$ corresponding to the v-th receive antenna can be determined by

$$\nabla f_v\left(X_{u,m_p}(k_p), \hat{\boldsymbol{\omega}}_{i-1}\right) = \left[\frac{\partial f_v\left(X_{u,m_p}(k_p), \hat{\boldsymbol{\omega}}_{i-1}\right)}{\partial \hat{\omega}_{i,0}} \quad \cdots \quad \frac{\partial f_v\left(X_{u,m_p}(k_p), \hat{\boldsymbol{\omega}}_{i-1}\right)}{\partial \hat{\omega}_{i,2LN_tN_r+1}}\right]^T, \quad (4.19)$$

where

$$\frac{\partial f_v\left(X_{u,m_p}(k_p), \hat{\boldsymbol{\omega}}_i\right)}{\partial \hat{\omega}_{i,l+2L(u-1)+2LN_t(v-1)}} = X_{u,m_p}(k_p) e^{-j\frac{2\pi l k_p}{N}} e^{j\frac{2\pi}{N}N_m\hat{\varepsilon}^{(i)}_{k_p}} \hat{\rho}^c_{k_p},\ l = 0,...,L-1,$$

$$\frac{\partial f_v\left(X_{u,m_p}(k_p), \hat{\boldsymbol{\omega}}_i\right)}{\partial \hat{\omega}_{i,l+L+2L(u-1)+2LN_t(v-1)}} = j\frac{\partial f_v\left(X_{u,m_p}(k_p), \hat{\boldsymbol{\omega}}_i\right)}{\partial \hat{\omega}_{i,l+2L(u-1)+2LN_t(v-1)}},$$

$$\frac{\partial f_v\left(X_{u,m_p}(k_p), \hat{\boldsymbol{\omega}}_i\right)}{\partial \hat{\omega}_{i,2LN_tN_r}} = \left(1+\hat{\eta}^{(i)}\right)\Omega_{i,p,v},$$

$$\Omega_{i,p,v} = e^{j\frac{2\pi}{N}N_m\hat{\varepsilon}^{(i)}_{k_p}}\left[j\frac{2\pi}{N}N_m\hat{\rho}^c_{k_p} + \frac{1}{N}\sum_{n=0}^{N-1} j\frac{2\pi}{N}n e^{j\frac{2\pi}{N}n\left[\hat{\varepsilon}^{(i)}_{k_p}-\varepsilon^c_\eta\right]}\right]\sum_{u=1}^{N_t} X_{u,m_p}(k_p)\hat{H}^{(i)}_{u,v}(k_p)$$

and

$$\frac{\partial f_v\left(X_{u,m_p}(k_p), \hat{\boldsymbol{\omega}}_i\right)}{\partial \hat{\omega}_{i,2LN_tN_r+1}} = \left(k_p + \hat{\varepsilon}^{(i)}\right)\Omega_{i,p,v},\ u = 1,..,N_t.$$

Note that $\frac{\partial f_v\left(X_{u,m_p}(k_p),\hat{\boldsymbol{\omega}}_i\right)}{\partial\hat{\omega}_{i,l+2L(u-1)+2LN_t(\rho-1)}}=0$, $\frac{\partial f_v\left(X_{u,m_p}(k_p),\hat{\boldsymbol{\omega}}_i\right)}{\partial\hat{\omega}_{i,l+L+2L(u-1)+2LN_t(\rho-1)}}=0$ with

$\rho=1,...,N_r$ and $\rho\neq v$.

Subsequently, we can formulate the following vector RLS-based joint CIR, CFO, SFO estimation algorithm as follows:

Initialization: Select $\hat{\boldsymbol{\omega}}_1$ using the ML CFO-SFO estimation (to be described in Sub-section 4.3.4) and $\mathbf{P}_1=\gamma^{-1}\mathbf{I}_{2LN_rN_t+2}$, where γ is the regularization parameter, $\mathbf{I}_{2LN_rN_t+2}$ is the $(2LN_rN_t+2)\times(2LN_rN_t+2)$ identity matrix.

Iterative Procedure:

1) Update the parameters at the *i*-th iteration

$$\mathbf{X}_{i,N_r}=\left[\nabla f_1\left(X_{u,m_i}(k_i),\hat{\boldsymbol{\omega}}_{i-1}\right)\ \cdots\ \nabla f_{N_r}\left(X_{u,m_i}(k_i),\hat{\boldsymbol{\omega}}_{i-1}\right)\right], \tag{4.20}$$

$$\mathbf{K}_i=\mathbf{P}_{i-1}\mathbf{X}^*_{i,N_r}\left(\lambda\mathbf{I}_{N_r}+\mathbf{X}^T_{i,N_r}\mathbf{P}_{i-1}\mathbf{X}^*_{i,N_r}\right)^{-1}, \tag{4.21}$$

with λ denoting the forgetting factor.

$$\mathbf{P}_i=\lambda^{-1}\left(\mathbf{P}_{i-1}-\mathbf{K}_i\mathbf{X}^T_{i,N_r}\mathbf{P}_{i-1}\right), \tag{4.22}$$

$$\mathbf{e}_{i,N_r}=\left[\left(Y^c_{1,m_i}(k_i)-f_1\left(X_{u,m_i}(k_i),\hat{\boldsymbol{\omega}}_{i-1}\right)\right)\ \cdots\ \left(Y^c_{N_r,m_i}(k_i)-f_{N_r}\left(X_{u,m_i}(k_i),\hat{\boldsymbol{\omega}}_{i-1}\right)\right)\right]^T, \tag{4.23}$$

with $u=1,..,N_t$

2) Update estimates at the *i*-th iteration

$$\hat{\boldsymbol{\omega}}_i=\hat{\boldsymbol{\omega}}_{i-1}+\mathbf{K}_i\mathbf{e}_{i,N_r}, \tag{4.24}$$

In the MIMO-OFDM receiver (Figure 4.2), the CIR, CFO, SFO estimates are updated on a symbol-by-symbol basis for the MIMO-ML sub-carrier detector, while the tracking block updates the CIR, CFO and SFO estimates in an iteration-by-iteration manner. Moreover, since the number of the CIR coefficients is much smaller than the FFT size, a simplified FFT with a reduced-complexity can be employed to

generate channel transfer function for both the MIMO-ML sub-carrier detector in the demodulator and reconstruction of the transmitted signal in the tracking block.

Like other iterative estimation techniques, the vector RLS-based estimation approach also requires appropriate initial guesses of estimated parameters to achieve its proper convergence. For this reason, a ML estimator is introduced to obtain coarse estimates of CFO and SFO to be used as initial guesses for estimated parameters in the vector RLS-based iterative estimation.

4.3.4 ML Coarse CFO and SFO Estimator at Multiantenna Receiver

Due to the possibility of multiple local minima caused by the non-linearity of the cost function of CIR, CFO and SFO, the initial guesses of the estimated parameters for adaptive estimation must fall in a specific vicinity of their actual values. Consequently, the large initial errors between the initial guesses and the true values would cause instability of the vector RLS-based iterative computation. To alleviate such deterioration, we extend the ML coarse estimator of CFO and SFO [47] in a SISO-OFDM receiver to obtain coarse estimates of the initial CFO and SFO values in a MIMO-OFDM one.

Let m_1 and (m_1+1) be the time indices of the first and second long training symbols in preamble of a burst, respectively. Based on the FD observations in these two identical training symbols at the v-th receive antenna, we define the following term

$$Y_v(k) \equiv \frac{Y_{v,m_1+1}(k)}{Y_{v,m_1}(k)} = e^{j\frac{2\pi N_s}{N}[k\eta+\varepsilon(1+\eta)]} + E_v(k), \tag{4.25}$$

where $v = 1,...,N_r$, $N_s = N + N_g$ and the FD error sample $E_v(k)$ can be expressed by

$$E_v(k) = \frac{W_{v,m_1+1}(k) - W_{v,m_1}(k)e^{j\frac{2\pi N_s}{N}\varepsilon_k}}{e^{j\frac{2\pi(N_g+m_1N_s)}{N}\varepsilon_k}\rho_{kk}\sum_{u=1}^{N_t} X_{u,m_1}(k)H_{u,v}(k) + W_{v,m_1}(k)}.$$

The ICI parts are herein absorbed in $W_{v,m}(k)$ with $m = m_1$, and $(m_1 + 1)$, and assumed to be Gaussian distributed [12], [31]. As a result, the FD error sample $E_v(k)$ can also be approximated to be uncorrelated, Gaussian-distributed. This assumption is well supported by the measured Gaussian-shape histograms of the real and imaginary parts of $E(k)$ and its measured auto-correlation that is approximately a delta function as shown in Figure 4.3.

Hence, based on the use of the FD received sub-carriers at N_r receive antennas corresponding to two long training symbols, we define the following ML cost function

$$f(\varepsilon,\eta) = \sum_{k\in I_p}\sum_{v=1}^{N_r}\left|Y_v(k) - e^{j\frac{2\pi N_s}{N}[k\eta+\varepsilon(1+\eta)]}\right|^2, \tag{4.26}$$

where I_p is the set of sub-carrier indices of pilot tones in preamble.

As a result, in the absence of CIR knowledge, the coarse estimates of CFO and SFO can be obtained by

$$\hat{\varepsilon},\hat{\eta} = \arg\min_{\varepsilon,\eta}\sum_{k\in I_p}\sum_{v=1}^{N_r}\left|Y_v(k) - e^{j\frac{2\pi N_s}{N}[k\eta+\varepsilon(1+\eta)]}\right|^2. \tag{4.27}$$

The above coarse CFO and SFO estimates are then used as initial guesses of CFO and SFO for the vector RLS-based joint CIR, CFO and SFO estimation & tracking (in Section 4.3.3) while the coarse CIR estimates are obtained by using the RLS algorithm with the preamble and the available coarse CFO and SFO estimates.

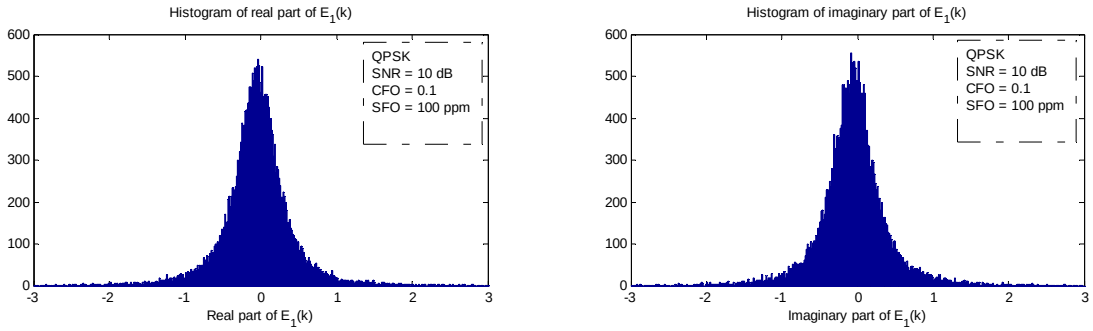

(a) Histograms (probability density functions) of the real and imaginary parts of $E_1(k)$ at the 1-st receive antenna

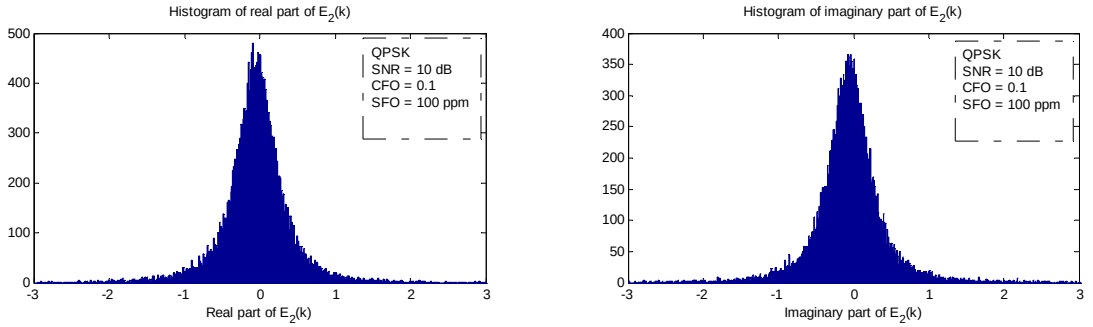

(b) Histograms (probability density functions) of the real and imaginary parts of $E_2(k)$ at the 2-nd receive antenna

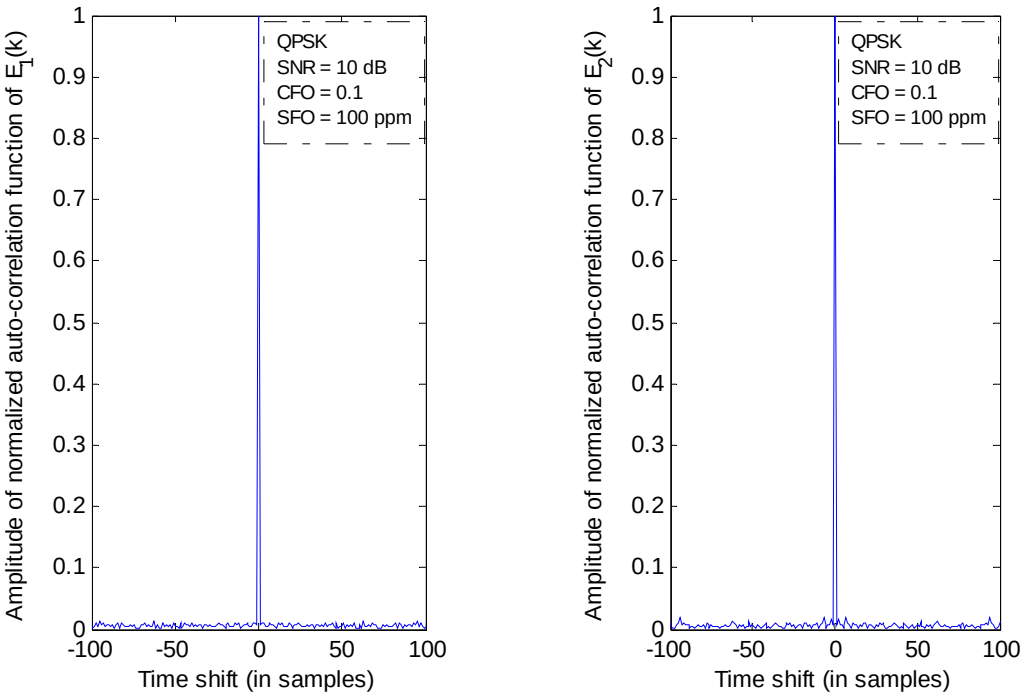

(c) auto-correlation function at the *1*-st receive antenna and the *2*-nd receive antenna.

Figure 4.3: Probability density and auto-correlation functions of the FD error samples.

4.4 Simulation results and discussions

Computer simulation has been conducted to evaluate the performance of the proposed algorithm for the joint estimation of CIR, CFO and SFO in an OFDM system with various MIMO configurations. In the investigation, we set the OFDM-related parameters based on the IEEE 802.11a standard [38]. Signal constellation of QPSK is employed for OFDM symbols of 48 data subcarriers and 4 equally spaced pilot tones of the same power. For each transmit antenna, a burst format of two long identical training symbols and 225 data OFDM symbols is used in the simulation. For each transmit-receive antenna pair, we consider an exponentially decaying Rayleigh fading channel with L=5 and a RMS delay spread of 25ns. For the coarse CFO estimation, the used step size for searching the ML CFO estimates is 0.0001.

Figure 4.4 shows the measured mean squared errors[2] (MSE) of the CIR, CFO and SFO estimates and their corresponding Cramer-Rao lower bounds (CRLBs[3]). Unlike CRLBs in Chapter 3, the CRLB values herein are derived under an assumption that pilot-aided CIR, CFO and SFO estimation employ 4 pilot tones in each OFDM symbol. It is observed that a forgetting factor smaller than 0.995 results in instability. In addition, the numerical results demonstrate that the proposed estimation algorithm achieves fast convergence, high stability and the best MSE performance with forgetting factor λ=0.995 and regularization parameter $\gamma = 10$.

[2] Normalized to the signal power.
[3] Derivation of these CRLBs is presented in Appendix E

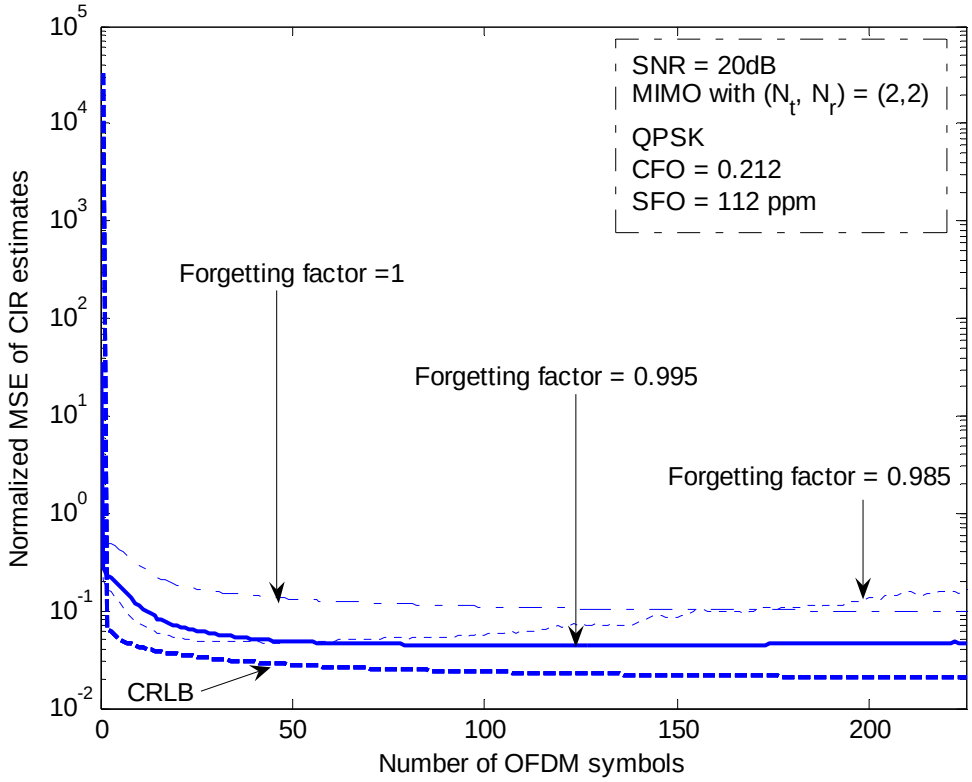

(a) CIR

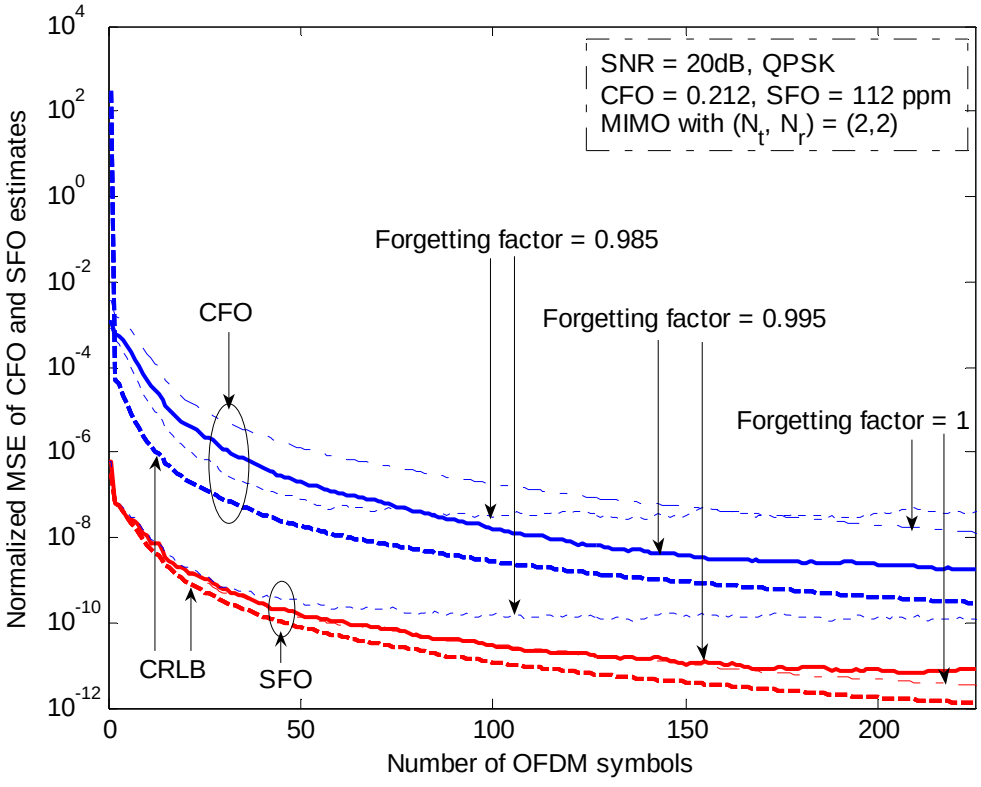

(b) CFO and SFO

Figure 4.4: Normalized MSEs and CRLBs of CIR, CFO and SFO estimates.

To further assess the performance of the pilot-aided joint estimation of CIR, CFO and SFO, we study the BER performance of the MIMO-ML data detector using the estimates of CIR, CFO and SFO from the proposed estimation algorithm in various scenarios. Figure 4.5 shows the BER-versus-SNR performance curves in Rayleigh fading channels under various single-input multiple-output (SIMO) configurations. As reference, the *ideal* BER performances with perfect channel estimation and synchronization (SFO=CFO=0) are included. The *analytical* (theoretical BER of QPSK [51] and asymptotic union bounds [50]) and *simulation* BER results for the *ideal* cases are in excellent agreement under any SNR value for SISO case and $SNR > 5dB$ for SIMO cases (asymptotic union bounds [50] applicable to high SNRs).

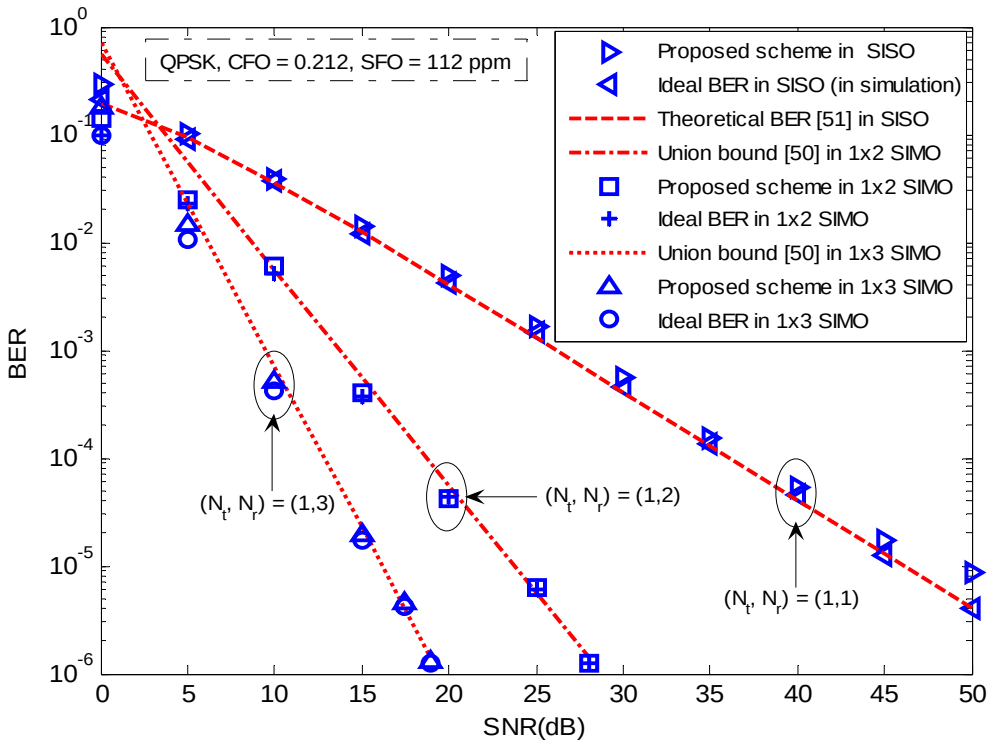

Figure 4.5: BER performance of the SIMO-ML sub-carrier detector versus SNR with QPSK constellation over Rayleigh fading channel.

As observed in Figure 4.5, the proposed joint CIR, CFO and SFO estimation algorithm provides a near-optimum receiver performance that is very close to the *ideal* BER performance.

Figure 4.6 shows the BER performance of the proposed approach versus SNR values under different MIMO configurations. Curve A shows unacceptable BER performance in the absence of coarse CFO and SFO estimator. These results illustrate that bad guesses of CFO and SFO lead to wrong convergence of the proposed estimation scheme in the presence of large residual CFO and SFO values. Also, without CFO and SFO compensation, the dominant effect of ICI keeps BER at around 5E-2 under SNR > 10 dB (Curve B). With the aid of the coarse CFO-SFO estimator and the CFO-SFO compensators, the proposed estimation and tracking algorithm (Curves D and G) is able to provide a near-optimum BER performance that is very close to the ideal BER one.

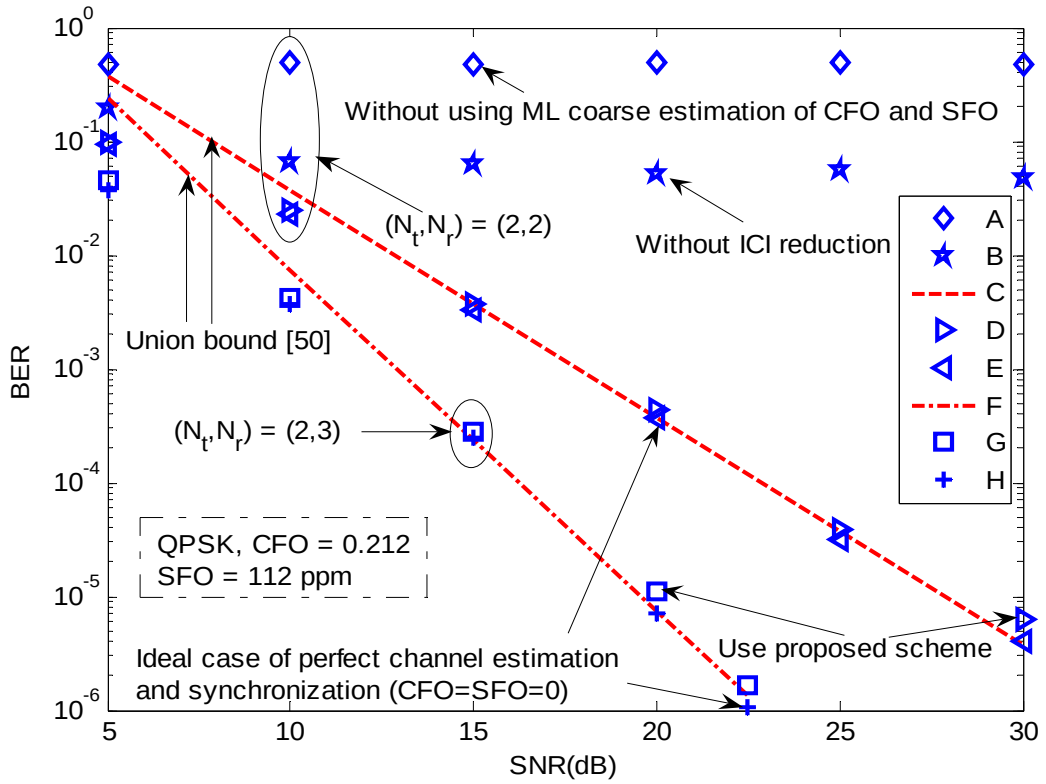

Figure 4.6: BER performance of the MIMO-ML sub-carrier detector versus SNR with QPSK constellation over Rayleigh fading channel.

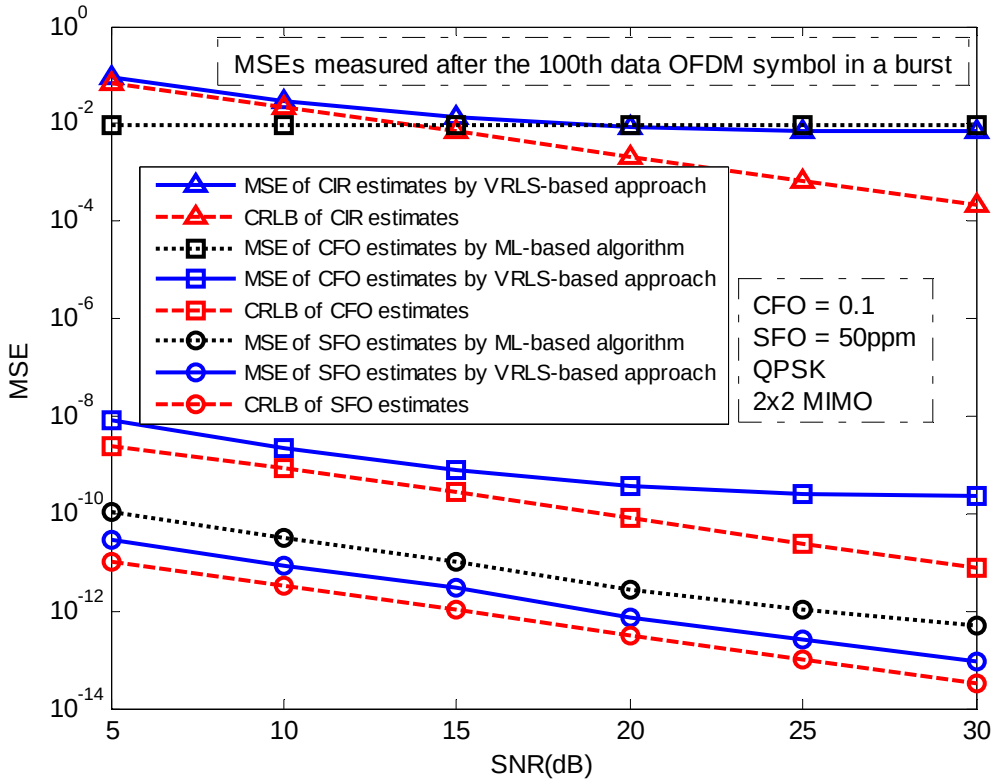

Figure 4.7: MSEs and CRLBs of CIR, CFO and SFO estimates by the proposed VRLS-based approach and the ML-based algorithm [31] under RMS delay spread of 150ns.

To investigate the proposed VRLS-based tracking approach in a more critical channel scenario with RMS delay spread of 150ns, Figures 4.7 shows the MSE performance of the VRLS-based approach with $\lambda = 0.995$ and $\gamma = 10$ under various SNR values. As can be seen in Figure 4.7, the CFO and SFO estimates by the VRLS-based approach are more accurate than those by the ML-based algorithm [31] that assumes perfect channel estimation has been established priori to the CFO and SFO estimation.

4.5 Chapter Summary

For multi-antenna channel estimation and synchronization in MIMO scenarios, the vector RLS algorithm [49] was deployed to function as an adaptive filter with multiple outputs instead of the standard RLS-based adaptive filter [8] with a single output. Based on the vector RLS algorithm, a pilot-aided approach was proposed to

perform the joint estimation of CIR, CFO and SFO for burst-mode MIMO-OFDM systems over quasi-static Rayleigh multi-path fading channels. With the aid of a coarse CFO-SFO estimator and CFO-SFO compensators, the proposed vector RLS-based estimation and tracking approach is able to attain fast convergence, high stability and low MSE values when compared with CRLB values. As a result, over large ranges of CFO and SFO values, the proposed vector RLS-based estimation approach provides a near-optimum BER performance that is remarkably close to the ideal one in the case of perfect channel estimation and synchronization. Finally, the proposed estimation and tracking approach is compatible with any space-time coded transmission.

Chapter 5

Turbo Processing for Joint Channel Estimation, Synchronization and Decoding in MIMO-OFDM Systems

As previously mentioned in Chapter 4, the integration of MIMO and OFDM techniques has offered spectacular benefits to broadband wireless communication transmissions. For further improvement in the performance of coded MIMO-OFDM systems, turbo processing has been well recognized as a very strong solution to perform channel estimation and decoding in an iterative fashion [62]. In fact, the principle behind the astonishing performance of turbo processing is the iterative exchange of extrinsic *a posteriori* probabilities (soft information) among constituent functional blocks in MIMO-OFDM receivers. Focusing on the issue, Chapter 5 introduces a turbo joint channel estimation, synchronization and decoding scheme for convolutionally coded MIMO-OFDM systems. Finally, various simulation results are presented to verify its expected performance.

5.1 Introduction

Feedback processing has been extensively employed in turbo engines as well as electronics circuits to give better performance. Similarly, the same concept can also be beneficially used in decoding, giving rise to the so-called turbo decoding. Indeed, the invention of the turbo codes [52] in 1993 has been widely recognized as one of the most revolutionary milestones in the world of encoding and decoding techniques. Specifically, such codes have a performance [52] that is extremely close to the Shannon limit, and also inspire the use of the extrinsic *a posteriori* probabilities (soft

information) for feedback processing. This turbo principle can be employed for a variety of signal processing tasks such as in detection, equalization, interference cancellation, synchronization as well as channel estimation.

The use of the turbo principle for detection, equalization and interference cancellation has been intensively explored in the last decade [53]-[59]. Recently, some turbo algorithms have been proposed for channel estimation and synchronization in coded OFDM systems [60]-[66]. In particular, [63]-[66] exploit using soft estimates of the data tones to iteratively enhance the channel estimation in SISO-OFDM systems under the assumption that perfect synchronization has been established. Unlike these studies, [62] employs a semi-blind channel estimation scheme using hard estimates of data tones to successively improve the channel estimates in a MIMO-OFDM receiver with a turbo decoder. Taking both channel estimation and synchronization into account, [60]-[61] investigate turbo algorithms for estimating the channel impulse response (CIR) and carrier frequency offset (CFO) but without considering the sampling frequency offset (SFO) effect in *single-input single-output* OFDM systems. However, as demonstrated in [47], the detrimental effect of SFO (even for a very small SFO) will likely lead to a significant degradation to the OFDM receiver performance even when perfect CIR and CFO knowledge are available. Specifically, SFO induces a sampling delay that drifts linearly in time over an OFDM symbol. Without any SFO compensation, this delay hampers the OFDM receiver as soon as the product of the relative SFO and the number of subcarriers becomes comparable to one [36]. Consequently, OFDM receivers become more vulnerable to the SFO effect as the used FFT size increases.

To the best of our knowledge, all existing turbo algorithms for either joint or sequential estimation of the channel response and frequency offset in *coded* OFDM system

have not taken care of the SFO effect. In this chapter, we propose a turbo scheme for joint estimation of CIR, CFO and SFO in a convolutionally coded MIMO-OFDM system with the transmitter configuration based on that in [67]. In particular, with the aid of the vector RLS algorithm [49], the proposed turbo estimation scheme exploits the soft estimates of the data tones obtained by using the extrinsic APPs at the outputs of the soft-input soft-output decoder [68] to successively enhance the estimates of CIR, CFO and *SFO* and in turn the overall receiver performance.

The major advantages of using the soft estimates of data tones are two-folds. First, they eliminate the need of pilot tones which have to be embedded among data tones in an OFDM symbol, thus enhancing the spectral efficiency of MIMO-OFDM systems. Second, the use of the soft estimates alleviates the detrimental effect of error propagation that usually occurs when the hard estimates are used in feedback processing, i.e, decision-directed modes. Finally, simulation results demonstrate that the proposed turbo joint channel estimation, synchronization and decoding scheme is able to provide fast convergence and a near-ideal BER performance that is remarkably close to the performance in the case of perfect channel estimation and synchronization.

5.2 System Model

Figure 4.1 shows a simplified block diagram of a convolutionally coded MIMO-OFDM transmitter with N_t transmit antennas and M-ary modulation (e.g., M-QAM). This receiver configuration is similar to the space-time bit-interleaved coded modulation (STBICM) [67]. The input bit stream is first convolutionally encoded before being serial-to-parallel (S/P) converted to N_t sequences. These sequences are bit-wise interleaved independently to yield the N_t bit streams d_i^u with $u = 1,..., N_t$ before being converted to N_t sequences of Q-bit tuples, $\{\mathbf{d}_{m,k}^u\}$, where

$\mathbf{d}_{m,k}^{u} = [d_{m,k,q}^{u}, q = 0,1,...,Q-1]$ with $u = 1,...,N_t$ and $Q = \log_2 M$ bits. Following this, each *Q*-bit tuple, $\mathbf{d}_{m,k}^{u}$, is mapped to a complex-valued symbol, $X_{u,m}(k) \in \mathbf{A}$, where **A** is the M-ary modulation signaling set, and *u*, *m* and *k* denote the indices of the transmit antennas, OFDM symbols and sub-carriers, respectively. Each OFDM symbol consists of $K<N$ information bearing sub-carriers, where *N* is FFT size. After cyclic prefix (CP) insertion and digital-to-analogous converter (DAC), the transmitted baseband signal at the *u*-th transmit antenna can be written as

$$s_u(t) = \frac{1}{N} \sum_{m=-\infty}^{+\infty} \sum_{k=-K/2}^{K/2-1} X_{u,m}(k) e^{j\frac{2\pi k}{NT}(t - T_g - mT_s)} U(t - mT_s), \tag{5.1}$$

where *T* is the sampling period at the output of IFFT, N_g denotes the number of CP samples, $T_g = N_g T$, $T_s = (N + N_g)T$ is the OFDM symbol length after CP insertion, $u(t)$ is the unit step function, and $U(t) = u(t) - u(t - T_s)$.

As previously described in Chapter 4, the quasi-static channel response between the *u*-th transmit antenna and the *v*-th receive antenna can be represented by

$$h_{u,v}(\tau) = \sum_{l=0}^{L-1} \tilde{h}_{u,v,l} \delta(\tau - \tau_l), \tag{5.2}$$

where $\tilde{h}_{u,v,l}$ and τ_l are the complex gain and delay of the *l*-th path, respectively. *L* is the total number of resolvable (effective) paths.

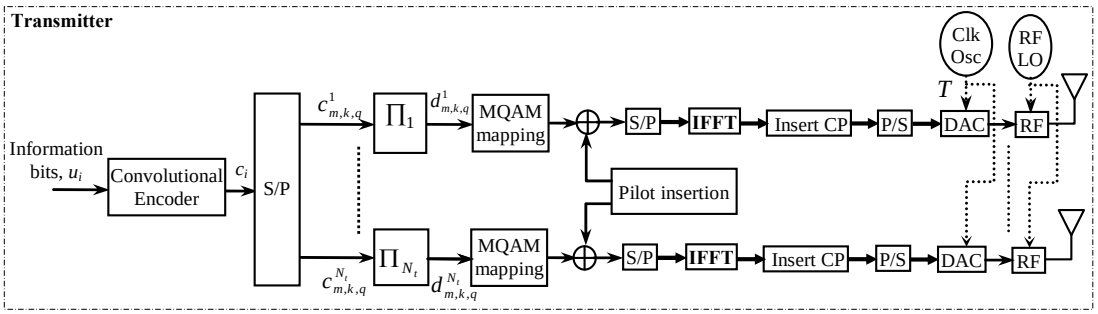

Figure 5.1: Burst-mode coded MIMO-OFDM transmitter.

In the presence of the net CFO Δf (as mentioned in Chapter 4), the received signal at the *v*-th receive antenna element can be determined by

$$r_v(t) = e^{j2\pi\Delta ft}\sum_{u=1}^{N_t}\sum_{l=0}^{L-1}\tilde{h}_{u,v,l}s_u(t-\tau_l)+w_v(t)\,. \tag{5.3}$$

After sampling the received signal $r_v(t)$ at time instant $t_n = nT'$ (due to the presence of SFO) and CP removal, the *n*-th received sample of the *m*-th OFDM symbol in the time-domain at the *v*-th receive antenna element is given by

$$r_{v,m,n} = \frac{e^{j\frac{2\pi}{N}(N_m+n)\varepsilon_\eta}}{N}\sum_{k=-K/2}^{K/2-1}e^{j\frac{2\pi k}{N}n(1+\eta)}e^{j\frac{2\pi k}{N}\eta N_m}\sum_{u=1}^{N_t}X_{u,m}(k)H_{u,v}(k)+w_{v,m,n}\,, \tag{5.4}$$

where $n = 0,1,...,N-1$ and $N_m = N_g + m(N+N_g)$. The complex-valued Gaussian noise sample, $w_{v,m,n}$, has zero mean and a variance of σ^2. $H_{u,v}(k) = \sum_{l=0}^{L-1}h_{u,v,l}e^{-j\frac{2\pi k}{N}l}$ is the channel frequency response (CFR) at the *k*-th sub-carrier for the pair of the *u*-th transmit antenna and the *v*-th receive antenna, and $\mathbf{h}_{u,v} = [h_{u,v,0}\ \ h_{u,v,1}\ \cdots\ h_{u,v,L-1}]^T$ is the corresponding effective channel impulse response (CIR).

After FFT, the received FD sample at the *v*-th receive antenna is $Y_{v,m}(k) = \sum_{n=0}^{N-1}r_{v,m,n}e^{-j\frac{2\pi}{N}nk}$. Based on (5.4), we obtain the following

$$Y_{v,m}(k) = \sum_{i=-K/2}^{K/2-1}e^{j\frac{2\pi}{N}N_m\varepsilon_i}\rho_{i,k}\sum_{u=1}^{N_t}X_{u,m}(i)H_{u,v}(i)+W_{v,m}(k)\,, \tag{5.5}$$

where $\rho_{i,k} = \frac{1}{N}\sum_{n=0}^{N-1}e^{j\frac{2\pi}{N}n(\varepsilon_i+i-k)} \approx \mathrm{sinc}(\varepsilon_i+i-k)e^{j\pi(\varepsilon_i+i-k)}$ stands for the ICI

coefficient, $\varepsilon_i = i\eta + \varepsilon_\eta$, $\mathrm{sinc}(x) = \dfrac{\sin(\pi x)}{(\pi x)}$, and $W_{v,m}(k) = \sum_{n=0}^{N-1} w_{v,m}(n+N_m) e^{-j\frac{2\pi}{N}nk}$.

As discussed in Chapter 4, to mitigate ICI, the received time-domain sample in (5.4) can be multiplied by $e^{-j\frac{2\pi\varepsilon_\eta^c n}{N}}$ prior to FFT as shown in Figure 5.2, where

$$r_{v,m,n}^c = r_{v,m,n} e^{-j\frac{2\pi}{N}n\varepsilon_\eta^c}, \tag{5.6}$$

$\varepsilon_\eta^c = (1+\eta^c)\varepsilon^c$, and ε^c and η^c are the estimates of CFO and SFO, respectively.

After FFT, the resulting FD sub-carriers at the *v*-th receive antenna is

$$Y_{v,m}^c(k) = \sum_{n=0}^{N-1} r_{v,m,n}^c e^{-j\frac{2\pi}{N}nk}. \tag{5.7}$$

After some manipulation, (5.7) can be shown to be

$$Y_{v,m}^c(k) = \sum_{i=-K/2}^{K/2-1} e^{j\frac{2\pi}{N}N_m\varepsilon_i} \rho_{i,k}^c \sum_{u=1}^{N_t} X_{u,m}(i) H_{u,v}(i) + W_{v,m}^c(k), \tag{5.8}$$

where $W_{v,m}^c(k) = \sum_{n=0}^{N-1} w_{v,m}(n+N_m) e^{-j\frac{2\pi}{N}n(1+\eta^c)\varepsilon^c} e^{-j\frac{2\pi}{N}nk}$ and

$$\rho_{i,k}^c = \frac{1}{N}\sum_{n=0}^{N-1} e^{j\frac{2\pi}{N}n\left[\varepsilon_i - (1+\eta^c)\varepsilon^c + i - k\right]}.$$

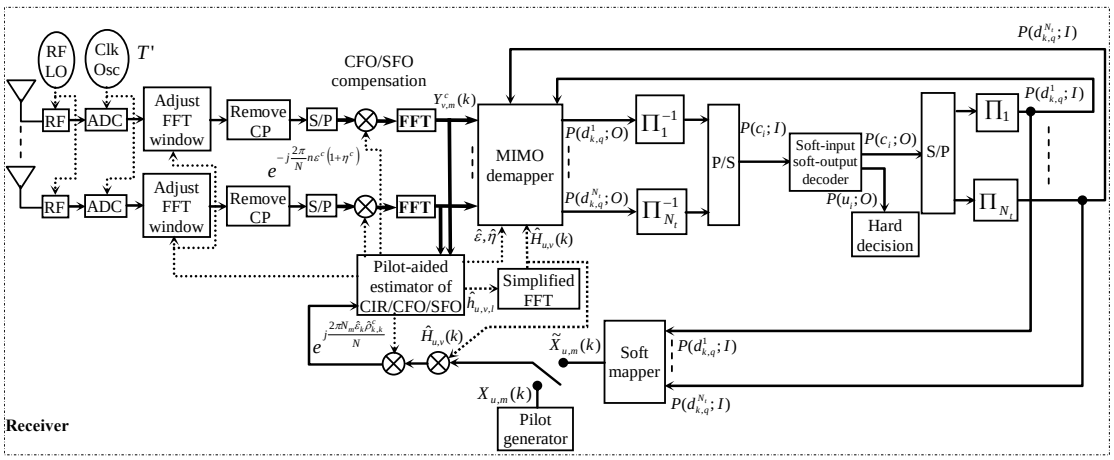

Figure 5.2: Burst-mode MIMO-OFDM receiver using the proposed turbo joint channel estimation, synchronization and decoding scheme.

The vector representation of the FD received samples at all receive antennas corresponding to the subcarrier *k* can be expressed by

$$\mathbf{Y}_m^c(k) = e^{j\frac{2\pi}{N}N_m\varepsilon_k}\rho_{k,k}^c\mathbf{H}(k)\mathbf{X}_m(k) + \tilde{\mathbf{W}}_m^c(k), \tag{5.9}$$

where the (*u*,*v*)-th entry of $\mathbf{H}(k)$ is given by $[\mathbf{H}(k)]_{u,v} = H_{u,v}(k)$. Note that $\tilde{\mathbf{W}}_m^c(k)$ includes both AWGN and ICI parts, $\mathbf{X}_m(k) = [X_{1,m}(k)\cdots X_{N_t,m}(k)]^T$ and each of the complex elements in $\tilde{\mathbf{W}}_m^c(k)$ has a variance of N_0.

5.3 Turbo Processing

In the section, we describe in details the proposed turbo joint channel estimation, synchronization and decoding scheme. To give an overall picture of the turbo processing in the proposed receiver, Figure 5.3 shows an information-flow graph for illustrating how the extrinsic *a posteriori* probabilities (APPs) are iteratively exchanged among the constituent functional blocks in the receiver.

First, the initial estimates of CIR, CFO and SFO are obtained by using pilot tones in the preamble. These initial CIR, CFO, SFO estimates are fed into the MIMO-demapper to generate the (initial) extrinsic APPs of the coded bits $d_{m,k,q}^u$. This is denoted by $P(d;O)$ in the figure, where, for the sake of notational simplicity, the subscripts *u*, *m*, *k* and *q* in $d_{m,k,q}^u$ have been omitted in $P(d;O)$ and the notation is based on [68]. Subsequently, after deinterleaving and P/S converter, the extrinsic APPs $P(d;O)$ become $P(c;I)$ to be used as input *a priori* probabilities of the soft-input soft-output decoder [68]. Based on these $P(c;I)$ values, this soft-input soft-output module generates more reliable soft estimates of the coded bits $P(c;O)$. After S/P converter and interleaving, the extrinsic APPs $P(c;O)$ become $P(d;I)$ to be used

as *a priori* probabilities of the MIMO-demapper (at the next iteration) and the soft mapper.

Lastly, based on the more reliable soft estimates of the coded bits $P(d;I)$, the resulting better soft estimates of data tones generated by the soft mapper are fed to the joint CIR, CFO and SFO estimator to generate better CIR, CFO and SFO estimates for the MIMO-demapper at the next iteration.

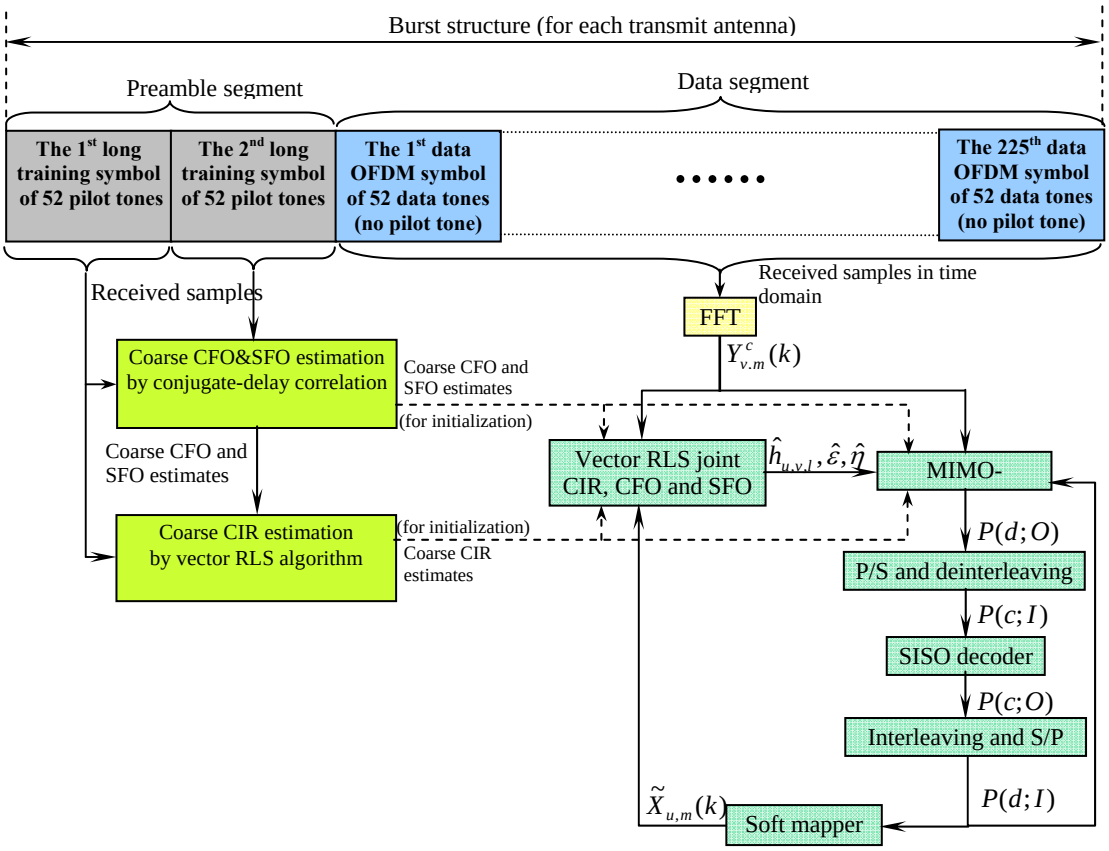

Figure 5.3: Turbo processing for joint channel estimation, synchronization and decoding.

Naturally, by using the better CIR, CFO and SFO estimates and more reliable soft estimates of the coded bits $P(d;I)$, the MIMO-demapper will generate more reliable soft estimates of the coded bits $d^u_{m,k,q}$ in the next iteration of this turbo processing. In other words, the turbo processing procedure operates in an iterative fashion over a block of interleaved bits to successively produce better estimates of CIR, CFO and SFO, which in turn, give more reliable soft estimates of coded and transmitted infor-

mation bits, which then produce better CIR, CFO and SFO estimates, and so on. The following describes the constituent functional blocks in the information-flow graph of Figure 5.3 in more details.

5.3.1 MIMO- Demapper

The goal of the MIMO-demapper is to compute the extrinsic *a posteriori* probabilities of coded bits to be used as input *a priori* probabilities for the soft-input soft-output decoder in [68]. Following the notation used in [68], the extrinsic APP of the coded bits at the output of MIMO-demapper can be defined as follows.

$$P(d^u_{m,k,q}=b;O)=\frac{P\left(d^u_{m,k,q}=b\middle|\mathbf{Y}^c_m(k),\hat{\mathbf{H}}(k),\hat{\varepsilon},\hat{\eta}\right)}{P(d^u_{m,k,q}=b;I)}, \tag{5.10}$$

where $b\in\{0,1\}$, and the letters *I* and *O* denote, respectively, the input and output of the soft-input soft-output decoder as well as the MIMO-demapper. In particular, the term $P\left(d^u_{m,k,q}=b\middle|\mathbf{Y}^c_m(k),\hat{\mathbf{H}}(k),\hat{\varepsilon},\hat{\eta}\right)$ can be determined by using

$$P\left(d^u_{m,k,q}=b\middle|\mathbf{Y}^c_m(k),\hat{\mathbf{H}}(k),\hat{\varepsilon},\hat{\eta}\right)=\sum_{\mathbf{x}\in\mathbf{X}^{(b)}_{u,m,k,q}}P\left(\mathbf{X}_m(k)=\mathbf{x}\middle|\mathbf{Y}^c_m(k),\hat{\mathbf{H}}(k),\hat{\varepsilon},\hat{\eta}\right), \tag{5.11}$$

where $\mathbf{X}^{(b)}_{u,m,k,q}$ is the set of the vectors $\mathbf{X}_m(k)=\left[X_{1,m}(k)\cdots X_{N_t,m}(k)\right]^T$ that corresponds to $d^u_{m,k,q}=b$,

$$P\left(\mathbf{X}_m(k)=\mathbf{x}\middle|\mathbf{Y}^c_m(k),\hat{\mathbf{H}}(k),\hat{\varepsilon},\hat{\eta}\right)=\frac{P\left(\mathbf{Y}^c_m(k)\middle|\mathbf{X}_m(k)=\mathbf{x},\hat{\mathbf{H}}(k),\hat{\varepsilon},\hat{\eta}\right)P\left(\mathbf{X}_m(k)=\mathbf{x}\right)}{P\left(\mathbf{Y}^c_m(k)\right)},$$

$$P\left(\mathbf{Y}^c_m(k)\middle|\mathbf{X}_m(k)=\mathbf{x},\hat{\mathbf{H}}(k),\hat{\varepsilon},\hat{\eta}\right)=\left(\frac{1}{\pi N_0}\right)^{N_r}e^{-\frac{\left\|\mathbf{Y}^c_m(k)-e^{j\frac{2\pi}{N}N_m\hat{\varepsilon}_k}\hat{\rho}^c_{k,k}\hat{\mathbf{H}}(k)\mathbf{x}\right\|^2}{N_o}},$$

$P\left(\mathbf{Y}_m^c(k)\right) = \sum_{\mathbf{x}\in\breve{\mathbf{X}}_m} P\left(\mathbf{Y}_m^c(k)\middle|\mathbf{X}_m(k)=\mathbf{x},\hat{\mathbf{H}}(k),\hat{\varepsilon},\hat{\eta}\right)P\left(\mathbf{X}_m(k)=\mathbf{x}\right)$ with $\breve{\mathbf{X}}_m$ being the set of all possible values of the vector $\mathbf{X}_m(k)$,

$P\left(\mathbf{X}_m(k)=\mathbf{x}\right) = \prod_u \prod_q P(d_{m,k,q}^u = d_{m,k,q}^u(\mathbf{x}); I)$ due to the use of interleaving and

$d_{m,k,q}^u(\mathbf{x})$ denotes the value of the corresponding bit $d_{m,k,q}^u$ in the vector **x**.

5.3.2 Soft-Input Soft-Output Decoder

The purpose of soft-input soft-output module is to obtain more reliable soft estimates of the coded bits $P(c;O)$ based on the *a priori* probabilities $P(c;I)$ and knowledge of the trellis section used for convolutional encoding at transmitter. Detailed operations of $P(c;O)$ is well documented in [68]. In addition, the soft-input soft-output decoding with turbo processing also generates more reliable soft estimates of transmitted information bits after each iteration of turbo processing.

5.3.3 Soft Mapper

Based on the extrinsic APPs of the coded bits at the outputs of the soft-input soft-output decoder, these soft estimates of data tones can be simply obtained by

$$\tilde{\mathbf{X}}_m(k) = E\left[\mathbf{X}_m(k)\right] = \sum_{\mathbf{x}\in\breve{\mathbf{X}}_m} \mathbf{x}P\left(\mathbf{X}_m(k)=\mathbf{x}\right). \qquad (5.12)$$

In turbo processing, the reliabilities of the soft estimates of the coded bits are successively enhanced due to the spectacular benefits of the iterative extrinsic APP exchanges. As a result, soft estimates of the data tones will also become successively more reliable. Naturally, this gives better overall BER performance after each iteration.

5.3.4 Semi-Blind Joint CIR, CFO and SFO Estimation

By using the received samples, pilot tones (only for initialization in the preamble duration) and soft estimates of the data tones in the frequency domain, a turbo joint channel estimation and synchronization scheme can be used with the aid of the vector RLS algorithm [49] to estimate and track the CIR, CFO and SFO in convolutionally coded MIMO-OFDM systems. To exploit the vector RLS algorithm [49] for this estimation and tracking task, we introduce a least square (LS) cost function corresponding to the use of *i* soft estimates of data tones and pilot tones (only for initialization during preamble duration) over OFDM symbols in a burst as follows:

$$C\left(\hat{\mathbf{h}}_{u,v}^{(i)}, \hat{\varepsilon}^{(i)}, \hat{\eta}^{(i)}\right) = \sum_{p=1}^{i} \lambda^{i-p} \sum_{v=1}^{N_r} \left| e_{i,p,v} \right|^2 , \tag{5.13}$$

where λ is the forgetting factor, $\hat{\mathbf{h}}_{u,v}^{(i)} = \left[\hat{h}_{u,v,0}^{(i)}, \hat{h}_{u,v,1}^{(i)}, ... \hat{h}_{u,v,L-1}^{(i)}\right]^T$, $u = 1,..., N_t$, $v = 1,..., N_r$, $p = 1,..., i$ denotes the *p*-th tone index in the set of *i* tone indices used for this adaptive estimation,

$$e_{i,p,v} = Y_{v,m_p}^{c}\left(k_p\right) - f_v\left(\tilde{X}_{u,m_p}\left(k_p\right), \hat{\boldsymbol{\omega}}_i\right),$$

$$f_v\left(\tilde{X}_{u,m_p}\left(k_p\right), \hat{\boldsymbol{\omega}}_i\right) = e^{j\frac{2\pi}{N} N_{m_p} \hat{\varepsilon}_{k_p}^{(i)}} \hat{\rho}_{k_p}^{c} \sum_{u=1}^{N_t} \tilde{X}_{u,m_p}(k_p) \hat{H}_{u,v}^{(i)}(k_p),$$

$$\hat{H}_{u,v}^{(i)}(k_p) = \sum_{l=0}^{L-1} \hat{h}_{u,v,l}^{(i)} e^{-j\frac{2\pi k_p l}{N}}, \qquad \hat{\varepsilon}_{k_p}^{(i)} = k_p \hat{\eta}^{(i)} + (1+\hat{\eta}^{(i)})\hat{\varepsilon}^{(i)},$$

$$\hat{\rho}_{k_p}^{c} = \frac{1}{N} \sum_{n=0}^{N-1} e^{j\frac{2\pi}{N} n\left[k_p \hat{\eta}^{(i)} + (1+\hat{\eta}^{(i)})\hat{\varepsilon}^{(i)} - (1+\eta^c)\varepsilon^c\right]}.$$

$\tilde{X}_{u,m_p}\left(k_p\right)$ is the value of the *p*-th *soft* estimate of data tone or pilot tone (only for initialization) at sub-carrier k_p of the m_p^{th} OFDM symbol from the *u*-th transmit antenna in this adaptive estimation.

To exploit the vector RLS algorithm [49] for the joint estimation of unknown CIR, CFO and SFO, the non-linear estimation error $e_{i,p,v}$ needs to be linearized about the existing estimates of CIR, CFO and SFO by using the following first-order Taylor's series approximation:

$$e_{i,p,v} \approx Y^{c}_{v,m_p}(k_p) - \left\{ f_v\left(\tilde{X}_{u,m_p}(k_p), \hat{\boldsymbol{\omega}}_{i-1}\right) + \nabla f_v^{T}\left(\tilde{X}_{u,m_p}(k_p), \hat{\boldsymbol{\omega}}_{i-1}\right)\left(\hat{\boldsymbol{\omega}}_i - \hat{\boldsymbol{\omega}}_{i-1}\right)\right\}, \quad (5.14)$$

where the $(2LN_tN_r+2)\times 1$ weight vector $\hat{\boldsymbol{\omega}}_i = \left[\hat{\omega}_{i,0}\ \ \hat{\omega}_{i,1}\ \ \ldots\ \ \hat{\omega}_{i,2LN_tN_r+1}\right]^T$ contains the CIR, CFO and SFO estimates at time instant *i* of the vector RLS algorithm. More specifica-lly, elements of $\hat{\boldsymbol{\omega}}_i$ are assigned as follows:

$$\hat{\omega}_{i,l+2L(u-1)+2LN_t(v-1)} = \mathrm{Re}\left\{\hat{h}^{(i)}_{u,v,l}\right\},\ \hat{\omega}_{i,l+L+2L(u-1)+2LN_t(v-1)} = \mathrm{Im}\left\{\hat{h}^{(i)}_{u,v,l}\right\},\ \hat{\omega}_{i,2LN_tN_r} = \hat{\varepsilon}^{(i)}$$

and $\hat{\omega}_{i,2LN_tN_r+1} = \hat{\eta}^{(i)}$ with $u = 1,\ldots,N_t$, $v = 1,\ldots,N_r$ and $l = 0,\ldots,L-1$.

The gradient vector of $f_v\left(\tilde{X}_{u,m_p}(k_p), \hat{\boldsymbol{\omega}}_{i-1}\right)$ corresponding to the *v*-th receive antenna is determined by

$$\nabla f_v\left(\tilde{X}_{u,m_p}(k_p), \hat{\boldsymbol{\omega}}_{i-1}\right) = \left[\frac{\partial f_v\left(\tilde{X}_{u,m_p}(k_p), \hat{\boldsymbol{\omega}}_{i-1}\right)}{\partial \hat{\omega}_{i-1,0}} \ \cdots\ \frac{\partial f_v\left(\tilde{X}_{u,m_p}(k_p), \hat{\boldsymbol{\omega}}_{i-1}\right)}{\partial \hat{\omega}_{i-1,2LN_tN_r+1}}\right]^T, \quad (5.15)$$

where $\dfrac{\partial f_v\left(\tilde{X}_{u,m_p}(k_p), \hat{\boldsymbol{\omega}}_i\right)}{\partial \hat{\omega}_{i,l+2L(u-1)+2LN_t(v-1)}} = \tilde{X}_{u,m_p}(k_p) e^{-j\frac{2\pi l k_p}{N}} e^{j\frac{2\pi}{N}N_m\hat{\varepsilon}^{(i)}_{k_p}} \hat{\rho}^{c}_{k_p}$, $l = 0,\ldots,L-1$,

$$\frac{\partial f_v\left(\tilde{X}_{u,m_p}(k_p), \hat{\boldsymbol{\omega}}_i\right)}{\partial \hat{\omega}_{i,l+L+2L(u-1)+2LN_t(v-1)}} = j\frac{\partial f_v\left(\tilde{X}_{u,m_p}(k_p), \hat{\boldsymbol{\omega}}_i\right)}{\partial \hat{\omega}_{i,l+2L(u-1)+2LN_t(v-1)}},$$

$$\frac{\partial f_v\left(\tilde{X}_{u,m_p}(k_p), \hat{\boldsymbol{\omega}}_i\right)}{\partial \hat{\omega}_{i,2LN_tN_r}} = \left(1+\hat{\eta}^{(i)}\right)\Omega_{i,p,v},$$

$$\Omega_{i,p,v} = e^{j\frac{2\pi}{N}N_m\hat{\varepsilon}^{(i)}_{k_p}}\left[j\frac{2\pi}{N}N_m\hat{\rho}^{c}_{k_p} + \frac{1}{N}\sum_{n=0}^{N-1} j\frac{2\pi}{N}n e^{j\frac{2\pi}{N}n\left[\hat{\varepsilon}^{(i)}_{k_p}-\varepsilon^{c}_{\eta}\right]}\right]\sum_{u=1}^{N_t}\tilde{X}_{u,m_p}(k_p)\hat{H}^{(i)}_{u,v}(k_p),$$

$$\frac{\partial f_v\left(\tilde{X}_{u,m_p}(k_p),\hat{\boldsymbol{\omega}}_i\right)}{\partial \hat{\omega}_{i,2LN_tN_r+1}} = \left(k_p + \hat{\varepsilon}^{(i)}\right)\Omega_{i,p,v},\ u = 1,..,N_t.$$

Note that for $\rho = 1,...,N_r$ and $\rho \neq v$,

$$\frac{\partial f_v\left(\tilde{X}_{u,m_p}(k_p),\hat{\boldsymbol{\omega}}_i\right)}{\partial \hat{\omega}_{i,l+2L(u-1)+2LN_t(\rho-1)}} = 0, \quad \frac{\partial f_v\left(\tilde{X}_{u,m_p}(k_p),\hat{\boldsymbol{\omega}}_i\right)}{\partial \hat{\omega}_{i,l+L+2L(u-1)+2LN_t(\rho-1)}} = 0.$$

Subsequently, the proposed vector RLS-based joint CIR, CFO and SFO estimation using soft estimates of data tones can be formulated as follows.

Initialization: $\mathbf{P}_1 = \gamma^{-1}\mathbf{I}_{2LN_rN_t+2}$, where γ is the regularization parameter.

Iterative Procedure: At the *i*-th iteration with the forgetting factor λ, update

Parameters:

$$\mathbf{X}_{i,N_r} = \left[\nabla f_1\left(\tilde{X}_{u,m_i}(k_i),\hat{\boldsymbol{\omega}}_{i-1}\right) \ \cdots \ \nabla f_{N_r}\left(\tilde{X}_{u,m_i}(k_i),\hat{\boldsymbol{\omega}}_{i-1}\right)\right], \quad (5.16)$$

$$\mathbf{K}_i = \mathbf{P}_{i-1}\mathbf{X}^*_{i,N_r}\left(\lambda\mathbf{I}_{N_r} + \mathbf{X}^T_{i,N_r}\mathbf{P}_{i-1}\mathbf{X}^*_{i,N_r}\right)^{-1}, \quad (5.17)$$

$$\mathbf{P}_i = \lambda^{-1}\left(\mathbf{P}_{i-1} - \mathbf{K}_i\mathbf{X}^T_{i,N_r}\mathbf{P}_{i-1}\right), \quad (5.18)$$

$$\mathbf{e}_{i,N_r} = \left[\left(Y^c_{1,m_i}(k_i) - f_1\left(\tilde{X}_{u,m_i}(k_i),\hat{\boldsymbol{\omega}}_{i-1}\right)\right)...\left(Y^c_{N_r,m_i}(k_i) - f_{N_r}\left(\tilde{X}_{u,m_i}(k_i),\hat{\boldsymbol{\omega}}_{i-1}\right)\right)\right]^T, u = 1,...,N_t \quad (5.19)$$

Estimates: $$\hat{\boldsymbol{\omega}}_i = \hat{\boldsymbol{\omega}}_{i-1} + \mathbf{K}_i\mathbf{e}_{i,N_r}, \quad (5.20)$$

5.3.5. Coarse CFO and SFO estimation

Accurate yet simple coarse estimation of CFO and SFO can be based on the conjugate-delay correlation of the two *identical* and *known* training sequences in the pre-amble of the burst (as shown in Figure 5.3), i.e., based on (5.4), we can obtain the following approximation

$$E\left\{r_{v,m_2,n}r^*_{v,m_1,n}\right\}\approx\frac{e^{j\frac{2\pi}{N}\left(N+N_g\right)\varepsilon_\eta}}{N^2}\left|\sum_{k=-K/2}^{K/2-1}e^{j\frac{2\pi k}{N}n(1+\eta)}e^{j\frac{2\pi k}{N}\eta N_{m_1}}\sum_{u=1}^{N_t}X_{u,m_1}(k)H_{u,v}(k)\right|^2, \tag{5.21}$$

where m_1 and $m_2=m_1+1$ denote the indices of the 1st and 2nd training sequences. Therefore, the combined CFO-SFO perturbation is

$$\hat{\varepsilon}_\eta=\frac{N}{2\pi\left(N+N_g\right)}\Phi\left[E\left\{r_{v,m_2,n}r^*_{v,m_1,n}\right\}\right]. \tag{5.22}$$

where $\Phi\left[E\left\{r_{v,m_2,n}r^*_{v,m_1,n}\right\}\right]$ is the angle of $E\left\{r_{v,m_2,n}r^*_{v,m_1,n}\right\}$. Under the assumption of $\eta<<1$ (e.g., for a typical SFO values of around 50ppm or 5E-5 in practice), and the use of the two *identical* long training sequences in the pre-amble of a burst, the coarse (initial) CFO and SFO estimates can be determined separately by

$$\hat{\varepsilon}=\frac{1}{2\pi\left(N+N_g\right)N_r}\Phi\left[\sum_{v=1}^{N_r}\sum_{n=0}^{N-1}r_{v,m_2,n}r^*_{v,m_1,n}\right]. \tag{5.23}$$

and

$$\hat{\eta}=0 \tag{5.24}$$

where $\Phi\left[\sum_{v=1}^{N_r}\sum_{n=0}^{N-1}r_{v,m_2,n}r^*_{v,m_1,n}\right]$ is the angle of $\sum_{v=1}^{N_r}\sum_{n=0}^{N-1}r_{v,m_2,n}r^*_{v,m_1,n}$ .The above coarse CFO and SFO estimates are then used in the coarse CIR estimation that employs the vector RLS algorithm with the known $\mathbf{X}_m(k)$'s during the pre-amble.

5.4 Simulation Results and Discussions

Computer simulation has been conducted to evaluate the performance of the proposed turbo joint channel estimation, synchronization and decoding scheme for a convolutionally coded MIMO-OFDM system. In the simulation, we set the OFDM-related

parameters similar to the IEEE standard 802.11a [38]. Signal constellation of QPSK is employed for OFDM symbols of 52 data tones. For convolutional encoding at transmitter, the rate-1/2 non-recursive systematic code is employed. At the receiver, the soft-input soft-output decoding algorithm [68] is deployed to generate soft estimates of transmitted data bits as well as the extrinsic *a posteriori* probabilities of coded bits for turbo processing in the joint CIR, CFO and SFO estimation. For each transmit-receive antenna pair, we consider an exponentially decaying Rayleigh fading channel with a channel length of 5 and a RMS delay spread of 25ns.

Figure 5.4 shows the measured mean squared errors (MSE) of the CIR estimate and relevant Cramer-Rao lower bounds (CRLBs). The numerical results demonstrate that the proposed estimation algorithm has a fast convergence and the best MSE performance with forgetting factor $\lambda = 1$ and regularization parameter $\gamma = 10$. For comparison, the CRLB values of the CIR estimates obtained by using pilot-aided estimation with *perfect* information of 4 pilot tones (a pilot design in IEEE standard 802.11a [38]) and of *all* (52) tones in each data OFDM symbol are also plotted in Figure 5.4. As can be seen in Figure 5.4, the numerical results show that the MSE values of the CIR estimates obtained by the proposed turbo estimation scheme using just 1 APP exchange iteration are even smaller than the lower bound (CRLB as derived in Appendix E) of the CIR estimates obtained by pilot-aided joint CIR, CFO and SFO estimation using 4 pilots in each OFDM symbol. The reason is that the turbo principle (the iterative extrinsic APP exchange) enables the joint CIR, CFO and SFO estimation to exploit efficiently the soft information of *all* (52) data tones in each OFDM symbol. In addition, numerical results show that the turbo estimation scheme converges to its best MSE performance after just 3 APP exchange iterations.

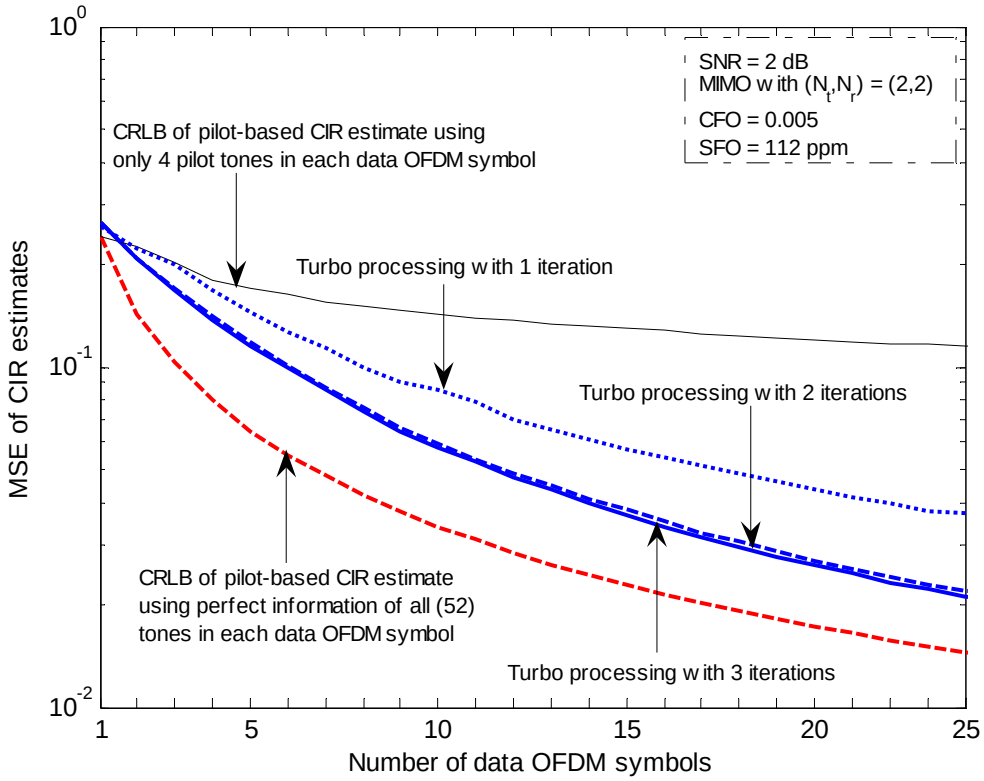

Figure 5.4: MSE and CRLB of CIR estimates.

In the same manner, Figures 5.5 and 5.6 show the MSE results of the CFO and SFO estimates and relevant CRLBs.

Figure 5.7 shows the BER performance of the proposed turbo principle-based scheme with various numbers of iterations of the turbo processing. For reference, the ideal BER performance (Curve E) in the case of perfect channel estimation and synchronization (CFO=SFO=0) is also demonstrated in Figure 5.7. As can be seen, the proposed turbo scheme approaches the ideal BER performance by using just three iterations of turbo processing (Curve D). Also, without the turbo processing, the worst-case BER performance (Curve A) in the case of using only preamble for the vector RLS-based joint channel estimation and synchronization is plotted in Figure 5.7. In particular, without the use of the turbo principle, the vector RLS-based joint channel estimation and synchronization using only pilot tones in preamble (Curve A) results in an unacceptable receiver performance (BER values around 0.5). The reason

is that using only preamble for the vector RLS-based estimation of CIR, CFO and SFO is able to provide just coarse CIR, CFO and SFO estimates (for the subsequent tracking phase) that are not accurate enough for an acceptable performance of the ML symbol detection. As compared with the preamble-aided, vector RLS-based joint channel estimation and synchronization (Curve A), the turbo scheme provides a remarkable BER performance improvement even by using the turbo processing with only 1 iteration (Curve B).

To investigate the effect of CFO and SFO on the performance of the proposed turbo scheme, Figures 5.8 and 5.9 show the BER performance of the proposed turbo algorithm under various CFO and SFO values, respectively. For reference, the ideal BER performance in the case of *perfect* channel estimation and synchronization (i.e., *zero* CFO and SFO) is also plotted. As shown, the proposed turbo estimation scheme is highly robust against a wide range of SFO values.

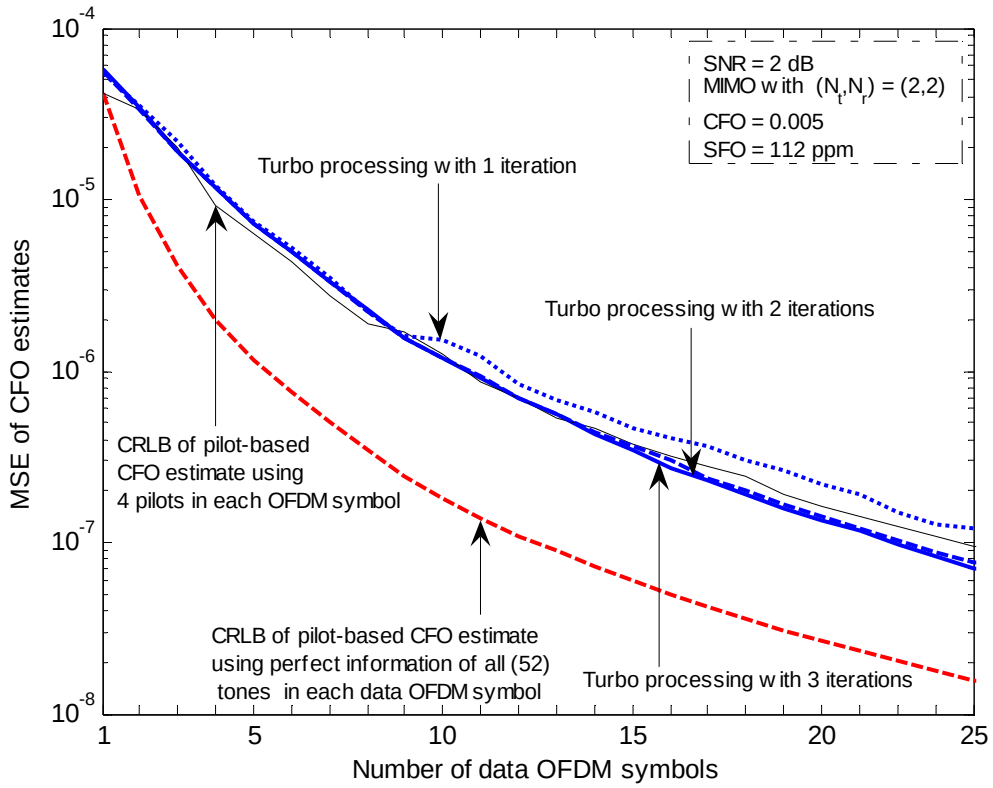

Figure 5.5: MSE and CRLB of CFO estimates.

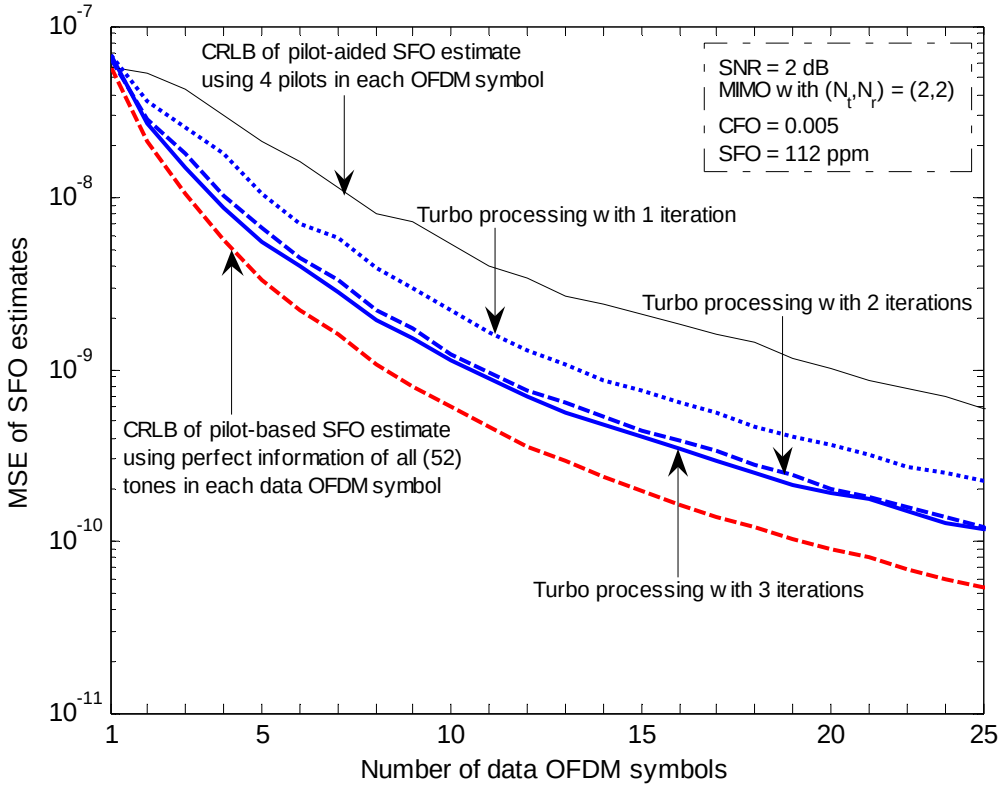

Figure 5.6: MSE and CRLB of SFO estimates.

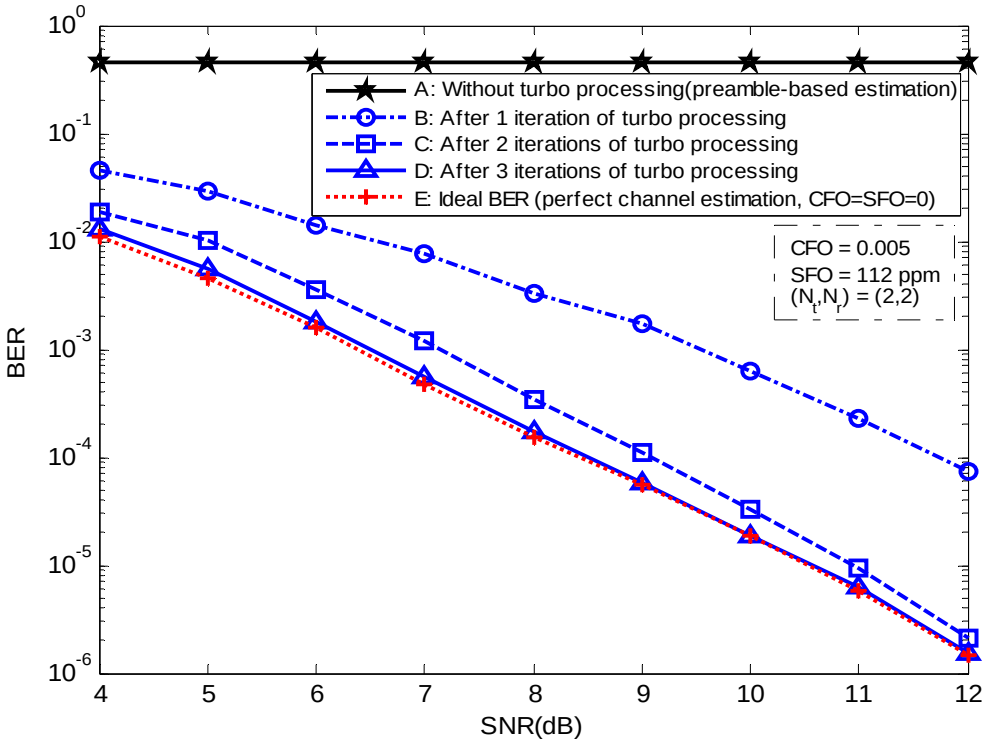

Figure 5.7: BER performance of the proposed turbo scheme.

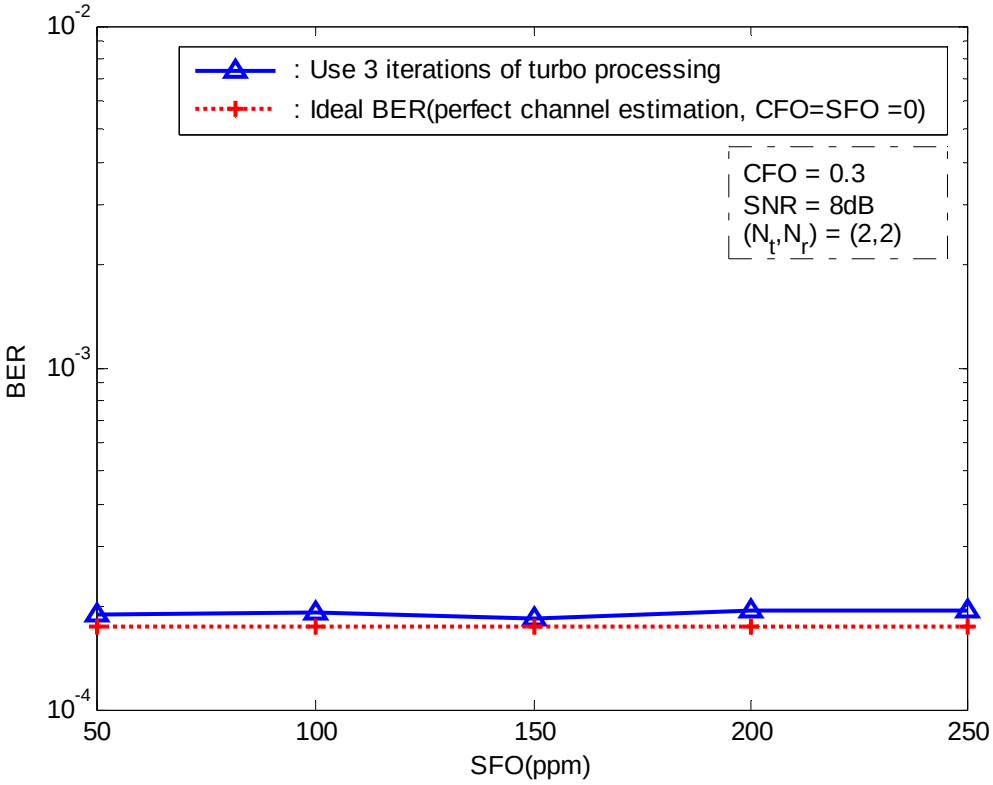

Figure 5.8: BER performance of the proposed turbo joint channel estimation, synchronization and decoding scheme under various SFO values.

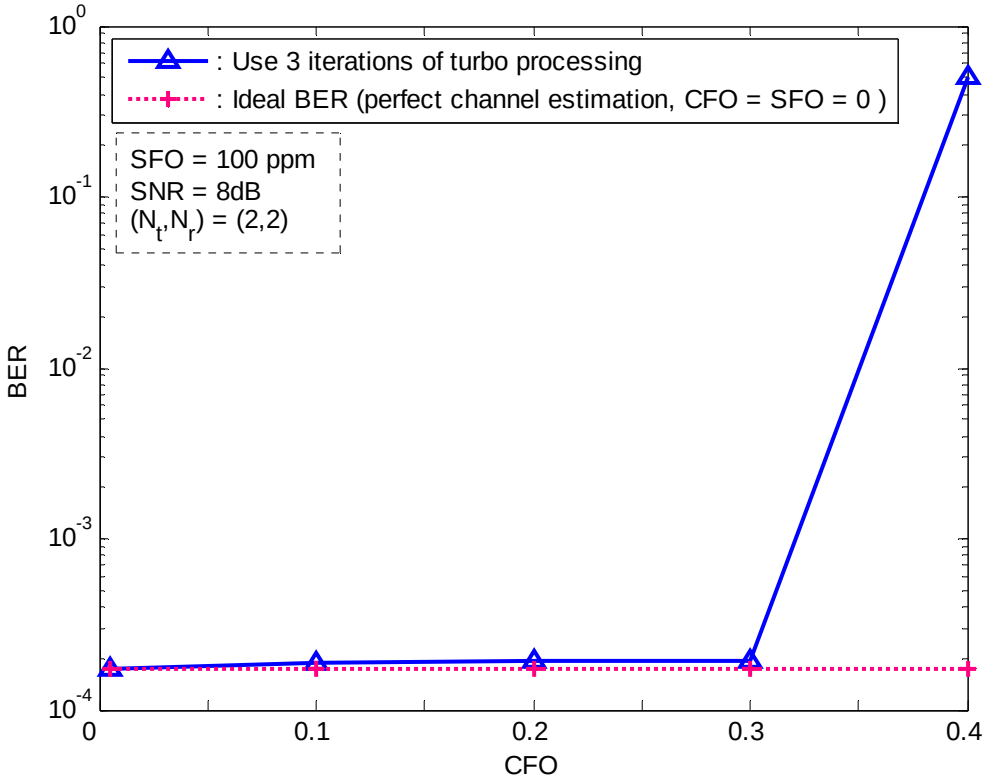

Figure 5.9: BER performance of the proposed turbo joint channel estimation, synchronization and decoding scheme under various CFO values.

5.5 Chapter Summary

In this chapter, a turbo joint channel estimation, synchronization and decoding scheme was developed for convolutionally coded MIMO-OFDM systems over quasi-static Rayleigh multi-path fading channels. The astonishing benefits of iteratively exchanging the extrinsic *a posteriori* probabilities in the turbo principle enable the proposed turbo scheme to provide a near-ideal BER performance after just three exchange iterations. Simulation results show that the joint CIR, CFO and SFO estimation using the iterative extrinsic APP exchange offers a fast convergent and low MSE performance over quasi-static Rayleigh multi-path fading channels.

Chapter 6

Summary and Future Work

Considered as one of the early broadband wireless communication techniques, the frequency hopping spread spectrum (FHSS) strategy has been employed to provide highly secure data transmissions. Later, the invention of the orthogonal frequency division multiplexing (OFDM) scheme has offered the high spectral efficiency and robustness against frequency-selective fading channels for broadband wireless communications. Recently, the revolutionary concept of multiple-input multiple-output (MIMO) architectures has provided a spectacular increase in the spectral efficiency for wireless communication channels. However, along with these potential benefits, the primary challenges in broadband wireless communications are the channel impairments which include intentional interference, multi-path propagation and imperfect synchronization. To mitigate such detrimental effects to the receiver performance, this thesis proposed several algorithms for estimating and compensating these channel impairments in early and recent broadband wireless systems as presented in previous chapters. In this chapter, we summarize these algorithm contributions and suggest some possible aspects for future work.

6.1 Summary of Thesis Contributions

In Chapter 2, we presented the literature of the existing anti-jamming algorithms for FHSS systems. Then, a detailed investigation on the FH/MFSK systems in the presence of a follower partial-band jammer was carried out. Based on formulating a signal model of the FH/MFSK signal corrupted by a follower jamming signal, a maximum likelihood (ML)–based algorithm was proposed to perform the joint follower jamming

rejection and symbol detection in FH/MFSK systems over quasi-static flat Rayleigh fading channels. Finally, the performance of the ML-based scheme was verified by various analytical and simulation results, and compared with the existing approaches.

In Chapter 3, we considered the performance of SISO-OFDM systems over quasi-static Rayleigh multipath fading channels in the presence of the carrier and sampling frequency offsets. By exploiting the standard RLS algorithm, a pilot-aided joint channel estimation and synchronization approach was proposed for burst-mode SISO-OFDM systems. In addition, Chapter 3 introduced a simple ICI reduction technique in the time domain and ML-based coarse estimation of CFO-SFO to further widen the allowable ranges of CFO and SFO values for the proposed approach. The simulation results showed that the proposed joint channel estimation and synchronization scheme is able to provide a near-optimum receiver performance over quasi-static Rayleigh multipath fading channels.

In Chapter 4, we addressed the joint estimation of CIR, CFO and SFO in MIMO-OFDM systems. Unlike the case of SISO-OFDM receivers where the standard RLS algorithm is employable, the joint estimation of CIR, CFO and SFO in MIMO scenarios requires the use of an adaptive filtering algorithm which can function as an adaptive filter with multiple outputs. To meet the requirement, the vector RLS-based joint channel estimation and synchronization scheme was proposed for MIMO-OFDM systems. The analytical and simulation results showed that the proposed scheme offers low MSE estimates and a near-optimum BER performance.

In chapter 5, a turbo joint channel estimation, synchronization and decoding scheme was developed for convolutionally coded MIMO-OFDM systems over quasi-static Rayleigh multi-path fading channels. By exploiting the soft information at the output of a soft-input soft-output decoder in a turbo manner, the joint CIR, CFO and

SFO estimation with the aid of the vector recursive least-squares (RLS) adaptive filtering algorithm is performed in a doubly iterative and semi-blind fashion. The astonishing benefits of iteratively exchanging the extrinsic APPs in the turbo principle enable the proposed turbo scheme to provide a low MSE and near-ideal BER performance after just three iterations of the iterative extrinsic APP exchange.

6.2 Suggestions of Future Work

Based on the individual chapters in this thesis, some possible issues of future work are as follows.

In Chapter 2, the ML-based jamming rejection scheme was proposed under an assumption that perfect timing synchronization of hopping sequences has been established at receivers. As a result, a possible future work would be to consider the anti-jamming issues in the presence of imperfect timing synchronization of hopping sequences. For instance, a joint jamming rejection, timing synchronization and symbol detection issue would be an interesting study.

In Chapter 3, the proposed pilot-aided joint estimation and synchronization scheme is applicable to *burst-mode* SISO-OFDM transmissions such as wireless LAN systems, where CIR, CFO and SFO are assumed to be time-invariant within one burst duration. For mobile wireless communication applications, where these channel parameters are usually assumed to be unchanged within one OFDM symbol duration, joint channel estimation and synchronization issues in such scenarios are desirable for further study.

For uncoded MIMO-OFDM transmissions, a vector RLS-based joint channel estimation and synchronization scheme was proposed in Chapter 4. Hence, an optimal

pilot design for the joint CIR, CFO and SFO estimation in MIMO scenarios would be an interesting issue for further investigation.

Unlike Chapters 3 and 4 with investigations in *uncoded* transmissions, Chapter 5 deals with *coded* MIMO-OFDM systems. Specifically, a turbo joint channel estimation, synchronization and decoding scheme was proposed for convolutionally coded MIMO-OFDM systems. As a result, an overall design of coded MIMO-OFDM systems using the turbo principle to optimize the receiver performance is a very interesting and practical research topic for future study.

Finally, this thesis has suggested a variety of research issues in FH and OFDM systems for broadband wireless communications. After obtaining the experimental performance of the proposed approaches for OFDM systems via the ongoing FPGA hardware implementation, we will study the mentioned suggestions of future work and hope that more feasible and higher performance algorithms would be developed for channel impairment mitigation in broadband wireless OFDM transmissions.

References

[1] Gergory D. Durgin, *Space-time wireless channels*, Prentice Hall, Upper saddle River, NJ, 2003.

[2] Marvin K. Simon, Jim K. Omura, Robert A. Scholtz and Barry K. Levvitt, *Spread spectrum communications handbook*, McGraw- Hill, 1994.

[3] Robert W. Chang and Richard A. Gibby, "A theoretical study of performance of an orthogonal multiplexing data transmission scheme", *IEEE Trans. on Communi. Technology*, vol. com-16, no. 4, Aug. 1968.

[4] G.L. Stuber, J.R. Barry, S.W. McLaughlin, Ye Li, M.A. Ingram and T.G. Pratt, "Broadband MIMO-OFDM wireless communications," *Proceedings of the IEEE*, vol.92, no.2, pp.271-294, Feb. 2004.

[5] R. E. Ziemer, R. L. Peterson and D. E. Borth, *Introduction to Spread Spectrum Communications*, Englewood Cliffs, NJ: Prentice-Hall, 1995.

[6] O. Besson, P. Stoica and Y. Kamiya, "Direction finding in the presence of an intermittent interference", *IEEE Trans. Signal Processing*, vol. 50, pp. 1554–1564, July 2002.

[7] E. B. Felstead, "Follower jammer considerations for frequency hopped spread spectrum," in *Proc. IEEE MILCOM 98*, Oct. 18-21, 1998, vol. 2, pp. 474 –478.

[8] John G. Proakis, *Digital Communications*, 3rd ed. New York: McGraw-Hill, 1995.

[9] Ezio Biglieri, John Proakis and Shlomo Shamai, "Fading channels: information-theoretic and communications aspects", *IEEE Trans. Inform. Theory*, vol. 44, pp. 6, Oct. 1998.

[10] M. Speth, S. Fechtel, G. Fock, and H. Meyr, "Optimum receiver design for OFDM-based broadband transmission - part II: A case study," *IEEE Trans. Commu.*, vol. 49, pp. 571–578, April 2001.

[11] V. Abhayawardhana and I.Wassell, "Iterative symbol offset correction algorithm for coherently modulated OFDM systems in wireless communication," *in Proceeding of the 13th IEEE International Symposium on Personal Indoor and Mobile Radio Communications*, vol. 2, pp. 545–549, September 2002.

[12] M. Speth, S. A. Fechtel, G. Fock, and H. Meyr, "Optimum receiver design for wireless broad-band systems using OFDM - part I," *IEEE Trans. Commun.*, vol. 47, no. 11, pp. 1668–1677, Nov. 1999.

[13] J. R. Vig and A. Ballato, *Frequency Control Devices*, available at http://www.ieee-uffc.org/freqcontrol/VigBallato/fcdevices.pdf

[14] A. A. Hassan, W. E. Stark, and J. E. Hershey, "Frequency-hopped spread spectrum in the presence of a follower partial-band jammer," *IEEE Trans. Commun.*, vol. 41, pp. 1125 – 1131, July 1993.

[15] H. M. Kwon, L. E. Miller, and J. S. Lee, “Evaluation of a partial band jammer with Gaussian-shaped spectrum against FH/MFSK”, *IEEE Trans. Commun.*, vol. 38, pp. 1045–1049, July 1990.

[16] K. C. Teh, A. C. Kot, and K. H. Li, “Partial-band jammer suppression in FFH spread-spectrum system using FFT”, *IEEE Trans. Veh. Technol*., vol. 48, pp. 478-486, Mar. 1999.

[17] Y. Kamiya and O. Besson, “Interference rejection for frequency hopping communication systems using a constant power algorithm”, *IEEE Trans. Commun.*, vol. 51, pp. 627 – 633, Apr. 2003.

[18] L. Acar and R. T. Compton, “The performance of an LMS adaptive array with frequency-hopped signals,” *IEEE Trans. Aerosp. Electron. Syst.*, vol. 21, pp. 360-371, May 1985.

[19] A. Krieger, “An adaptive algorithm for interference suppression in spread spectrum communication systems,” in *Proc. 24th Asilomar Conf.*, 1990, pp. 373-377.

[20] D. Torrieri and K. Bakhru, “An anticipative adaptive array for frequency-hopping communications,” *IEEE Trans. Aerosp. Electron. Syst.*, vol. 24, pp. 449-456, July 1988.

[21] F. Eken, “Use of antenna nulling with frequency-hopping against the follower jammer,” *IEEE Trans. Antennas Propagat.*, vol. 39, pp. 1391-1397, Sept. 1991.

[22] Chi Chung Ko, Hung Nguyen-Le and Lei Huang, “Joint interference suppression and symbol detection in slow FH/MFSK system with an antenna array”, in *Proceeding of the 63rd IEEE Veh. Techno. Conf.*, May, 2006.

[23] C. C. Ko, J. Zhang and A. Nehorai, “Separation and tracking of multiple broadband sources with one electromagnetic vector sensor”, *IEEE Trans. Aerospace and Electronic Systems*, vol. 38, 2002, pp. 1109 -1116.

[24] C. C. Ko and C. S. Siddharth, “Rejection and tracking of an unknown broadband source in a 2-element array through least square approximation of inter-element delay”, *IEEE Signal Processing Letters*, vol. 6, 1999, pp. 122 - 125.

[25] K. T. Wong, "Blind beamforming/Geolocation for Wideband-FFHs with unknown hop sequences", *IEEE Trans. Aerospace and Electronic Systems*, vol. 37, no.1, Jan. 2001, pp. 65-76.

[26] Mika Stanhlberg, “Radio attacks against two popular mobile networks”, HUT TML2000, available at http://gbppr.dyndns.org/PROJ/mil/celljam/stahlberg.pdf.

[27] Paolo Codenotti, Alexander Sprintson, and Jehoshua Bruck, “Anti-jamming schedules for wireless broadcast systems”, ETR070, California Institute of Technology, July, 2005, available at http://www.paradise.caltech.edu/papers/etr070.pdf.

[28] Hamid Krim and Mats Viberg, “Two Decades of Array Signal Processing Research”, *IEEE Signal Processing Magazine*, July 1996.

[29] Yingwei Yao and Georgios B. Giannakis, “Blind carrier frequency offset estimation in SISO, MIMO, and multiuser OFDM systems”, *IEEE Trans. Commun.*, vol. 53, no. 1, pp. 173-183, Jan. 2005.

[30] Pei-Yun Tsai, Hsin-Yu Kang, and Tzi-Dar Chiueh, "Joint weighted least-squares estimation of frequency and timing offset for OFDM systems over fading channels," *IEEE Trans. Veh. Technol.*, Volume 54, Issue 1, pp. 211-223, Jan. 2005.

[31] Christian Oberli, "ML-based tracking algorithms for MIMO-OFDM", *IEEE Trans. Wireless Commun.*, vol. 6, no. 7, pp. 2630-2639, July 2007.

[32] Myeongchoel Shin, Hakju Lee, and Chungyong Lee, "Enhanced channel-estimation technique for MIMO-OFDM systems," *IEEE Trans. Veh. Technol*., pp. vol. 53, no. 1, pp. 261-265, Jan. 2004.

[33] Imad Barhumi, Geert Leus, and Marc Moonen, "Optimal training design for MIMO OFDM systems in mobile wireless channels," *IEEE Trans. Signal Process.*, vol. 51, no. 6, pp. 1615-1624, June 2003.

[34] Jong-Ho Lee, Jae Choong Han, and Seong-Cheol Kim, "Joint carrier frequency synchronization and channel estimation for OFDM systems via the EM algorithm," *IEEE Trans. Veh. Technol.*, vol. 55, no. 1, pp. 167-172, Jan. 2006.

[35] Darryl Dexu Lin, Ryan A. Pacheco, Teng Joon Lim, and Dimitrios Hatzinakos, "Joint estimation of channel response, frequency offset, and phase noise in OFDM", *IEEE Trans. on Signal Process.*, vol. 54, pp. 3542-3554, Sept. 2006.

[36] Sophie Gault, Walid Hachem, and Philippe Ciblat, "Joint sampling clock offset and channel estimation for OFDM signals: Cramer–Rao bound and algorithms", *IEEE Trans. on Signal Process.*, vol. 54, pp. 1875-1885, May 2006.

[37] M. M. Freda, J. F. Weng, and T. Le-Ngoc, "Joint channel estimation and synchronization for OFDM systems", *in Proc. IEEE VTC*, Sept. 26-29, 2004, vol. 3, pp. 1673-1677.

[38] IEEE Computer Society, *IEEE Std 802.11a-1999*, Dec 1999.

[39] Steven M. Kay, *Fundamentals of Statistical Signal Processing*, PTR Prentice-Hall, New Jersey, 1998.

[40] Helmut Bolcskei, "MIMO-OFDM wireless systems: basics, perspectives, and challenges", *IEEE Wireless Communications*, pp. 31-37, Aug. 2006.

[41] Xiaoli Ma, Mi-Kyung Oh, Georgios B. Giannakis, "Hopping pilots for estimation of frequency offset and multiantenna channel in MIMO-OFDM", *IEEE Trans. Commun.*, vol. 53, no. 1, pp. 162-172, Jan. 2005.

[42] Hlaing Minn and Naofal Al-Dhahir, "Optimal Training signals for MIMO OFDM channel estimation", *IEEE Trans. Wireless Communi.*, vol. 5, no. 5, pp. 1158-1168, May. 2006.

[43] Marcello Cicerone, Osvaldo Simeone and Umberto Spagnolini, "Channel estimation for MIMO-OFDM systems by modal analysis/filtering", *IEEE Trans. Communi.*, vol. 54, no. 11, pp. 2062-2074, Nov. 2006.

[44] Z. Jane Wang, Zhu Han, and K. J. Ray Liu, "A MIMO-OFDM channel estimation approach using time of arrivals", *IEEE Trans. Communi.*, vol. 4, no. 3, pp. 1207-1213 May 2005.

[45] Kyeong Jin Kim and Ronald A. Iltis, “Frequency offset synchronization and channel estimation for the MIMO-OFDM system using Rao-Blackwellized Gaussian-Hermite filter”, *in Proc. IEEE WCNC*, pp. 860-865, April 2006.

[46] Jun Li, Guisheng Liao, and Shan Ouyang, “Jointly tracking dispersive channels and carrier frequency-offset in MIMO-OFDM systems”, *in Proc. IEEE ICCS*, vol. 2, pp. 816-819, June 2006.

[47] Hung Nguyen-Le, Tho Le-Ngoc, Chi Chung Ko, “Joint channel estimation and synchronization with inter-carrier interference reduction for OFDM”, *in Proceeding of ICC’07*, June 24-28, 2007, Glasgow, UK.

[48] Harry L. Van Trees, *Optimum Array Processing*, Wiley, 2002.

[49] Jerry M. Mendel, *Lessons in estimation theory for signal processing, communications, and control*, Prentice-Hall, 1995.

[50] Xu Zhu and Ross D. Murch, “Performance analysis of maximum likelihood detection in MIMO antenna system”, *IEEE Trans. Communi.*, vol. 50, no. 2, pp. 187-191, Feb. 2002.

[51] Hiroshi Harada and Ramjee Prasad, *Simulation and Software Radio for Mobile Communications*, Boston: Artech, 2002.

[52] C. Berrou, A. Glavieux, and P. Thitimajshima, “Near Shannon limit error-correcting coding and decoding: Turbo codes,” *in Proceeding of ICC 1993*, Geneva, Switzerland, May 1993, pp. 1064-1070.

[53] Dan Raphaeli and Yoram Zarai, “Combined turbo equalization and turbo decoding**”** *in Proceeding of IEEE Globecom* Nov. 1997, pp. 639-643.

[54] Xiaodong Wang and H. Vincent Poor, “Iterative (Turbo) soft interference cancellation and decoding for coded CDMA” , *IEEE Trans. on Commnu*., vol. 47, no. 7, July, 1999.

[55] Hesham El Gamal and Evaggelos Geraniotis, “Iterative multiuser detection for coded CDMA signals in AWGN and fading channels”, *IEEE J. Select Areas Commun.* vol. 18,. no. 1, Jan. 2000.

[56] Paul D. Alexander, Mark C. Reed, John A. Asenstorfer and Christian B. Schlegel “Iterative multiuser interference reduction: Turbo CDMA”, *IEEE Trans. on Commnu*., vol. 47, no. 7, July, 1999.

[57] Mutlu Koca and Bernard C. Levy, “Broadband beamforming for joint interference cancellation and turbo equalization”, *IEEE Trans. on Wireless Commnu*., vol. 4, no. 5, Sept, 2005.

[58] Stefano Tomasin, Alexei Gorokhov, Haibing Yang and Jean-Paul Linnartz, “Iterative interference cancellation and channel estimation for mobile OFDM”, *IEEE Trans. on Wireless Commnu*., vol. 4, no. 1, Jan, 2005.

[59] Andreas Wolfgang, Sheng Chen and Lajos Hanzo, “Parallel interference cancellation based turbo space-time equalization in the SDMA uplink”, *IEEE Trans. on Wireless Commnu*., vol. 6, no. 2, Feb, 2007.

[60] Xuan Huan Nguyen and Jinho Choi, “Iterative OFDM receiver with channel estimation and frequency-offset compensation”, *in Proceeding of IEEE Int. Conf. Communi.*, June 2006.

[61] Si Li, Tho Le-Ngoc, Soon Chan Kwon and Jong-Soo Seo, “Turbo coded OFDM receiver using joint synchronization, channel estimation and decoding”, *in Proceeding of IEEE WCNC*, 2007.

[62] Jianhua Liu and Jian Li, “Turbo processing for an OFDM-based MIMO system”, *IEEE Trans. on Wireless Commnu.*, vol. 4, no. 5, Sept., 2005.

[63] Xuan Huan Nguyen and Jinho Choi, “Iterative channel estimation and turbo decoding in OFDM systems”, *in Proceeding of IEEE VTC 2005*, pp. 166- 170, Sept. 2005.

[64] Jerome Bonnet and Gunther Auer, “Optimized iterative channel estimation for OFDM”, *in Proceeding of IEEE VTC Fall 2006*, pp. 1 - 5 , Sept. 2006.

[65] Se Bin Im and HyungJin Choi, “Robust iterative channel estimation for OFDM packet transmission system”, *in Proceeding of IEEE VTC Fall 2006*, Sept. 2006.

[66] Frieder Sanzi and Marc C. Necker, “Totally blind APP channel estimation for mobile OFDM systems”, *IEEE Commnu. Letter*, vol. 7, no. 11, Nov. 2003.

[67] Andrea M. Tonello, “Space-time bit-interleaved coded modulation with an iterative decoding strategy”, *in Proceeding of IEEE VTC 2000*.

[68] S. Benedetto, D. Divsalar, G. Montorsi and F. Pollara, “A soft-input soft-output APP module for iterative decoding of concatenated codes”, *IEEE Communi. Letters*, vol. 1, no. 1, Jan. 1997.

[69] Simon Haykin, Mathini Sellathurai, Yvo de Jong, and Tricia Willink, “Turbo-MIMO for wireless communications”, *IEEE Commnu. Magazine*, Oct. 2004.

[70] Hung Nguyen-Le, Tho Le-Ngoc, Chi Chung Ko, “Extended RLS-based joint estimation of channel response and frequency offsets for MIMO-OFDM”, *accepted for publication in Proceeding of IEEE Globecom 2007*.

[71] Chi Chung Ko, Hung Nguyen-Le and Lei Huang, “ML-based follower jamming rejection in slow FH/MFSK systems with an antenna array”, accepted for publication on *IEEE Trans. Communi.*

Appendix A

Blind ML Estimation of the Desired Signal's Channel Gains

In the unjammed portion of the hop, a joint ML estimation of d_0, α_1 and α_2 can be obtained from

$$\hat{\alpha}_1, \hat{\alpha}_2, \hat{d}_0 = \arg \min_{\alpha_1, \alpha_2, d_0} \left\{ \left\| \mathbf{r}_1 - \alpha_1 \mathbf{s}(d_0) \right\|^2 + \left\| \mathbf{r}_2 - \alpha_2 \mathbf{s}(d_0) \right\|^2, \; d_0 = 0,1,...,M-1 \right\}. \quad \text{(A.1)}$$

Differentiating $\left\| \mathbf{r}_1 - \alpha_1 \mathbf{s}(d_0) \right\|^2 + \left\| \mathbf{r}_2 - \alpha_2 \mathbf{s}(d_0) \right\|^2$ with respect to α_1 and α_2, respectively, and setting the results to zero, we have

$$\alpha_p = \frac{\mathbf{s}^H(d_0)\mathbf{r}_p}{\left\| \mathbf{s}(d_0) \right\|^2}, \; p = 1, 2. \quad \text{(A.2)}$$

Substituting (A.2) into (A.1) then yields

$$\hat{d}_0 = \arg \min_{d_0} \left\{ \left\| \mathbf{r}_1 - \frac{\mathbf{s}^H(d_0)\mathbf{r}_1\mathbf{s}(d_0)}{\left\| \mathbf{s}(d_0) \right\|^2} \right\|^2 + \left\| \mathbf{r}_2 - \frac{\mathbf{s}^H(d_0)\mathbf{r}_2\mathbf{s}(d_0)}{\left\| \mathbf{s}(d_0) \right\|^2} \right\|^2, d_0 = 0,1,...,M-1 \right\}. \quad \text{(A.3)}$$

Based on the estimate of transmitted symbol $\hat{d}_0$, the blind ML estimates of α_1 and α_2 are thus

$$\hat{\alpha}_p = \frac{\mathbf{s}^H(\hat{d}_0)\mathbf{r}_p}{\left\| \mathbf{s}(\hat{d}_0) \right\|^2}, \; p = 1, 2. \quad \text{(A.4)}$$

Appendix B

Beamforming Structure for Nulling the Desired Signal

Based on the estimates of the desired signal's channel gains $\hat{\alpha}_p, p = 1,2$, a simple beamforming structure with a weighting vector of $\mathbf{g} = [\hat{\alpha}_2 \quad -\hat{\alpha}_1]^T$ can be employed to null a signal with these gains. Specifically, the output from this beamforming is

$$y_n = \mathbf{g}^T \mathbf{r}_n, \tag{B.1}$$

where $\mathbf{r}_n = [r_{1,n} \quad r_{2,n}]^T$ has forms given by (2.4). Thus, if the estimated channel gains $\hat{\alpha}_p, p = 1,2$ are indeed closed to the actual channel gains $\alpha_p, p = 1,2$, the desired signal will be closed to being perfectly or completely rejected.

Appendix C

Proof of Inequality $\Gamma_2(d) < \Gamma_1(d)$

Substituting (2.16) and (2.17) into (2.18) and (2.19) yields

$$\xi_1(d) = \frac{\|\mathbf{z}_2(d)\|^2 - \|\mathbf{z}_1(d)\|^2 - \sqrt{\left(\|\mathbf{z}_2(d)\|^2 - \|\mathbf{z}_1(d)\|^2\right)^2 + 4\left|\mathbf{z}_2^H(d)\mathbf{z}_1(d)\right|^2}}{2\mathbf{z}_2^H(d)\mathbf{z}_1(d)}, \tag{C.1}$$

and

$$\xi_2(d) = \frac{\|\mathbf{z}_2(d)\|^2 - \|\mathbf{z}_1(d)\|^2 + \sqrt{\left(\|\mathbf{z}_2(d)\|^2 - \|\mathbf{z}_1(d)\|^2\right)^2 + 4\left|\mathbf{z}_2^H(d)\mathbf{z}_1(d)\right|^2}}{2\mathbf{z}_2^H(d)\mathbf{z}_1(d)}. \tag{C.2}$$

Substituting (C.1) and (C.2) into the numerator of (2.21), respectively, we deduce

$$\Gamma_1(d) = \|\mathbf{z}_1(d)\|^2 + \frac{\sqrt{\left(\|\mathbf{z}_2(d)\|^2 - \|\mathbf{z}_1(d)\|^2\right)^2 + 4\left|\mathbf{z}_2^H(d)\mathbf{z}_1(d)\right|^2}}{1 + |\xi_1(d)|^2}, \tag{C.3}$$

and

$$\Gamma_2(d) = \|\mathbf{z}_1(d)\|^2 - \frac{\sqrt{\left(\|\mathbf{z}_2(d)\|^2 - \|\mathbf{z}_1(d)\|^2\right)^2 + 4\left|\mathbf{z}_2^H(d)\mathbf{z}_1(d)\right|^2}}{1 + |\xi_2(d)|^2}. \tag{C.4}$$

As can be observed from (C.3) and (C.4), it is obvious that $\Gamma_2(d)$ is always smaller than $\Gamma_1(d)$.

APPENDIX D

Derivation of Cramér- Rao Lower Bound for Join Estimation of CIR, CFO and SFO in Chapter 3

The Cramér- Rao lower bounds [39] of the estimated parameters can be determined by

$$CRLB(\boldsymbol{\omega}) = diag\left(\mathbf{F}^{-1}(\boldsymbol{\omega})\right), \tag{D.1}$$

where the vector of true parameter values $\boldsymbol{\omega} = [\omega_0, ..., \omega_{2L+1}]$ with $\omega_l = \mathrm{Re}\{h_l\}$, $\omega_{l+L} = \mathrm{Im}\{h_l\}$, $\omega_{2L} = \varepsilon, \omega_{2L+1} = \eta$, for $l = 0,1,...,(L-1)$, and **F** is the Fisher information matrix.

The (*i*,*j*)-th entry of the Fisher information matrix can be obtained by

$$F_{i,j} = -E\left\{\frac{\partial^2 \Lambda}{\partial \omega_i \partial \omega_j}\right\}, \tag{D.2}$$

where Λ is the log-likelihood function of received signal samples used for estimation. It is assumed that the noise samples, $w_m(n)$, are independent complex-valued zero-mean Gaussian random variable with variance of σ^2. As a result, the log-likelihood function of received signal samples is given by

$$\Lambda = \Lambda_o - \frac{1}{\sigma^2}\sum_{m=1}^{M_S}\sum_{n=0}^{N-1}\left| r_{m,n} - \frac{1}{N} e^{j\frac{2\pi}{N}(N_m+n)\varepsilon_\eta} \sum_{k=-K/2}^{K/2-1} X_m(k) H(k) e^{j\frac{2\pi k}{N} n(1+\eta)} e^{j\frac{2\pi k}{N}\eta N_m} \right|^2, \tag{D.3}$$

where Λ_o is a constant and M_S is the number of OFDM symbol used for estimation.

As a result, the elements of the Fisher information matrix, namely **F**, are obtained by taking expectation of the following second-order partial derivatives

$$F_{l',l} = F_{l'+L,l+L} = -E\left\{\frac{\partial^2 \Lambda}{\partial \mathrm{Re}\{h_{l'}\}\partial \mathrm{Re}\{h_l\}}\right\} = \frac{2}{\sigma^2 N^2}\sum_{m=1}^{M_S}\sum_{n=0}^{N-1}\mathrm{Re}\{\rho_{l,l',m,n}\}, \tag{D.4}$$

$$F_{l',l+L} = F_{l'+L,l} = -E\left\{\frac{\partial^2 \Lambda}{\partial \mathrm{Im}\{h_{l'}\}\partial \mathrm{Re}\{h_l\}}\right\} = \frac{2}{\sigma^2 N^2}\sum_{m=1}^{M_S}\sum_{n=0}^{N-1}\mathrm{Im}\{\rho_{l,l',m,n}\}, \tag{D.5}$$

with $l' = 0,1,...,L-1$, $l = 0,1,...,L-1$,

$$\rho_{l,l',m,n} = \sum_{k'=-K/2}^{K/2-1}\sum_{k=-K/2}^{K/2-1} X_m^*(k')X_m(k)e^{j\frac{2\pi(k-k')n}{N}}e^{j\frac{2\pi(k-k')}{N}\eta(n+N_m)}e^{-j\frac{2\pi kl}{N}}e^{-j\frac{2\pi k'l'}{N}},$$

$$F_{l,2L} = F_{2L,l} = -E\left\{\frac{\partial^2 \Lambda}{\partial\varepsilon\partial \mathrm{Re}\{h_l\}}\right\} = \frac{-2}{\sigma^2 N^2}\sum_{m=1}^{M_S}\sum_{n=0}^{N-1}\mathrm{Re}\left\{j\frac{2\pi}{N}(n+N_m)(1+\eta)\zeta_{l,m,n}\right\}, \tag{D.6}$$

$$F_{l+L,2L} = F_{2L,l+L} = -E\left\{\frac{\partial^2 \Lambda}{\partial\varepsilon\partial \mathrm{Im}\{h_l\}}\right\} = \frac{-2}{\sigma^2 N^2}\sum_{m=1}^{M_S}\sum_{n=0}^{N-1}\mathrm{Re}\left\{\frac{2\pi}{N}(n+N_m)(1+\eta)\zeta_{l,m,n}\right\}, \tag{D.7}$$

with $\zeta_{l,m,n} = \sum_{k=-K/2}^{K/2-1}\sum_{k'=-K/2}^{K/2-1} X_m^*(k)H^*(k)X_m(k')e^{j\frac{2\pi(k'-k)}{N}\left[1+\eta(n+N_m)\right]}e^{-j\frac{2\pi k'l}{N}}$,

$$F_{l,2L+1} = F_{2L+1,l} = -E\left\{\frac{\partial^2 \Lambda}{\partial\eta\partial \mathrm{Re}\{h_l\}}\right\} = \frac{-2}{\sigma^2 N^2}\sum_{m=1}^{M_S}\sum_{n=0}^{N-1}\mathrm{Re}\{\Omega_{l,m,n}\}, \tag{D.8}$$

$$F_{l+L,2L+1} = F_{2L+1,l+L} = -E\left\{\frac{\partial^2 \Lambda}{\partial\eta\partial \mathrm{Im}\{h_l\}}\right\} = \frac{2}{\sigma^2 N^2}\sum_{m=1}^{M_S}\sum_{n=0}^{N-1}\mathrm{Im}\{\Omega_{l,m,n}\}, \tag{D.9}$$

with

$$\Omega_{l,m,n} = \sum_{k=-K/2}^{K/2-1}\sum_{k'=-K/2}^{K/2} X_m(k)X_m^*(k')e^{j\frac{2\pi(k-k')(n+\eta n+\eta N_m)}{N}}e^{-j\frac{2\pi kl}{N}}\left(j\frac{2\pi(n+N_m)\left(\varepsilon(k+1)-(k-k')H^*(k')\right)}{N}\right)$$

$$F_{2L,2L} = -E\left\{\frac{\partial^2 \Lambda}{(\partial\varepsilon)^2}\right\} = \frac{2}{\sigma^2 N}\sum_{m=1}^{M_S}\sum_{n=0}^{N-1}\left[\frac{2\pi}{N}(1+\eta)(n+N_m)\right]^2\left|\sum_{k=-K/2}^{K/2-1}X_m(k)e^{j\frac{2\pi kn}{N}}e^{j\frac{2\pi k}{N}\eta(n+N_m)}H(k)\right|^2$$

(4.32)

$$F_{2L,2L+1} = F_{2L+1,2L} = -E\left\{\frac{\partial^2 \Lambda}{\partial\eta\partial\varepsilon}\right\} = \frac{-2}{\sigma^2 N}\sum_{m=1}^{M_S}\sum_{n=0}^{N-1}\mathrm{Re}\left\{j\frac{2\pi}{N}(n+N_m)\left(\Phi_{m,n}+\Psi_{m,n}\right)\right\}, \tag{D.10}$$

with $\Phi_{m,n} = \left(1+j\frac{2\pi(n+N_m)\varepsilon_\eta}{N}\right)\left|\sum_{k=-K/2}^{K/2-1}X_m(k)e^{j\frac{2\pi k(n+\eta n+\eta N_m)}{N}}H^*(k)\right|^2$,

$$\Psi_{m,n} = j\frac{2\pi(n+N_m)}{N}(1+\eta)e^{j\frac{2\pi\varepsilon_\eta(n+N_m)}{N}}\sum_{k=-K/2}^{K/2-1}\sum_{k'=-K/2}^{K/2-1}X_m^*(k)X_m(k')e^{j\frac{2\pi(k-k')(n+\eta n+\eta N_m}{N}}k'H^*(k)H(k'),$$

$$F_{2L+1,2L+1} = -E\left\{\frac{\partial^2\Lambda}{(\partial\eta)^2}\right\} = \frac{-2}{\sigma^2N^2}\sum_{m=1}^{M_S}\sum_{n=0}^{N-1}\mathrm{Re}\{\Gamma_{m,n}+\Theta_{m,n}+\Pi_{m,n}\}, \qquad \text{(D.11)}$$

with

$$\Gamma_{m,n} = -\left|\sum_{k=-K/2}^{K/2-1}X_m^*(k)e^{-j\frac{2\pi k(n+\eta n+\eta N_m)}{N}}H^*(k)\right|^2\frac{4\pi^2(n+N_m)^2\varepsilon^2}{N^2},$$

$$\Theta_{m,n} = j\frac{4\pi}{N}\varepsilon(n+N_m)\sum_{k=-K/2}^{K/2-1}\sum_{k'=-K/2}^{K/2-1}X_m^*(k)X_m(k')e^{-j\frac{2\pi(k-k')(n+\eta n+\eta N_m}{N}}k'H^*(k)H(k'),$$

$$\Pi_{m,n} = -\left|\sum_{k=-K/2}^{K/2-1}X_m(k)e^{j\frac{2\pi k(n+\eta n+\eta N_m)}{N}}kH(k)\right|^2\frac{4\pi^2(n+N_m)^2}{N^2}.$$

Appendix E

Derivation of Cramér- Rao Lower Bound for Join Estimation of CIR, CFO AND SFO in Chapter 4

As shown in (4.5), the received subcarrier k_i in frequency domain at the *v*-th receive antenna can be expressed by

$$Y_{v,m}(k_i) = e^{j\frac{2\pi}{N}N_{m_i}\varepsilon_{k_i}}\delta_{k_i,k_i}\sum_{u=1}^{N_t} X_{u,m}(k_i)H_{u,v}(k_i) + W_{v,m}(k_i). \qquad \text{(E.1)}$$

Note that ICI components in (E.1) can be assumed to be additive and Gaussian distributed and to be absorbed in $W_{v,m}(k_i)$ [12], [31].

By collecting *K* subcarriers in each receive antenna, the resulting KN_r sub-carriers from N_r receive antennas can be represented in the vector form as follow,

$$\mathbf{y} = \left(\mathbf{I}_{N_r} \otimes \mathbf{\Phi}(\varepsilon,\eta)\right)\left(\mathbf{I}_{N_r} \otimes \mathbf{S}\right)\left(\mathbf{I}_{N_r} \otimes \mathbf{F}\right)\mathbf{h} + \mathbf{w} \qquad \text{(E.2)}$$

or

$$\mathbf{y} = \mathbf{c} + \mathbf{w}, \qquad \text{(E.3)}$$

where $\mathbf{y} = \left[Y_{1,m_1}(k_1) \ \ldots \ Y_{1,m_K}(k_K) \quad \cdots \quad Y_{N_r,m_1}(k_1) \ \ldots \ Y_{N_r,m_K}(k_K)\right]^T$,

$\mathbf{w} = \left[W_{1,m_1}(k_1) \ \ldots \ W_{1,m_K}(k_K) \quad \cdots \quad W_{N_r,m_1}(k_1) \ \ldots \ W_{N_r,m_K}(k_K)\right]^T$,

$\mathbf{c} = \left(\mathbf{I}_{N_r} \otimes \left(\mathbf{\Phi}(\varepsilon,\eta)\mathbf{SF}\right)\right)\mathbf{h}$,

$$\mathbf{\Phi}(\varepsilon,\eta) = diag\left(e^{j\frac{2\pi}{N}N_{m_1}\varepsilon_{k_1}}\delta_{k_1,k_1} \ \cdots \ e^{j\frac{2\pi}{N}N_{m_K}\varepsilon_{k_K}}\delta_{k_K,k_K}\right),$$

$$\mathbf{S}=\begin{bmatrix}\mathbf{x}(k_1) & \mathbf{0}_{1\times N_t} & \mathbf{0}_{1\times N_t(K-2)}\\ \mathbf{0}_{1\times N_t} & \mathbf{x}(k_2) & \mathbf{0}_{1\times N_t(K-2)}\\ \vdots & \ddots & \vdots\\ \mathbf{0}_{1\times N_t} & \mathbf{0}_{1\times N_t(K-2)} & \mathbf{x}(k_K)\end{bmatrix},\ \mathbf{x}(k_i)=\left[X_1(k_i)\ \ldots\ X_{N_t}(k_i)\right],$$

$$\mathbf{0}_{1\times N_t}=\underbrace{[0\cdots 0]}_{N_t\ \text{elements}},$$

$$\mathbf{h}=\left[\mathbf{h}_1^T\ \cdots\ \mathbf{h}_{N_r}^T\right]^T,\ \mathbf{h}_v=\left[h_{1,v,0}\ \ldots\ h_{1,v,L-1}\ \ \cdots\ \ h_{N_t,v,0}\ \ldots\ h_{N_t,v,L-1}\right]^T,\ v=1,\ldots,N_r,$$

$$\mathbf{F}=\begin{bmatrix}\mathbf{F}_1\\ \vdots\\ \mathbf{F}_K\end{bmatrix}\ \text{and}\ \mathbf{F}_i=\mathbf{I}_{N_t}\otimes\begin{bmatrix}1\ \cdots\ e^{-j\frac{2\pi}{N}(L-1)k_i}\end{bmatrix}.$$

Based on (E.3), the Fisher information matrix [39] can be computed by

$$\mathbf{M}=\frac{2}{\sigma_w^2}\mathrm{Re}\left[\frac{\partial\mathbf{c}^H}{\partial\boldsymbol{\omega}}\frac{\partial\mathbf{c}}{\partial\boldsymbol{\omega}^T}\right],\tag{E.4}$$

where $\boldsymbol{\omega}=\left[\mathbf{h}_R^T\ \ \mathbf{h}_I^T\ \ \varphi^T\right]^T$, $\mathbf{h}_R=\mathrm{Re}\{\mathbf{h}\}$, $\mathbf{h}_I=\mathrm{Im}\{\mathbf{h}\}$, $\boldsymbol{\varphi}=\left[\varepsilon\ \ \eta\right]^T$,

$$\frac{\partial\mathbf{c}^H}{\partial\mathbf{h}_R}=\mathbf{I}_{N_r}\otimes\left(\mathbf{F}^H\mathbf{S}^H\boldsymbol{\Phi}^H(\varepsilon,\eta)\right),\ \frac{\partial\mathbf{c}^H}{\partial\mathbf{h}_I}=-j\mathbf{I}_{N_r}\otimes\left(\mathbf{F}^H\mathbf{S}^H\boldsymbol{\Phi}^H(\varepsilon,\eta)\right),$$

$$\frac{\partial\mathbf{c}^H}{\partial\varphi}=\begin{bmatrix}\mathbf{h}^H\left(\mathbf{I}_{N_r}\otimes\left(\mathbf{F}^H\mathbf{S}^H\boldsymbol{\Phi}_\varepsilon^H\right)\right)\\ \mathbf{h}^H\left(\mathbf{I}_{N_r}\otimes\left(\mathbf{F}^H\mathbf{S}^H\boldsymbol{\Phi}_\eta^H\right)\right)\end{bmatrix},\ \frac{\partial\mathbf{c}}{\partial\mathbf{h}_R^T}=\mathbf{I}_{N_r}\otimes\left(\boldsymbol{\Phi}(\varepsilon,\eta)\mathbf{SF}\right),$$

$$\frac{\partial\mathbf{c}}{\partial\mathbf{h}_I^T}=j\mathbf{I}_{N_r}\otimes\left(\boldsymbol{\Phi}(\varepsilon,\eta)\mathbf{SF}\right)\ \text{and}\ \frac{\partial\mathbf{c}}{\partial\varphi^T}=\left[\left(\mathbf{I}_{N_r}\otimes\left(\boldsymbol{\Phi}_\varepsilon\mathbf{SF}\right)\right)\mathbf{h}\quad\left(\mathbf{I}_{N_r}\otimes\left(\boldsymbol{\Phi}_\eta\mathbf{SF}\right)\right)\mathbf{h}\right].$$

After some manipulation, the Fisher information matrix can be rewritten by

$$\mathbf{M}=\frac{2}{\sigma_w^2}\mathrm{Re}\begin{bmatrix}\mathbf{C} & j\mathbf{C} & \mathbf{D} & \mathbf{E}\\ -j\mathbf{C} & \mathbf{C} & -j\mathbf{D} & -j\mathbf{E}\\ \mathbf{D}^H & j\mathbf{D}^H & \mathbf{C}_\varepsilon & \mathbf{G}\\ \mathbf{E}^H & j\mathbf{E}^H & \mathbf{G}^H & \mathbf{C}_\eta\end{bmatrix}\tag{E.5}$$

or

$$\mathbf{M} = \frac{2}{\sigma_w^2}\begin{bmatrix} \mathbf{M}_{11} & \mathbf{M}_{12} \\ \mathbf{M}_{12}^T & \mathbf{M}_{22} \end{bmatrix}, \tag{E.6}$$

where $\mathbf{M}_{11} = \begin{bmatrix} \mathrm{Re}\{\mathbf{C}\} & -\mathrm{Im}\{\mathbf{C}\} \\ \mathrm{Im}\{\mathbf{C}\} & \mathrm{Re}\{\mathbf{C}\} \end{bmatrix}$, $\mathbf{M}_{12} = \begin{bmatrix} \mathrm{Re}\{\mathbf{D}\} & \mathrm{Re}\{\mathbf{E}\} \\ \mathrm{Im}\{\mathbf{D}\} & \mathrm{Im}\{\mathbf{E}\} \end{bmatrix}$,

$\mathbf{M}_{22} = \begin{bmatrix} \mathrm{Re}\{\mathbf{C}_\varepsilon\} & \mathrm{Re}\{\mathbf{G}\} \\ \mathrm{Re}\{\mathbf{G}^H\} & \mathrm{Re}\{\mathbf{C}_\eta\} \end{bmatrix}$, $\mathbf{C} = \mathbf{I}_{N_r} \otimes \left(\mathbf{F}^H \mathbf{S}^H \boldsymbol{\Phi}^H(\varepsilon,\eta)\boldsymbol{\Phi}(\varepsilon,\eta)\mathbf{SF}\right)$,

$\mathbf{D} = \mathbf{I}_{N_r} \otimes \left(\mathbf{F}^H \mathbf{S}^H \boldsymbol{\Phi}^H(\varepsilon,\eta)\boldsymbol{\Phi}_\varepsilon \mathbf{SF}\right)$, $\mathbf{E} = \left(\mathbf{I}_{N_r} \otimes \left(\mathbf{F}^H \mathbf{S}^H \boldsymbol{\Phi}^H(\varepsilon,\eta)\boldsymbol{\Phi}_\eta \mathbf{SF}\right)\right)\mathbf{h}$,

$\mathbf{C}_\varepsilon = \mathbf{h}^H \left(\mathbf{I}_{N_r} \otimes \left(\mathbf{F}^H \mathbf{S}^H \boldsymbol{\Phi}_\varepsilon^H \boldsymbol{\Phi}_\varepsilon \mathbf{SF}\right)\right)\mathbf{h}$, $\mathbf{C}_\eta = \mathbf{h}^H \left(\mathbf{I}_{N_r} \otimes \left(\mathbf{F}^H \mathbf{S}^H \boldsymbol{\Phi}_\eta^H \boldsymbol{\Phi}_\eta \mathbf{SF}\right)\right)\mathbf{h}$,

$\mathbf{G} = \mathbf{h}^H \left(\mathbf{I}_{N_r} \otimes \left(\mathbf{F}^H \mathbf{S}^H \boldsymbol{\Phi}_\varepsilon^H \boldsymbol{\Phi}_\eta \mathbf{SF}\right)\right)\mathbf{h}$.

By applying a lemma for the inverse of partitioned matrices [48, Appendix A], the inverse of the Fisher information matrix can be determined by

$$\mathbf{M}^{-1} = \frac{\sigma_w^2}{2}\begin{bmatrix} \left(\mathbf{M}_{11} - \mathbf{M}_{12}\mathbf{M}_{22}^{-1}\mathbf{M}_{21}\right)^{-1} & -\left(\mathbf{M}_{11} - \mathbf{M}_{12}\mathbf{M}_{22}^{-1}\mathbf{M}_{21}\right)^{-1}\mathbf{M}_{12}\mathbf{M}_{22}^{-1} \\ -\left(\mathbf{M}_{22} - \mathbf{M}_{21}\mathbf{M}_{11}^{-1}\mathbf{M}_{12}\right)^{-1}\mathbf{M}_{21}\mathbf{M}_{11}^{-1} & \left(\mathbf{M}_{22} - \mathbf{M}_{21}\mathbf{M}_{11}^{-1}\mathbf{M}_{12}\right)^{-1} \end{bmatrix}, \tag{E.7}$$

Therefore, the Crame Rao lower bound of estimated parameters $\boldsymbol{\omega}$, *CRLB(**ω**)*, can be determined by

$$CRLB(\boldsymbol{\omega}) = diag\left(\mathbf{M}^{-1}\right). \tag{E.8}$$